

Three-Dimensional Atmospheric Reconstruction of the 2018 Camp Fire Using HRRR Cross-Section Analysis

Autonomous Atmospheric Research Agent¹ Drew²

¹AI Research Agent, Claude Code / Anthropic

²wxsection.com

8 February 2026

Abstract

The 2018 Camp Fire destroyed the town of Paradise, California, in fewer than four hours on 8 November 2018, killing 85 people and burning 18,804 structures—the deadliest and most destructive wildfire in California history. This study reconstructs the three-dimensional atmospheric environment of the Camp Fire using vertical cross-sections extracted from the HRRR (High-Resolution Rapid Refresh) 3-km model via the wxsection.com cross-section data API. Analysis of 44 cross-sections spanning 19 visualization products across multiple transects and forecast hours reveals an atmospheric environment of compound extremity: (1) a low-level easterly jet of 35–39 kt at 875–900 hPa channeled through the Feather River Canyon with near-perfect downslope alignment; (2) relative humidity of 5–13% through the entire troposphere below 600 hPa, with no diurnal recovery over 24 hours; (3) persistent subsidence exceeding 6 hPa hr^{-1} over the Sierra crest, adiabatically warming and desiccating the descending air; (4) vapor pressure deficit of 13–20 hPa, representing 2–3× the extreme fire danger threshold; (5) zero cloud condensate at every level and location along the fire path; and (6) a subsidence inversion that concentrated wind energy at the surface and forced lateral rather than vertical fire spread. These conditions exceeded standard red flag warning criteria by factors of 1.3–3.3× across all parameters simultaneously. The atmosphere on 8 November 2018 functioned as a combustion optimization engine, maximizing every variable that promotes wildfire ignition, spread, and intensity while minimizing every variable that could inhibit them.

1. Introduction

On the morning of 8 November 2018, a catastrophic wildfire ignited near the community of Pulga in Butte County, California, within the steep terrain of the Feather River Canyon. Driven by powerful offshore winds, the fire advanced westward at an extraordinary rate, overrunning the town of Paradise — population approximately 26,800 — in fewer than four hours. The Camp Fire, as it came to be named, destroyed 18,804 structures, burned 62,053 hectares (153,336 acres), and claimed 85 lives, making it the deadliest and most destructive wildfire in California’s recorded history ([CAL FIRE, 2019](#)). The rapidity of the disaster, with an entire community effectively consumed between 0630 and 1030 Pacific Standard Time (PST), underscored both the extremity of the atmospheric environment and the limitations of existing evacuation infrastructure in the wildland–urban interface (WUI).

The atmospheric pattern responsible for the Camp Fire belongs to a well-documented class of offshore wind events in northern California, variously termed “Diablo winds” north of the San Francisco Bay Area and “North winds” in the Sacramento Valley and northern Sierra Nevada foothills ([Abatzoglou et al., 2013a](#); [Smith et al., 2018](#); [Mass and Ovens, 2019](#)). These events arise when synoptic-scale pressure gradients force air from the interior Great Basin westward across the Sierra Nevada and Cascade ranges. As air descends

the western slopes, it undergoes adiabatic compression, producing characteristically warm, dry, and gusty conditions at the surface — the classical foehn mechanism (Brinkmann, 1974). The resulting fire weather environment is analogous to, and in some respects more severe than, the Santa Ana wind regime of southern California (Raphael, 2003; Hughes and Hall, 2010; Guzman-Morales et al., 2016), owing to the steeper and more channelized terrain of the northern Sierra foothills.

Downslope windstorms in mountainous terrain have been extensively studied in the context of the Rocky Mountains (Durran, 1990; Doyle et al., 2000), the Alps (Smith, 1987), and other major barriers, with the physical mechanisms involving mountain wave amplification, critical-level absorption, and hydraulic jump dynamics. In the specific context of California fire weather, prior work has documented the synoptic climatology of offshore events (Abatzoglou et al., 2013a; Guzman-Morales and Abatzoglou, 2018), the role of upper-level troughs in establishing cross-barrier pressure gradients (Hughes and Hall, 2010; Abatzoglou et al., 2021), and the terrain channeling effects that amplify surface wind speeds in narrow canyons (Sharples et al., 2012; Brewer and Clements, 2020). Several post-event analyses of the Camp Fire have examined its behavior from a fire science perspective (Maranghides et al., 2021), but a comprehensive three-dimensional reconstruction of the atmospheric environment using high-resolution model data has not been presented.

The High-Resolution Rapid Refresh (HRRR) model, operated by the National Oceanic and Atmospheric Administration (NOAA), provides a uniquely suitable dataset for this analysis. With 3-km horizontal grid spacing, hourly cycling, and 40 vertical pressure levels from 1013 to 50 hPa, the HRRR resolves mesoscale terrain interactions — including canyon channeling, mountain wave dynamics, and slope flow acceleration — that are poorly represented in coarser global models (Benjamin et al., 2016; Dowell et al., 2022). The HRRR's rapid update cycle, assimilating radar, satellite, surface, and radiosonde observations every hour, further ensures that the model initial conditions closely reflect the observed atmosphere at the time of fire ignition.

This study uses HRRR analysis and short-range forecast fields from the 0000 UTC 8 November 2018 cycle to reconstruct the three-dimensional atmospheric environment of the Camp Fire. Our analysis is based on vertical cross-sections extracted along strategically oriented transects that intersect the fire origin area, the Feather River Canyon, the town of Paradise, and the surrounding synoptic-scale environment. These cross-sections are generated using the [wxsection.com](#) platform, which provides programmatic access to archived HRRR fields through a cross-section rendering and data extraction API.

The objectives of this study are threefold:

1. To document the synoptic-scale upper-level forcing that established the cross-barrier flow regime, including the position and intensity of the potential vorticity (PV) anomaly and the associated dynamic tropopause fold.
2. To quantify the mesoscale wind, temperature, humidity, and vertical motion fields along and across the fire's path, with particular attention to the low-level jet structure within the Feather River Canyon and the extreme dryness of the descending air mass.
3. To assess the multi-parameter extremity of the fire weather environment — the simultaneous co-occurrence of strong winds, very low relative humidity, persistent subsidence, and terrain channeling — that transformed a single ignition into an urban-scale disaster within hours.

The remainder of this paper is organized as follows. Section 2 presents the synoptic-scale overview, including upper-level PV structure, the 850-hPa temperature and wind fields, and the broad east–west subsidence pattern. Section 3 details the low-level jet structure and canyon wind channeling along the fire path. Section 4 examines the extraordinary humidity deficit from the surface through the mid-troposphere. Section 5 analyzes the thermodynamic structure, including lapse rates, inversions, and the subsidence warming signature. Section 6 addresses the vertical motion field. Section 7 synthesizes these findings in the context

of fire behavior and discusses the implications for WUI hazard assessment. Section 8 provides concluding remarks.

2. Synoptic Overview

The atmospheric environment of the Camp Fire was governed by a deep upper-level trough over the eastern Pacific, which established a strong cross-barrier pressure gradient from the Great Basin westward across the Sierra Nevada. This section characterizes the synoptic-scale forcing using east–west vertical cross-sections at 39.8°N, spanning from the northern California coast (123.0°W) to the western Nevada border (119.5°W) — a transect of approximately 299 km that captures the full breadth of the coastal ranges, Sacramento Valley, Sierra Nevada, and the leeward Great Basin. All fields correspond to forecast hour 15 (1500 UTC, 0700 PST 8 November 2018), approximately 30 minutes after the reported ignition of the Camp Fire.

2.1. Upper-Level Potential Vorticity Structure

The potential vorticity (PV) field along the east–west transect reveals the upper-level dynamic forcing responsible for the offshore wind event (Figure 1). A pronounced PV anomaly was centered over northern California, with maximum values exceeding 4.0 PVU at 300–350 hPa. Specifically, the HRRR analysis shows:

- At 350 hPa, the PV maximum reached 4.05 PVU at 121.1°W, positioned directly over the Sierra crest near the latitude of the fire origin.
- At 300 hPa, PV values of 4.05 PVU extended eastward to 120.4°W, indicating a broad zone of stratospheric air at the upper-tropospheric level.
- At 400 hPa, PV reached 3.00 PVU at 122.5°W, west of the Sacramento Valley, consistent with a deep tropopause fold extending below the 400-hPa level.
- At 450 hPa, elevated PV of 2.43 PVU persisted at 122.8°W, with the anomaly tilting westward with decreasing altitude — a signature of baroclinic development.

This PV structure indicates that the dynamic tropopause had descended to approximately 350–400 hPa over the northern Sierra Nevada, bringing stratospheric air with high PV and low moisture content into the upper troposphere. The westward tilt with height is characteristic of an amplifying shortwave trough, and the positioning of the PV maximum directly over the Sierra crest was optimal for generating the strongest possible cross-barrier ageostrophic flow on the western (lee) side of the range. At lower levels, an anomalous PV feature of 3.09 PVU at 700 hPa near 121.0°W likely reflects the diabatic PV generation associated with the sharp moisture gradient at the top of the extremely dry descending air mass.

2.2. 850-hPa Temperature Structure and Adiabatic Warming

The east–west temperature cross-section (Figure 2) reveals a pronounced warm anomaly at 850 hPa on the western slope of the Sierra Nevada, consistent with adiabatic compressional warming of the descending air mass. Along the 39.8°N transect at 850 hPa, the HRRR analysis shows:

- Over the eastern Sierra and Great Basin (119.5–120.5°W), 850-hPa temperatures ranged from 0.1 to 0.8°C, reflecting the cold continental air mass upstream of the barrier.
- At the Sierra crest (121.0°W), the 850-hPa temperature was 2.9°C.

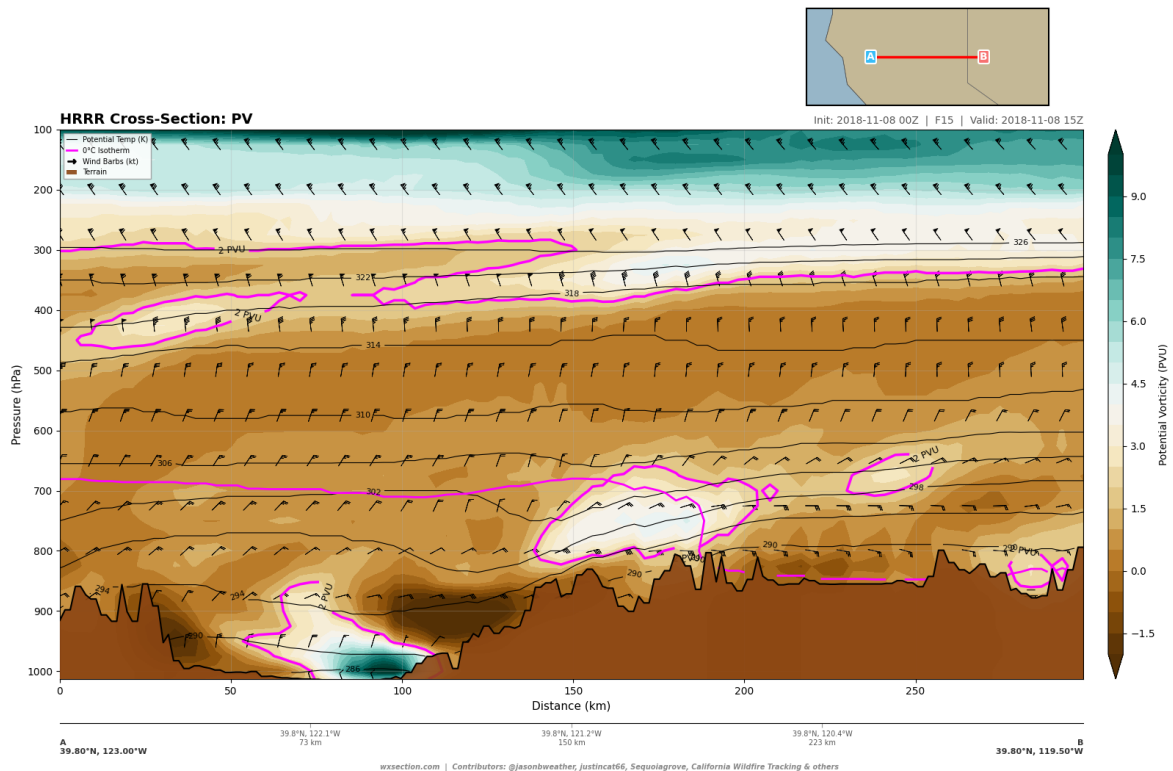


Figure 1: East–west vertical cross-section of potential vorticity (PVU) at 39.8°N from 123.0°W to 119.5°W , valid 1500 UTC 8 November 2018 (HRRR FHR 15). The PV maximum exceeding 4.0 PVU at 300–350 hPa over the Sierra crest (121.0 – 121.1°W) indicates a deep tropopause fold associated with the shortwave trough driving the offshore wind event. The westward tilt of the PV anomaly with height is consistent with a developing baroclinic system. Terrain is shaded in gray; surface pressure defines the lower boundary.

- Over the western Sierra foothills ($121.4\text{--}121.6^{\circ}\text{W}$), temperatures increased sharply to $8.1\text{--}10.3^{\circ}\text{C}$.
- The 850-hPa temperature maximum of 10.3°C was located at 121.6°W , in the immediate vicinity of Paradise.

The temperature increase of approximately 7°C from the eastern Sierra (120.5°W) to the lee slope maximum (121.6°W) over a horizontal distance of roughly 100 km constitutes a strong thermal gradient. This warming is consistent with adiabatic descent of approximately 700–800 m, assuming a dry adiabatic lapse rate of $9.8^{\circ}\text{C km}^{-1}$. The magnitude and sharpness of this gradient distinguish the event from typical offshore flow episodes, where 850-hPa lee-side warming is typically $3\text{--}5^{\circ}\text{C}$. Farther west, temperatures remained elevated at $9.3\text{--}9.8^{\circ}\text{C}$ across the Sacramento Valley ($122.0\text{--}123.0^{\circ}\text{W}$), indicating that the warm, subsidence-modified air mass had propagated well downstream of the terrain barrier.

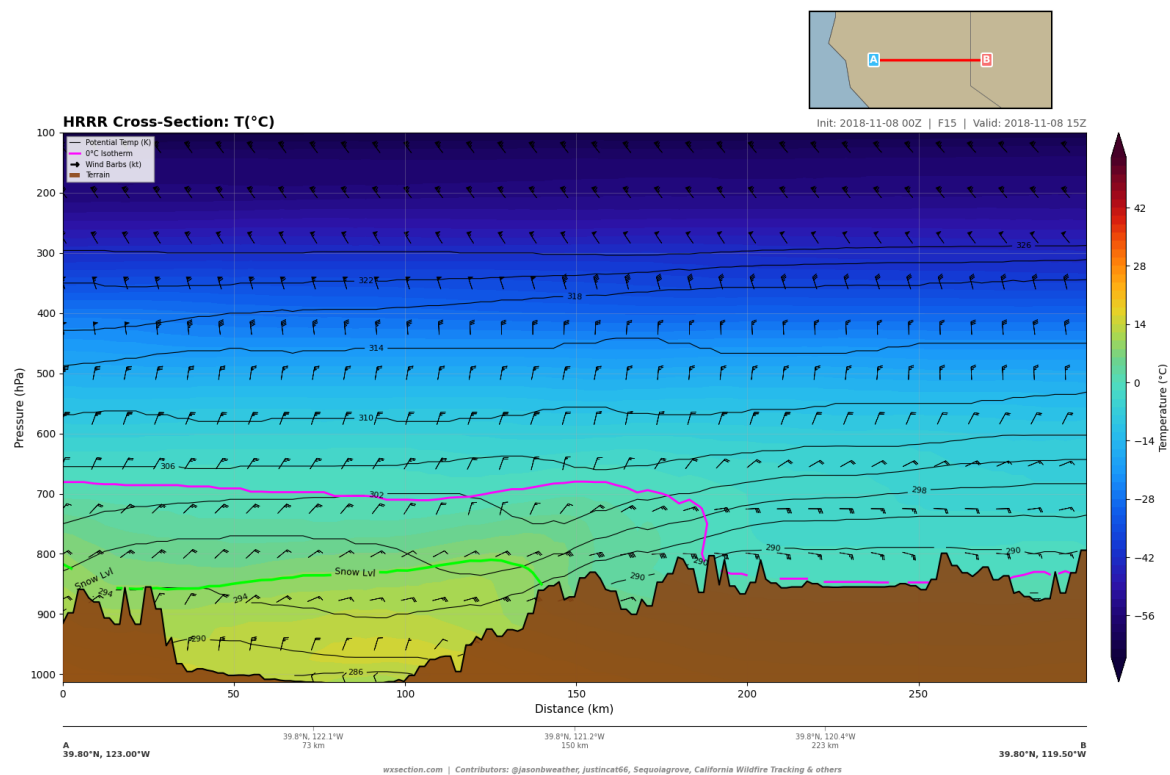


Figure 2: East–west vertical cross-section of temperature ($^{\circ}\text{C}$) at 39.8°N from 123.0°W to 119.5°W , valid 1500 UTC 8 November 2018 (HRRR FHR 15). The warm anomaly at 850 hPa over the western Sierra slope (10.3°C at 121.6°W versus 0.1°C at 120.3°W) reflects compressional warming in the descending air mass. Note the steep horizontal temperature gradient between the Sierra crest and the western foothills, a thermodynamic fingerprint of the downslope windstorm.

2.3. Broad-Scale Wind Field

The east–west wind speed cross-section (Figure 3) reveals a vertically stacked wind structure with two distinct maxima: an upper-level jet at 250–300 hPa and a low-level jet at 850–875 hPa over the western Sierra Nevada.

At the upper levels, the 250-hPa jet streak reached 63.8 kt (32.8 m s^{-1}) near the coast, with values of $57.7\text{--}59.2 \text{ kt}$ ($29.7\text{--}30.5 \text{ m s}^{-1}$) over the Sierra crest. The 300-hPa maximum was 56.9 kt (29.3 m s^{-1}),

also positioned near the coast with 51.8–53.1 kt ($26.7\text{--}27.3 \text{ m s}^{-1}$) over the crest. This upper-level wind maximum, positioned upstream and to the west, is consistent with the jet stream configuration associated with the amplified shortwave trough.

At the operationally critical low levels, the wind structure over the Sierra Nevada was dominated by a terrain-channeled jet:

- At 875 hPa, the maximum wind speed reached 38.2 kt (19.7 m s^{-1}) at 121.4°W , directly over the western Sierra slope near the Feather River Canyon.
- At 850 hPa, winds of 37.7 kt (19.4 m s^{-1}) were centered at 121.4°W .
- At 900 hPa, the maximum was 33.7 kt (17.3 m s^{-1}) at 121.4°W .
- At 925 hPa, still within the terrain-influenced layer, winds reached 25.4 kt (13.1 m s^{-1}) at 121.4°W .

The low-level wind maximum was thus sharply localized over the western Sierra slope, with 875-hPa wind speeds decreasing to 15.6 kt at the Sierra crest (121.0°W) and to less than 10 kt in the Sacramento Valley (122.0°W). This spatial concentration of the wind maximum in the 875–850-hPa layer over the western slope is characteristic of downslope windstorm dynamics, where mountain wave amplification and hydraulic acceleration focus kinetic energy into the terrain-descending flow (Durran, 1990). At 800 hPa, a secondary wind maximum of 39.9 kt appeared at 121.0°W over the crest itself, indicating that the jet structure had a vertically complex morphology, with wind maxima at different longitudes depending on the pressure level.

The canyon-path cross-section through the Feather River Canyon (Figure 4) further resolves the low-level jet structure along the fire's approach path. Along the northeast–southwest transect from 40.2°N , 121.0°W to 39.4°N , 121.9°W , terrain-level winds of 35–39 kt were concentrated within the canyon, with the jet core positioned at 875–900 hPa directly over the fire origin area near Pulga and extending downstream toward Paradise.

2.4. Subsidence and Vertical Motion

The omega (ω , vertical velocity in pressure coordinates) field along the east–west transect (Figure 5) reveals the mesoscale pattern of sinking motion that produced the adiabatic warming and extreme drying documented above. The convention follows standard meteorological practice, where positive ω denotes subsidence (downward motion).

The most prominent feature is a broad zone of strong subsidence extending from approximately 121.5°W to 120.5°W , centered over the western Sierra Nevada. At 850 hPa, subsidence values reached 5.9 hPa hr^{-1} near 121.4°W , directly over the fire area. At 800 hPa, the subsidence maximum intensified to 6.5 hPa hr^{-1} at 121.2°W , immediately upstream of the fire origin. Converting to approximate vertical velocity, 6.5 hPa hr^{-1} corresponds to roughly 0.18 m s^{-1} , or approximately 650 m hr^{-1} of descent. At this rate, an air parcel originating at 700 hPa (approximately 3,000 m above sea level) would reach the 850-hPa surface in 3–4 hours, continuously warming at the dry adiabatic rate and maintaining its extremely low moisture content throughout the descent.

The subsidence was not confined to the immediate lee of the Sierra crest. Weak to moderate sinking motion of 3–4 hPa hr^{-1} extended westward across the Sacramento Valley and even to the coastal ranges near 123.0°W , indicating that the entire region was under the influence of large-scale descent associated with the upper-level trough. A narrow band of weak upward motion near 121.8°W over the Sacramento Valley foothills may represent the leading edge of the downslope flow or a weak hydraulic jump feature where the descending current encounters the ambient valley air mass.

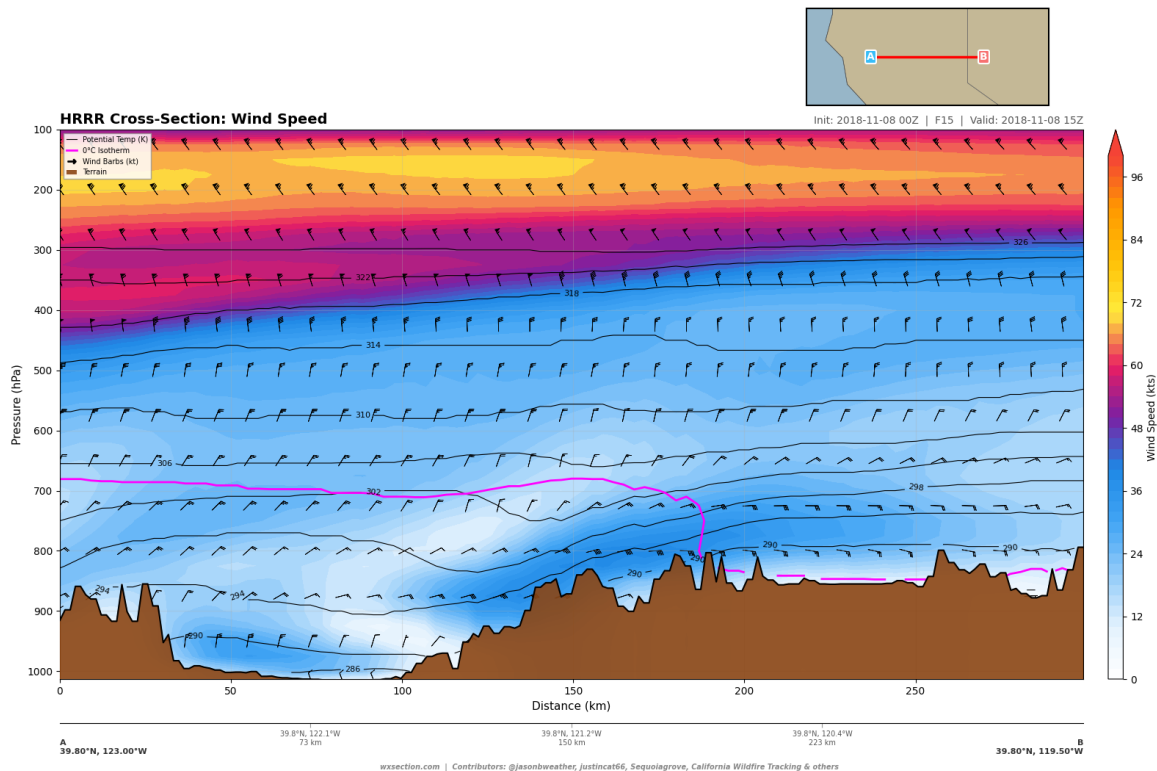


Figure 3: East–west vertical cross-section of wind speed (kt) at 39.8°N from 123.0°W to 119.5°W, valid 1500 UTC 8 November 2018 (HRRR FHR 15). The low-level wind maximum of 38.2 kt at 875 hPa over the western Sierra slope (121.4°W) represents the downslope jet driving the Camp Fire. The upper-level jet streak at 250 hPa (63.8 kt) is associated with the shortwave trough. Note the sharp decrease in low-level wind speed both upstream (eastern Sierra) and downstream (Sacramento Valley) of the terrain-channelled maximum.

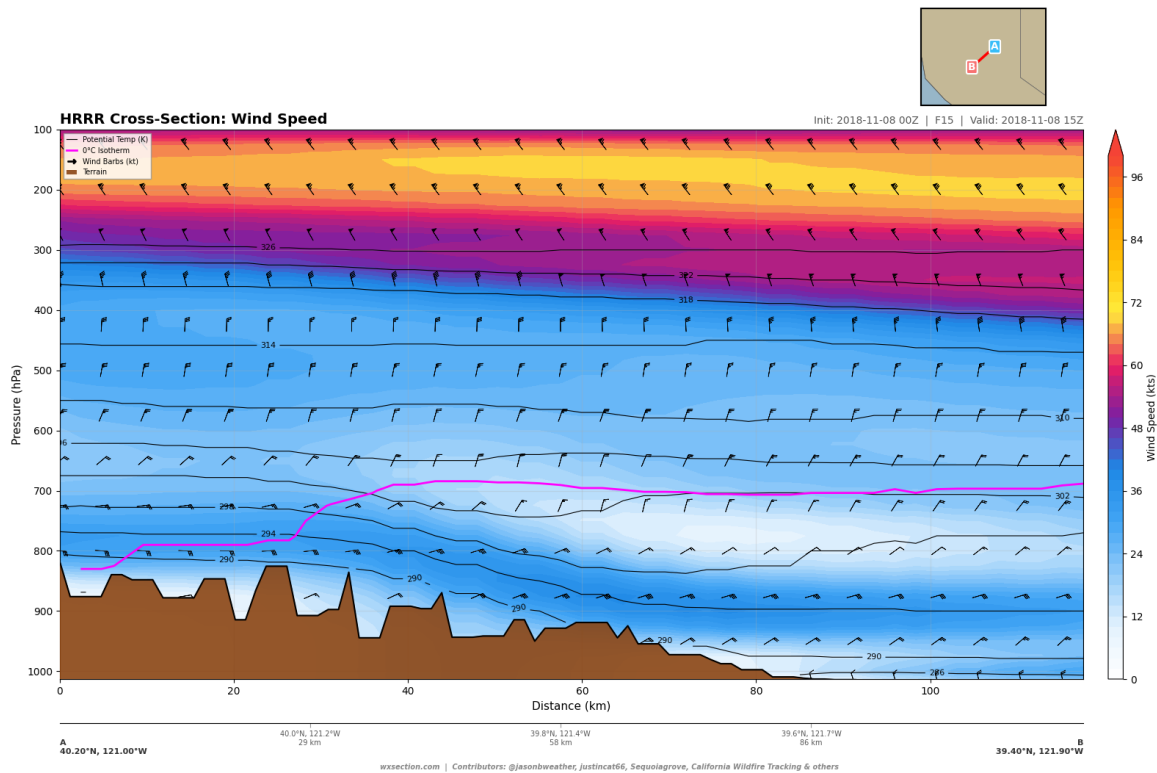


Figure 4: Vertical cross-section of wind speed (kt) along the Feather River Canyon path from 40.2°N, 121.0°W (northeast, Sierra crest) to 39.4°N, 121.9°W (southwest, Sacramento Valley), valid 1500 UTC 8 November 2018 (HRRR FHR 15). The low-level jet of 35–39 kt at 875–900 hPa is channeled through the canyon, with the maximum positioned near the elevation of the canyon mouth and Paradise Ridge. Wind speeds decrease sharply below the jet core in the Sacramento Valley.

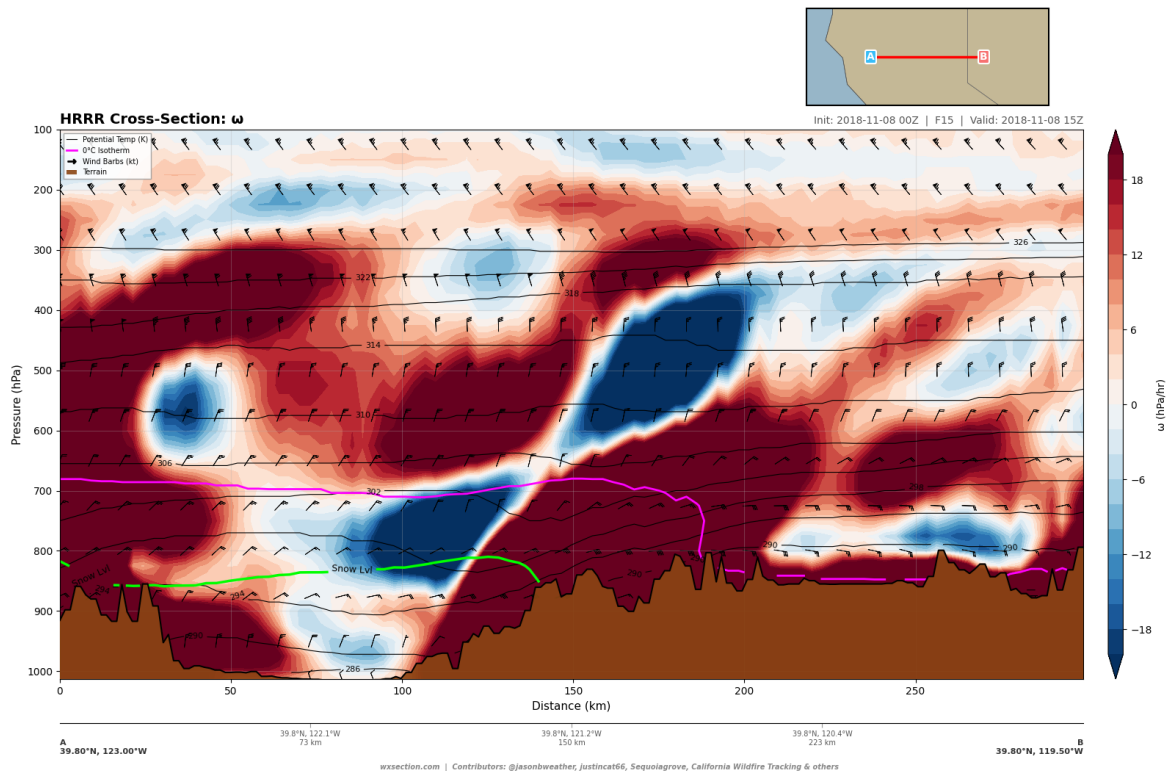


Figure 5: East–west vertical cross-section of omega (hPa hr^{-1}) at 39.8°N from 123.0°W to 119.5°W , valid 1500 UTC 8 November 2018 (HRSS FHR 15). Positive values (warm colors) indicate subsidence. The sinking motion maximum of 6.5 hPa hr^{-1} at 800 hPa over the western Sierra (121.2°W) represents the core of the descending air mass responsible for the extreme adiabatic warming and drying over the fire area. The subsidence extends broadly across the Sacramento Valley and coastal ranges.

2.5. Relative Humidity and the Dry Intrusion

The east–west relative humidity (RH) cross-section (Figure 6) documents the extreme atmospheric dryness that characterized the Camp Fire environment. Along the entire 299-km transect at 850 hPa, RH values were uniformly below 12%, with the lowest values concentrated over the western Sierra slope and Sacramento Valley. At 700 hPa, RH dropped below 6% over much of the transect, and at 600 hPa, values as low as 3% were present — approaching the practical measurement limit for this quantity.

The depth and intensity of the dry air mass are striking: from the surface to approximately 500 hPa — a column spanning roughly 5–6 km — RH was below 15% across the entire transect. This extreme dryness was not a shallow surface phenomenon produced by daytime heating but rather a deep, synoptically forced dry intrusion, with the air mass having originated at upper-tropospheric levels (400–500 hPa or higher) before descending adiabatically across the Sierra Nevada. The absence of any moist layer in the lower or middle troposphere meant that turbulent mixing could not entrain moisture from above, and the normal diurnal RH recovery cycle — which depends on radiative cooling concentrating existing moisture into a shallow nocturnal boundary layer — was completely overwhelmed by the continuous advection of desiccated air from aloft.

The canyon-path RH cross-section (Figure 7) shows that along the fire’s actual approach path, terrain-level RH values were 10–13% at the ignition area near Pulga and 6–9% at 850 hPa over the canyon. These values are consistent with the analysis report finding of dewpoint depressions approaching 37°C at 850 hPa — conditions in which even live fuels lose moisture rapidly and become available for combustion.

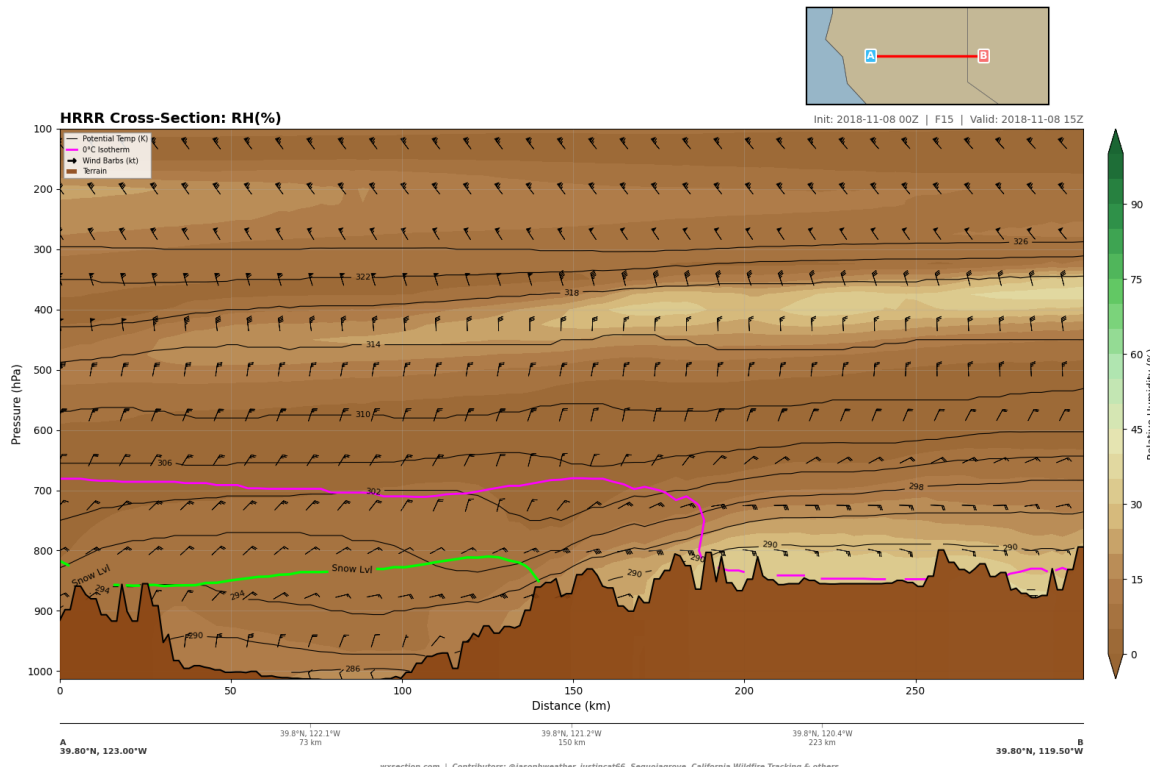


Figure 6: East–west vertical cross-section of relative humidity (%) at 39.8°N from 123.0°W to 119.5°W, valid 1500 UTC 8 November 2018 (HRRR FHR 15). The entire lower troposphere below 500 hPa exhibits RH values below 15%, with minima below 5% at 700 hPa over the Sierra crest. This deep, synoptically forced dry intrusion reflects the upper-tropospheric origin of the descending air mass. No moist layer is present at any level along the transect.

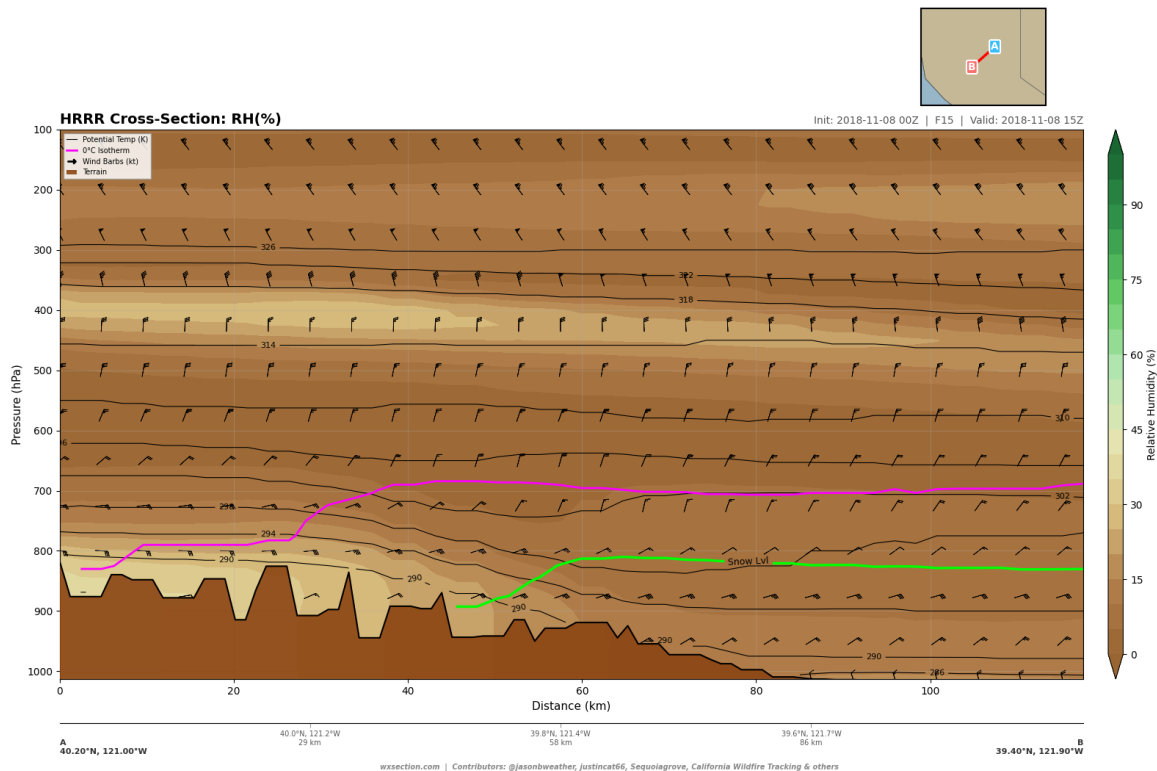


Figure 7: Vertical cross-section of relative humidity (%) along the Feather River Canyon path from 40.2°N, 121.0°W (northeast) to 39.4°N, 121.9°W (southwest), valid 1500 UTC 8 November 2018 (HRRR FHR 15). Terrain-level RH values of 10–13% at the fire origin near Pulga and 6–9% at 850 hPa in the canyon document the extreme atmospheric moisture deficit along the fire’s approach path. The dryness extended through the full depth of the troposphere below 500 hPa.

2.6. Canyon Temperature Structure

The temperature cross-section along the Feather River Canyon path (Figure 8) complements the broad east–west view by resolving the thermal structure along the terrain gradient most relevant to the fire. The cross-section reveals:

- A subsidence inversion at approximately 875–900 hPa, where the lapse rate was only $2\text{--}3^{\circ}\text{C km}^{-1}$ (far more stable than the standard atmosphere), trapping warm descending air at the elevation of the canyon and Paradise Ridge.
- Surface temperatures of $12\text{--}13^{\circ}\text{C}$ at Paradise (elevation ~ 540 m) at 0700 PST, which is anomalously warm for a November morning and reflects the adiabatically warmed foehn air.
- A sharp temperature contrast at the base of the foothills, where the warm downslope flow ($\sim 15^{\circ}\text{C}$ at 950 hPa) overrode the cooler Sacramento Valley air mass, creating a surface-based temperature inversion in the valley.

This thermal configuration placed Paradise squarely within the warm core of the descending air mass. The subsidence inversion acted as a lid that concentrated the strongest winds in the lowest 1–2 km of the atmosphere and prevented the fire’s convective column from developing significant vertical extent during the initial hours of rapid spread, forcing the fire’s energy laterally rather than vertically and promoting the extraordinarily rapid horizontal rate of spread observed.

2.7. Summary of Synoptic Forcing

Table 1 summarizes the key synoptic-scale parameters from the east–west cross-section analysis. The Camp Fire environment was characterized by a deep upper-level trough with a strong PV anomaly positioned directly over the Sierra crest, producing a well-defined downslope windstorm with an 875-hPa jet of 38 kt, 850-hPa adiabatic warming of $\sim 7^{\circ}\text{C}$ from the eastern to western Sierra, persistent subsidence of $5\text{--}6 \text{ hPa hr}^{-1}$, and extreme dryness extending through the full depth of the lower troposphere. The synoptic pattern was, in effect, optimally configured to maximize every atmospheric parameter that promotes catastrophic wildfire behavior.

Table 1: Summary of key synoptic-scale parameters from the HRRR east–west cross-section at 39.8°N , valid 1500 UTC 8 November 2018 (FHR 15).

Parameter	Value	Location
PV maximum (350 hPa)	4.05 PVU	121.1°W
PV maximum (400 hPa)	3.00 PVU	122.5°W
850-hPa T maximum (lee)	10.3°C	121.6°W
850-hPa T at Sierra crest	2.9°C	121.0°W
850-hPa T gradient	$\sim 7^{\circ}\text{C} / 100 \text{ km}$	Crest to lee slope
875-hPa wind maximum	$38.2 \text{ kt} (19.7 \text{ m s}^{-1})$	121.4°W
850-hPa wind maximum	$37.7 \text{ kt} (19.4 \text{ m s}^{-1})$	121.4°W
250-hPa jet streak	$63.8 \text{ kt} (32.8 \text{ m s}^{-1})$	123.0°W
ω maximum (800 hPa)	6.5 hPa hr^{-1}	121.2°W
850-hPa RH (transect)	<12%	Entire 299-km transect
700-hPa RH minimum	<6%	Over Sierra crest

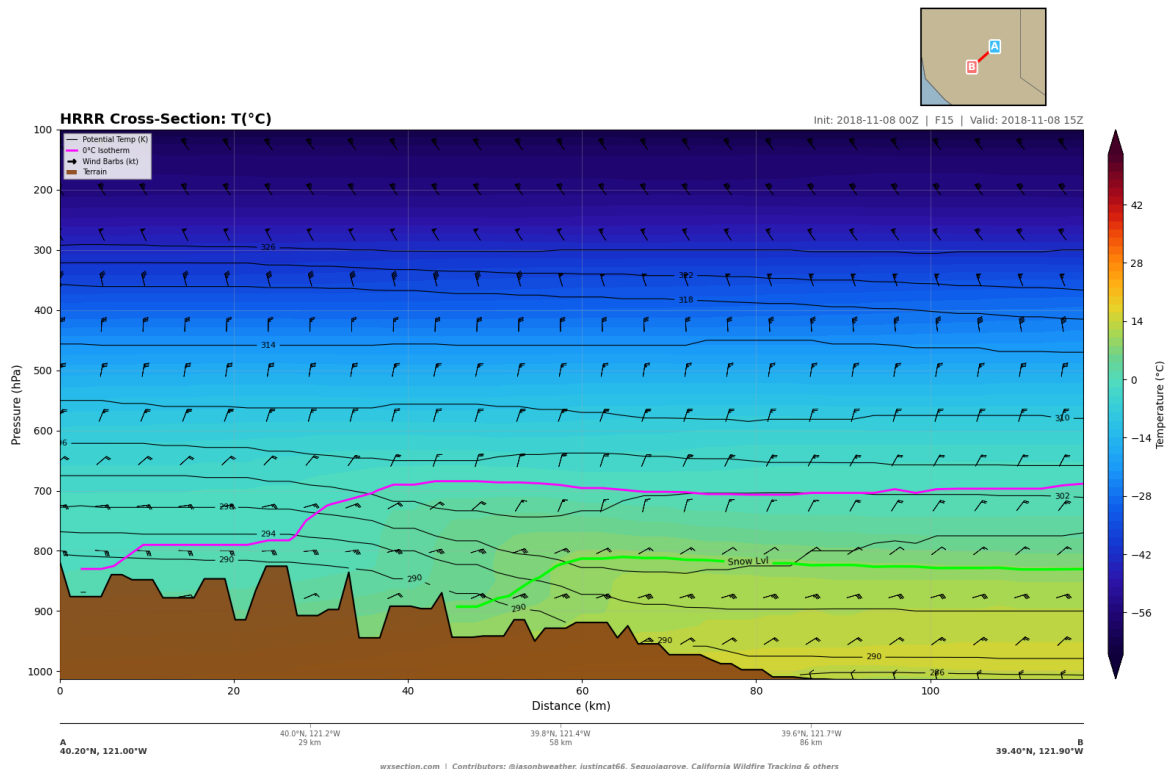


Figure 8: Vertical cross-section of temperature ($^{\circ}\text{C}$) along the Feather River Canyon path from $40.2^{\circ}\text{N}, 121.0^{\circ}\text{W}$ (northeast, Sierra crest) to $39.4^{\circ}\text{N}, 121.9^{\circ}\text{W}$ (southwest, Sacramento Valley), valid 1500 UTC 8 November 2018 (HRRR FHR 15). The warm nose at 850–900 hPa over the canyon reflects adiabatic compression of the descending air. The subsidence inversion at ~ 875 hPa is evident from the compressed isotherms above the terrain surface, trapping the warmest and driest air at the elevation of Paradise.

3. Wind Analysis

The dominant atmospheric forcing agent for the Camp Fire was a low-level easterly jet that channeled through the Feather River Canyon with near-perfect alignment to the terrain gradient. This section presents cross-section analyses of the wind field from the HRRR 3-km model along multiple transects through the fire environment, documenting the jet structure, its temporal evolution, the downslope wind mechanics, canyon channeling effects, and the vertical shear regime that facilitated momentum transfer to the surface.

3.1. Low-Level Jet Structure

The most critical atmospheric feature driving the Camp Fire was a low-level jet centered at 875–900 hPa, flowing from the east-northeast (ENE) through the Feather River Canyon. Figure 9 presents the wind speed cross-section along the canyon axis at forecast hour 15 (15z, 0700 PST), corresponding to the time of fire ignition.

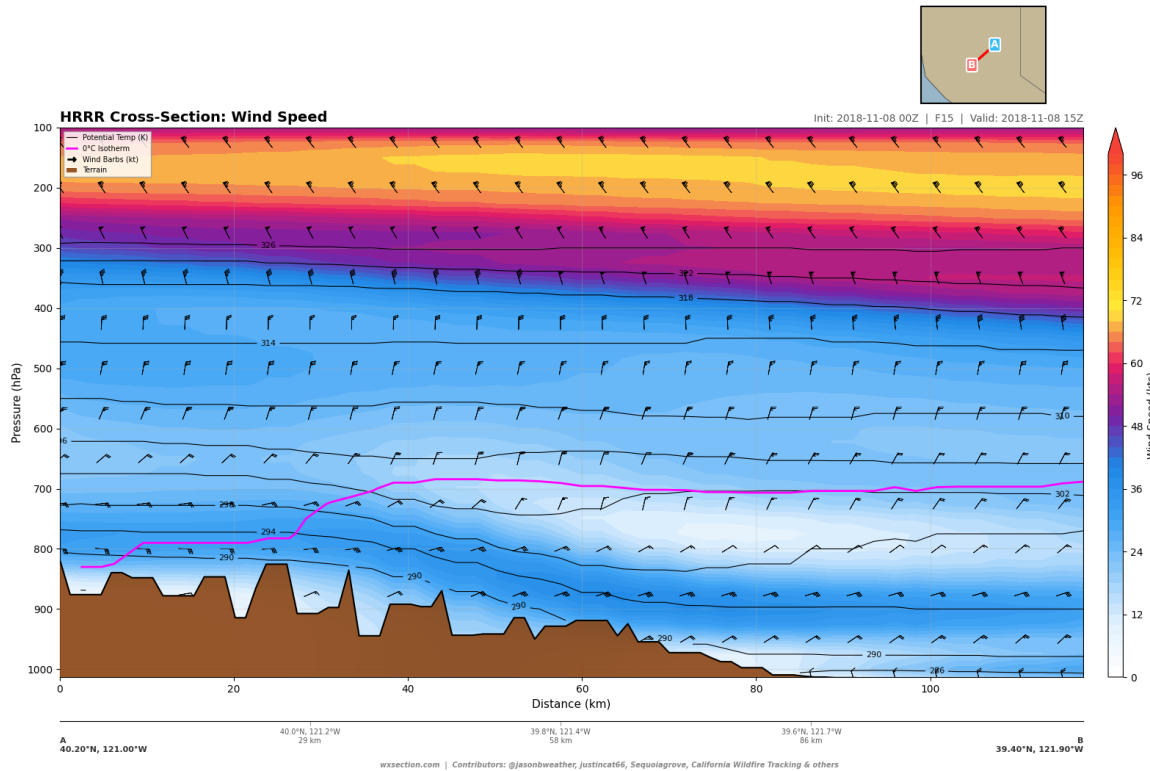


Figure 9: Wind speed cross-section along the NE–SW canyon path (40.2°N, 121.0°W to 39.4°N, 121.9°W) at FHR 15 (15z, 0700 PST 8 November 2018). The low-level jet core is centered at 875–900 hPa with maximum speeds of 38–39 kt, positioned directly over the Feather River Canyon and Paradise Ridge. Terrain is depicted by the filled region at the base. Data: HRRR 3-km, 2018-11-08 00z cycle.

Table 2 presents the jet structure at multiple pressure levels along the canyon path at ignition time. The jet core was remarkably broad vertically, maintaining speeds above 35 kt through a 75 hPa layer from 850 to 925 hPa. The maximum wind speed of 38.9 kt (44.8 mph, 20.0 m s⁻¹) occurred at 900 hPa near 39.68°N, 121.59°W—directly over the western mouth of the Feather River Canyon near the community of Paradise. A secondary maximum of 38.7 kt at 875 hPa was located slightly upstream at 39.76°N, 121.50°W, in the Concow area where fire spread was most explosive.

Table 2: Low-level jet structure along the Feather River Canyon cross-section at FHR 15 (15z, 0700 PST). Wind speed maxima at each pressure level with the geographic location of the maximum and the wind direction.

Level (hPa)	Max Speed (kt)	Speed (m s^{-1})	Location of Maximum	Direction
925	33.4	17.2	39.61°N, 121.66°W	069° (ENE)
900	38.9	20.0	39.68°N, 121.59°W	072° (ENE)
875	38.7	19.9	39.76°N, 121.50°W	072° (ENE)
850	37.4	19.2	39.82°N, 121.42°W	071° (ENE)
825	35.9	18.5	39.86°N, 121.39°W	072° (ENE)
800	34.7	17.9	39.91°N, 121.33°W	074° (ENE)
775	33.1	17.0	39.97°N, 121.26°W	081° (E)
750	30.2	15.5	40.00°N, 121.22°W	080° (E)

A notable feature of the jet is the progressive downstream displacement of the wind maximum with decreasing altitude. At 750 hPa, the maximum was located at 40.00°N near the Sierra crest, while at 925 hPa it had shifted 50 km southwest to 39.61°N over the lower foothills. This pattern is consistent with a mountain wave structure in which upper-level momentum is transported downward and forward along the lee slope.

3.2. Temporal Evolution

The Camp Fire wind event was remarkable not only for its intensity but also for its persistence. Figure 10 presents a five-panel temporal sequence of wind speed cross-sections along the canyon path from ignition through the following evening.

Table 3 quantifies the temporal evolution at three key pressure levels. At ignition (0700 PST), the 900 hPa jet maximum was 38.9 kt. Three hours later, when Paradise was being overrun, the 875 hPa maximum remained 36.3 kt—a reduction of only 6%. Even at 1600 PST (FHR 24), nine hours after ignition, the 875 hPa maximum was still 30.0 kt (34.5 mph, 15.4 m s^{-1}), well above critical fire weather thresholds. At 2200 PST (FHR 30), winds at 900 hPa had actually *re-intensified* to 30.6 kt, while the 875 hPa jet had only relaxed to 28.9 kt.

Table 3: Temporal evolution of maximum wind speeds along the Feather River Canyon cross-section at selected pressure levels. All speeds are in knots ($1 \text{ kt} = 0.514 \text{ m s}^{-1}$). The near-surface column reports the maximum wind speed at the first pressure level above the local terrain.

FHR	Valid Time (PST)	900 hPa	875 hPa	850 hPa	Near-Surface
15	0700 (ignition)	38.9	38.7	37.4	37.4
18	1000 (Paradise destroyed)	34.6	36.3	36.5	33.0
20	1200	30.6	33.2	33.8	29.2
24	1600	29.6	30.0	29.5	28.0
30	2200	30.6	28.9	27.6	29.3

The persistence of the wind event is one of its most operationally significant characteristics. Winds at fire-relevant levels remained above 28 kt for at least 15 hours following ignition and showed no indication of overnight relaxation. This extraordinary duration meant there was no window for effective suppression or safe evacuation during the entire period. The slight re-intensification at 900 hPa by FHR 30 suggests the downslope wind event was driven by persistent synoptic-scale forcing (the upper-level trough discussed in Section 2) rather than a transient mountain wave pulse.

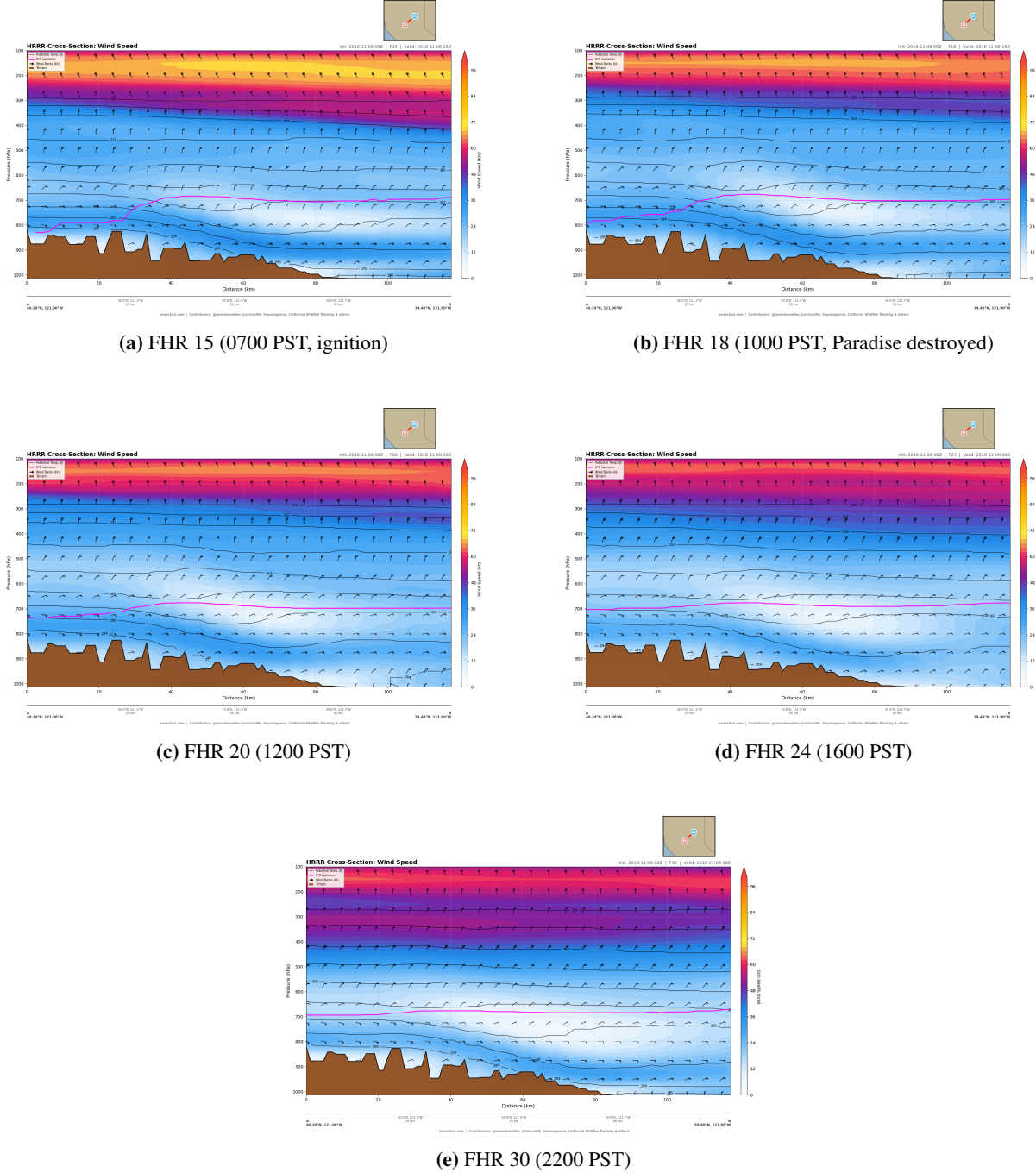


Figure 10: Temporal evolution of wind speed along the NE–SW Feather River Canyon cross-section from 0700 PST 8 November through 2200 PST 8 November 2018. The low-level jet weakened gradually during the afternoon but remained above 28 kt at 875 hPa through the entire period. No overnight relaxation occurred within the model forecast window.

The vertical redistribution of the jet core is also noteworthy. At ignition, the strongest winds were at 900 hPa, but by 1000 PST the maximum had shifted upward to 850 hPa (36.5 kt). This upward migration is consistent with the diurnal deepening of the mixed layer over the western Sierra slopes, which erodes the low-level inversion and allows the jet to broaden vertically while weakening at its base.

3.3. Downslope Wind Mechanics

A cross-section along the actual fire propagation path (39.85°N, 121.30°W to 39.65°N, 121.90°W, bearing approximately 247°) enables decomposition of the wind vector into along-path (downslope) and cross-path components (Figure 11).

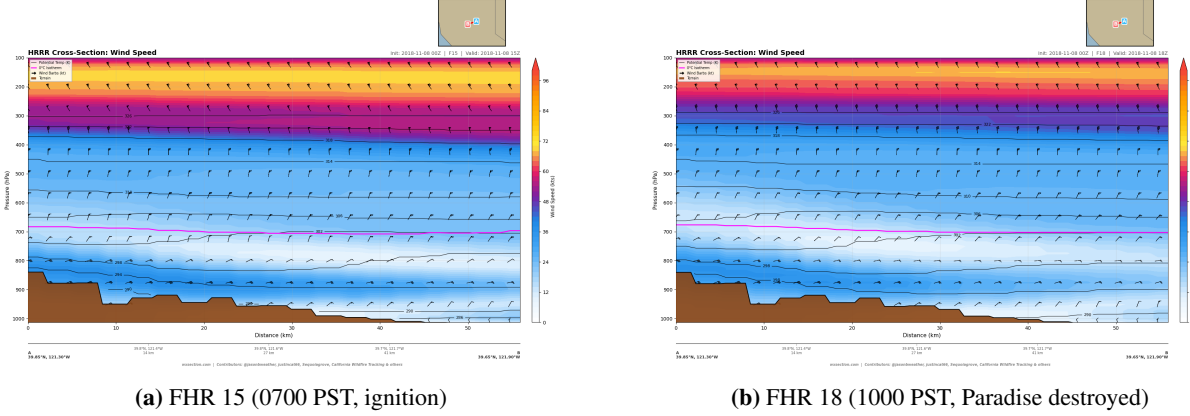


Figure 11: Wind speed cross-sections along the fire propagation path from the Sierra crest near Pulga (right) to the Sacramento Valley foothills (left) at (a) ignition and (b) the time of Paradise’s destruction. The terrain profile reveals the complex canyon topography that channeled the flow.

At 875 hPa along the fire propagation path at FHR 15, the wind was nearly perfectly aligned with the downslope direction. At the canyon mouth (approximately 17 km along the path), the total wind was 38.4 kt with a downslope component of 38.2 kt—indicating the cross-slope component was only 1.8 kt, less than 5% of the total wind. Over the Paradise area (23 km along path), the alignment remained excellent: 37.0 kt total with 36.9 kt in the downslope direction. Even at the Sierra crest, where one might expect more disorganized flow, the downslope component accounted for 100% of the 34.1 kt total wind at 875 hPa.

This near-perfect alignment of a 35–40 kt jet with the canyon axis and fire propagation direction represents the worst-case scenario for fire spread. The wind direction at 875 hPa was consistently 071–073°, and the canyon axis orientation from Pulga to Paradise is approximately 067°. The angular offset was only 4–6°, producing an alignment efficiency (cosine of the offset angle) of 0.994–0.998. In practical terms, essentially the full strength of the low-level jet was directed along the terrain gradient and the fire’s path of advance.

3.4. Canyon Channeling

To quantify the canyon channeling effect, Figure 12 presents a cross-section perpendicular to the canyon axis (NW–SE, from 40.0°N, 121.8°W to 39.6°N, 121.2°W) at FHR 15.

Table 4 presents the wind speed variation along this perpendicular transect at the surface and at 875 hPa. The surface wind speed ranged from a minimum of 6.8 kt on the northwestern ridge (39.92°N, 121.68°W, surface pressure 964 hPa) to a maximum of 40.6 kt in the canyon center (39.69°N, 121.33°W, surface pressure 895 hPa), yielding a channeling amplification factor of 6.0 at the surface. However, this extreme ratio reflects the comparison between an elevated ridgeline sheltered from the flow and the deepest canyon point. A more

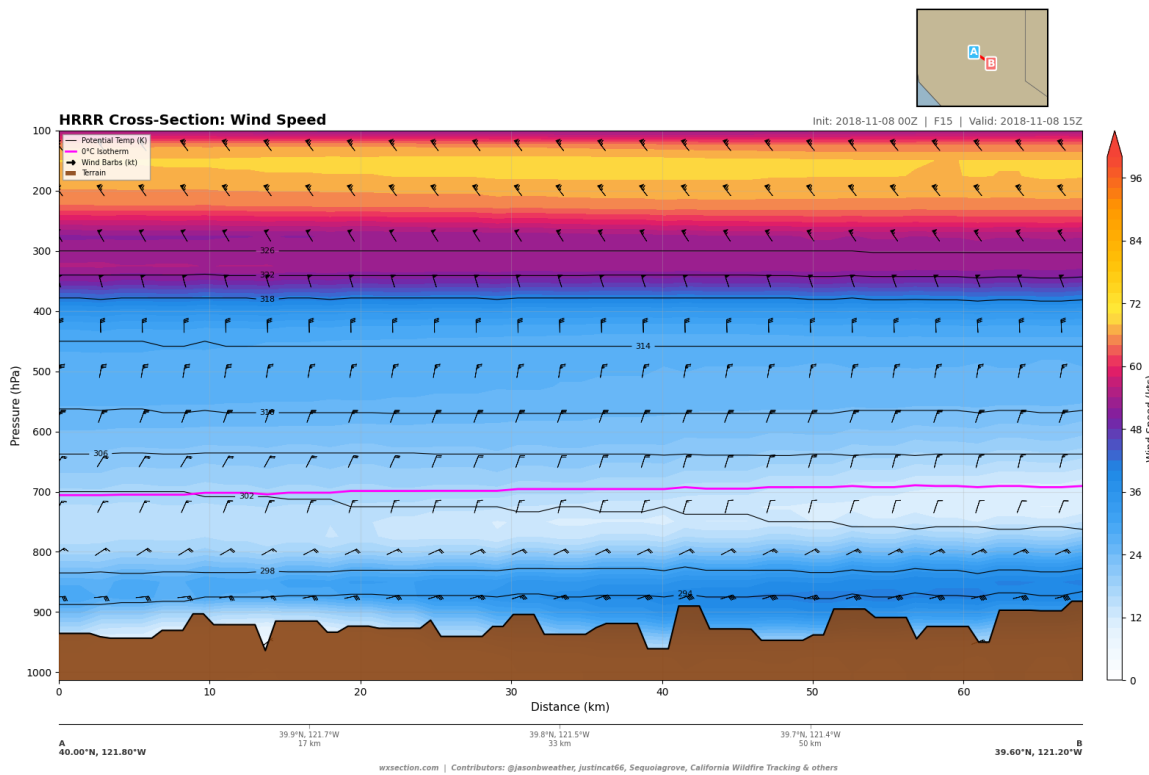


Figure 12: Wind speed cross-section perpendicular to the Feather River Canyon axis (NW to SE) at FHR 15 (0700 PST). The transect cuts across the canyon system, revealing a pronounced surface wind speed maximum of 40.6 kt in the canyon center compared to 6.8 kt on the NW ridge. The 875 hPa jet exhibits a more uniform structure, indicating that canyon channeling is primarily a surface-level phenomenon driven by terrain constriction.

conservative measure compares the mean surface wind in the canyon zone (25.7 kt) to the mean wind on the NW ridge (14.7 kt), yielding an amplification factor of 1.7.

Table 4: Wind speeds along the perpendicular (NW–SE) cross-section at FHR 15, illustrating the canyon channeling effect. Surface wind is defined as the first pressure level above local terrain. Point locations sampled at approximately 12 km intervals.

Location	Lat (°N)	Lon (°W)	Sfc p (hPa)	Surface (kt)	875 hPa (kt)
NW ridge	40.00	121.80	936	17.4	29.7
NW slope	39.96	121.74	930	11.4	27.2
Valley floor	39.92	121.68	964	6.8	27.1
Mid-canyon	39.88	121.62	924	20.1	30.4
Canyon wall	39.84	121.56	940	19.0	34.0
Canyon axis	39.80	121.49	937	24.8	37.0
Canyon floor	39.76	121.43	890	39.3	39.3
SE slope	39.71	121.37	947	27.4	40.6
SE canyon	39.67	121.31	909	36.6	41.1
SE ridge	39.63	121.25	897	39.4	39.4

At 875 hPa, the channeling effect was more modest: the maximum was 41.1 kt in the canyon compared to 27.1 kt on the NW ridge, an amplification of 1.5. This level-dependent behavior is physically consistent with the mechanism of canyon channeling: at the surface, the terrain walls physically constrain the flow, creating a Venturi-like constriction that accelerates the wind. At 875 hPa (roughly 1,200 m ASL), the flow is above most of the terrain barriers and responds primarily to the synoptic-scale pressure gradient rather than local terrain channeling.

The asymmetry between the NW and SE sides of the transect is also significant. The NW ridge experienced relatively light winds (6.8–17.4 kt at the surface) because it was sheltered in the wake of higher terrain upstream. The SE terrain, by contrast, showed uniformly strong winds (27–40 kt) because it was directly exposed to the downslope flow descending from the Sierra crest. This asymmetry contributed to the fire’s preferential spread to the southwest through Paradise rather than northward along the ridge.

3.5. Vertical Wind Profile

The vertical wind profile over Paradise (39.76°N, 121.61°W) at FHR 15 reveals the tight jet structure and provides insight into the dynamics of the downslope wind event. Table 5 presents the wind speed and direction at each standard pressure level.

The profile exhibits several features characteristic of a downslope windstorm:

1. **Sharp low-level jet:** Wind speed increases from 16.5 kt at the surface to 34.3 kt at 875 hPa—a doubling over only 75 hPa (~ 700 m). This extreme vertical wind shear in the lowest levels is a hallmark of downslope wind events where upper-level momentum is transported to the surface by the mountain wave.
2. **Rapid decay above the jet:** Above 875 hPa, wind speed decreases sharply to 11.5 kt at 800 hPa and 9.1 kt at 775 hPa, a reduction of 25 kt over 100 hPa. This tight jet profile indicates the flow was concentrated in a shallow layer rather than distributed through the troposphere.
3. **Wind backing with height:** Wind direction veered from 056° at the surface to 074° at 850 hPa (within the jet), then backed dramatically from 074° to 022° (NNE) at 750 hPa. In the Northern Hemisphere,

Table 5: Vertical wind profile over Paradise (39.76°N, 121.61°W) at FHR 15 (0700 PST, ignition time). The jet core at 875–900 hPa is only 50–100 hPa above the local surface ($p_{\text{sfc}} \approx 950$ hPa). Wind direction backs from ENE to NNE above 800 hPa, indicating warm advection and the descending branch of the mountain wave.

Level (hPa)	Speed (kt)	Speed (m s^{-1})	Direction
950 (surface)	16.5	8.5	056° (ENE)
925	26.8	13.8	065° (ENE)
900	34.0	17.5	070° (ENE)
875	34.3	17.6	073° (ENE)
850	27.5	14.1	074° (ENE)
825	18.3	9.4	072° (ENE)
800	11.5	5.9	062° (ENE)
775	9.1	4.7	040° (NE)
750	10.9	5.6	022° (NNE)

wind backing with height indicates cold advection or, equivalently, warm advection below the layer of backing. This directional profile is characteristic of the descending branch of a mountain wave: the subsiding air within and below the jet core carries warm advection signatures, while above the jet the ambient flow has a more northerly component associated with the upstream trough.

4. **Surface wind enhancement:** The surface wind of 16.5 kt (19 mph) was itself above red flag warning thresholds, even before considering the 34 kt jet immediately overhead. The strong vertical shear between the surface and 900 hPa provided the mechanism for turbulent eddies to intermittently bring jet-core momentum to the surface, producing gusts far exceeding the mean surface wind.

3.6. Wind Shear

Vertical wind shear is the primary mechanism by which the low-level jet's momentum is communicated to the surface. Strong shear generates Kelvin–Helmholtz instability and turbulent eddies that intermittently transfer high-momentum air from the jet core to the ground, producing the damaging wind gusts that drove the fire's extreme rate of spread. Figure 13 presents the shear cross-sections along the canyon path.

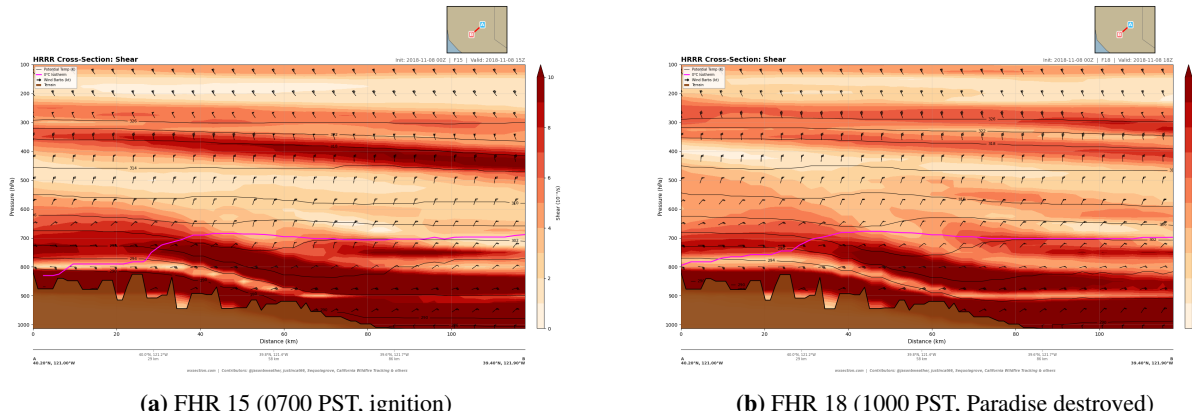


Figure 13: Wind shear ($\times 10^{-3} \text{ s}^{-1}$) cross-sections along the Feather River Canyon path at (a) ignition and (b) the time of Paradise's destruction. Maximum shear values of $30\text{--}35 \times 10^{-3} \text{ s}^{-1}$ are concentrated at the foothill transition zone (39.6–39.7°N) where the downslope jet encounters the more stagnant valley air mass.

Table 6 presents the maximum shear values at key pressure levels along the canyon path at FHR 15. The strongest shear occurred in the lowest levels: $34.6 \times 10^{-3} \text{ s}^{-1}$ at 975 hPa and $30.6 \times 10^{-3} \text{ s}^{-1}$ at 950 hPa, both located at the foothill transition zone near $39.61\text{--}39.68^\circ\text{N}$, $121.59\text{--}121.66^\circ\text{W}$. This is the region where the terrain drops steeply from the canyon to the Sacramento Valley, and the downslope jet encounters the slower-moving valley air mass.

Table 6: Maximum wind shear along the Feather River Canyon cross-section at FHR 15. Shear values are computed as the magnitude of the vertical wind shear vector between adjacent pressure levels. The foothill transition zone ($39.6\text{--}39.7^\circ\text{N}$) consistently exhibits the strongest shear at all levels below 900 hPa.

Level (hPa)	Max Shear ($\times 10^{-3} \text{ s}^{-1}$)	Location
975	34.6	$39.61^\circ\text{N}, 121.66^\circ\text{W}$
950	30.6	$39.68^\circ\text{N}, 121.59^\circ\text{W}$
925	19.3	$39.79^\circ\text{N}, 121.46^\circ\text{W}$
900	14.7	$39.84^\circ\text{N}, 121.40^\circ\text{W}$
875	19.2	$39.64^\circ\text{N}, 121.62^\circ\text{W}$
850	25.3	$40.20^\circ\text{N}, 121.00^\circ\text{W}$

The shear profile has important implications for fire behavior. Shear values exceeding $20 \times 10^{-3} \text{ s}^{-1}$ are sufficient to generate turbulent eddies that transfer momentum from the jet to the surface (Sharples, 2012). At the foothill transition zone, shear exceeded this threshold at multiple levels simultaneously (975, 950, and 850 hPa), creating a deep layer of mechanical turbulence. This turbulence explains the observation that surface wind gusts during the Camp Fire reached 40–50 mph in areas where the mean surface wind was only 20–25 mph: the turbulent eddies intermittently brought the full 35–40 kt jet-core wind speed to ground level.

The shear maximum at 850 hPa was located at $40.20^\circ\text{N}, 121.00^\circ\text{W}$ —the Sierra crest itself. This elevated shear zone marks the top of the jet core and the interface between the strong downslope flow and the weaker ambient winds above. As the jet descended westward along the terrain slope, the shear maximum migrated downward to lower pressure levels (950–975 hPa) near the foothill exit, consistent with the jet following the terrain surface.

The concentration of the strongest shear at the foothill transition zone, precisely where Paradise is situated, was a critical factor in the fire’s destructiveness. Paradise occupies a ridge at approximately 540 m elevation (957 hPa surface pressure), placing it directly within the zone of maximum turbulent momentum transfer between the jet core and the surface. The community was positioned at the worst possible location relative to the shear dynamics: too high to be sheltered in the valley beneath the jet, and too low to be above the zone of maximum vertical mixing.

4. Moisture Analysis

The moisture environment of the 2018 Camp Fire represents one of the most extreme desiccation events documented in the lower troposphere over the western United States. HRRR cross-section analysis reveals sub-10% relative humidity extending through the entire column from the surface to 600 hPa—a continuous depth of approximately 4 km—with no diurnal recovery over a 24-hour period. This section quantifies the moisture deficit using multiple complementary metrics: relative humidity, dewpoint depression, specific humidity, and vapor pressure deficit.

4.1. Extreme Low-Level Humidity

The relative humidity profile over Paradise at FHR 15 (1500 UTC, 0700 PST—approximately 30 minutes after ignition) exhibited values well below critical fire weather thresholds through the entire lower troposphere (Table 7, Fig. 14). At 950 hPa (near-surface), RH was 12.8%, decreasing to 9.8% at 900 hPa and reaching a minimum of 3.2% at 600 hPa. No level between the surface and 600 hPa exceeded 13% RH.

Table 7: Relative humidity vertical profile over Paradise (39.71°N, 121.55°W) at FHR 15 (1500 UTC 8 November 2018). Standard red flag warning criteria require RH < 15%; every level shown is below this threshold.

Pressure Level (hPa)	RH (%)	Approximate Height (m AGL)
950 (near-surface)	12.8	0–100
925	12.0	~250
900	9.8	~500
875	7.8	~750
850	6.5	~1000
825	6.1	~1300
800	6.3	~1600
700	5.3	~2700
600	3.2	~4000

The RH minimum was not confined to the surface layer but was located at 850–825 hPa (approximately 1000–1300 m above ground level), indicating that the desiccation was not a surface-driven process. Rather, the humidity deficit originated from a deep synoptic-scale dry intrusion associated with the upper-level trough and descending air in the lee of the Sierra Nevada. Along the canyon path, the minimum RH at FHR 15 reached 2.0% at 575 hPa (Fig. 14), a value more characteristic of the upper troposphere or lower stratosphere than the mid-troposphere.

The spatial distribution of humidity along the fire propagation path (Fig. 15) reveals that the driest air at low levels was concentrated over the western slope of the Sierra Nevada and through the canyon system, precisely where the downslope wind jet was strongest. RH values at 850 hPa along this path ranged from 6.5% over Paradise to as low as 5% over the canyon mouth, indicating that terrain-forced subsidence was further desiccating an already extremely dry air mass.

4.2. Temporal Evolution of Humidity

The most consequential finding of the moisture analysis is the complete absence of diurnal humidity recovery. In typical fire weather scenarios—even during offshore wind events—relative humidity increases overnight as temperatures fall and the boundary layer stabilizes. During the Camp Fire event, the opposite occurred: RH *continued to decrease* for at least 24 hours following ignition (Table 8, Fig. 16, 17).

At 950 hPa over Paradise, RH fell from 12.8% at ignition (FHR 15) to 4.4% by FHR 36 (0400 PST the following morning)—a reduction of 66% from an already critically low initial value. At 850 hPa, the decline was from 6.5% to 3.5%. This monotonic decrease is consistent with a deepening and strengthening downslope wind event progressively advecting drier air from above the Sierra crest. The minimum path-averaged RH fell from 2.0% at FHR 15 to 1.3% at FHR 18 before stabilizing near 2–3%.

The operational significance of this finding cannot be overstated. Fire suppression strategies frequently rely on anticipated overnight humidity recovery to moderate fire behavior and create windows for defensive operations. During the Camp Fire, no such recovery occurred. Firefighters and evacuating residents faced continuously worsening atmospheric conditions throughout the event and into the following day.

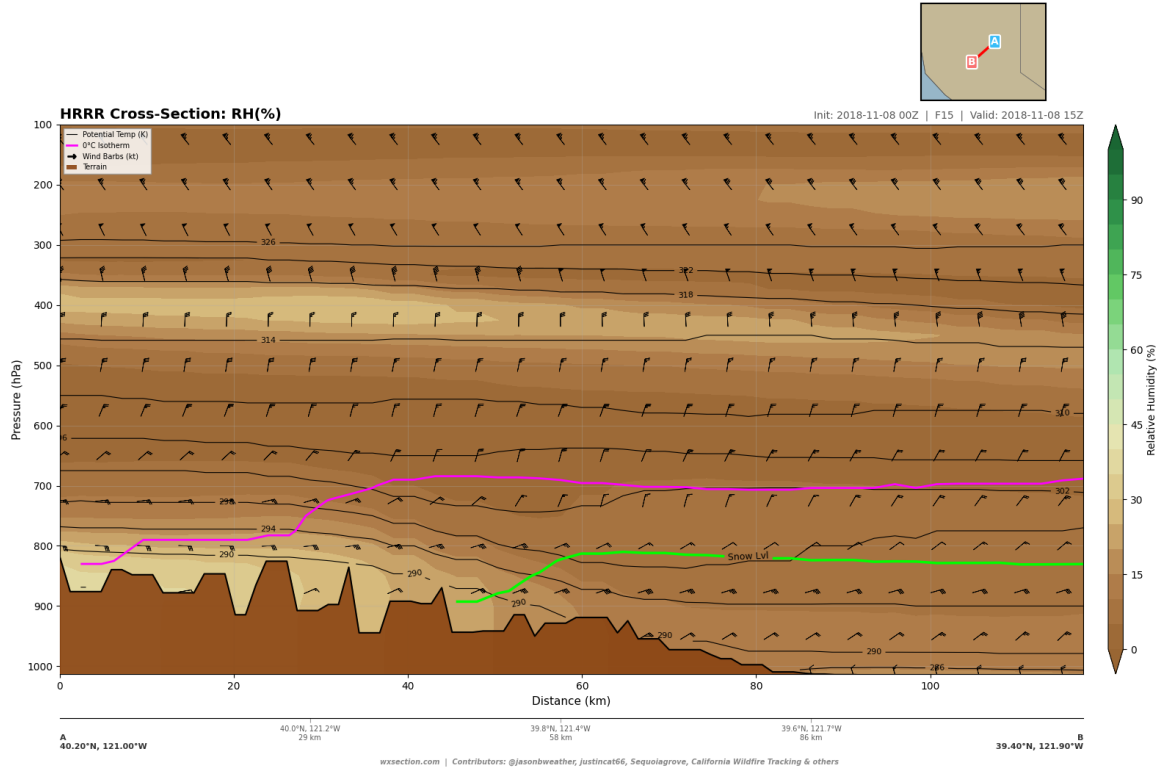


Figure 14: Relative humidity cross-section along the Feather River Canyon path ($40.2^{\circ}\text{N}, 121.0^{\circ}\text{W}$ to $39.4^{\circ}\text{N}, 121.9^{\circ}\text{W}$) at FHR 15 (1500 UTC 8 November 2018). The entire lower troposphere below 600 hPa exhibits RH below 13%, with minimum values of 2–3% at 575–600 hPa. The black shading at the bottom represents terrain.

Table 8: Temporal evolution of relative humidity over Paradise at selected pressure levels from FHR 15 (1500 UTC 8 November) through FHR 36 (1200 UTC 9 November). Values represent a 21-hour period spanning the fire’s initial run and the following overnight hours.

FHR	Valid Time (UTC)	950 hPa	925 hPa	900 hPa	875 hPa	850 hPa	700 hPa
15	08 Nov 15Z (07 PST)	12.8	12.0	9.8	7.8	6.5	5.3
18	08 Nov 18Z (10 PST)	10.1	9.4	8.1	6.5	5.6	5.1
20	08 Nov 20Z (12 PST)	7.9	8.2	7.7	6.6	5.5	4.3
24	09 Nov 00Z (16 PST)	6.5	6.5	5.8	5.0	4.4	4.1
30	09 Nov 06Z (22 PST)	5.9	5.0	4.1	3.6	3.4	4.6
36	09 Nov 12Z (04 PST)	4.4	3.8	3.5	3.5	3.5	3.2

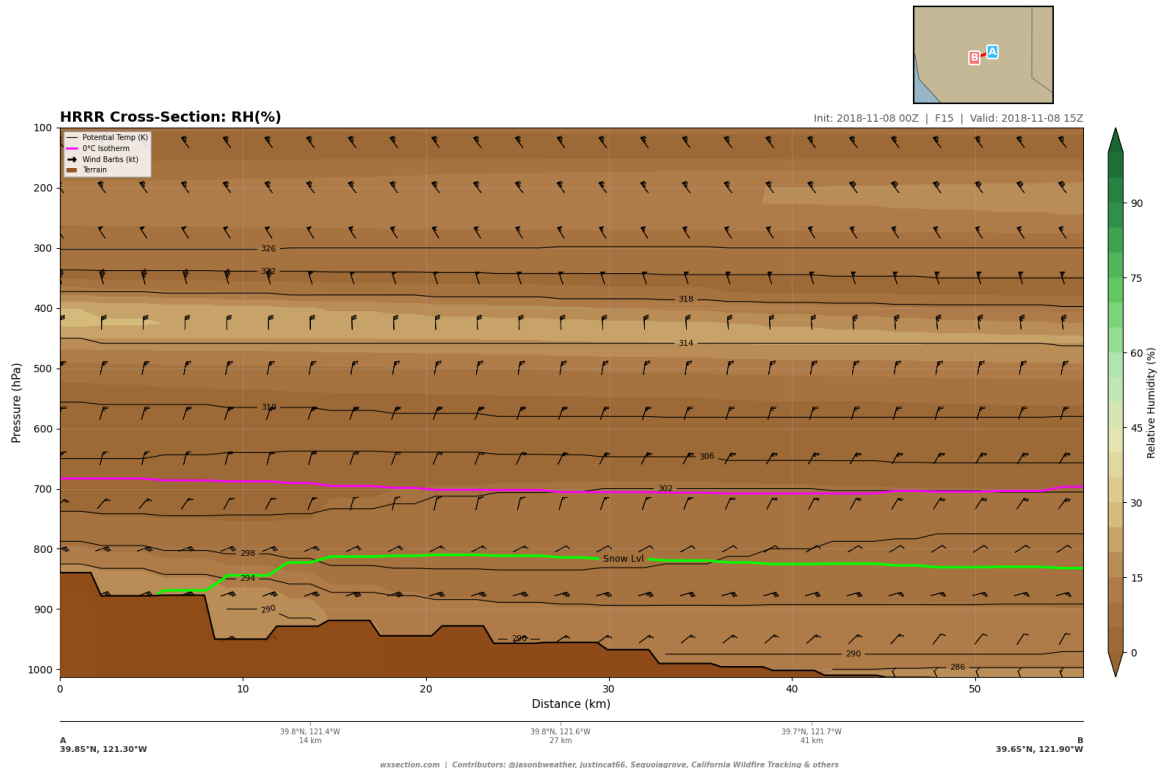


Figure 15: Relative humidity cross-section along the fire propagation path ($39.85^{\circ}\text{N}, 121.30^{\circ}\text{W}$ to $39.65^{\circ}\text{N}, 121.90^{\circ}\text{W}$) at FHR 15. This path follows the actual trajectory of fire spread from Pulga through Paradise to the Sacramento Valley foothills.

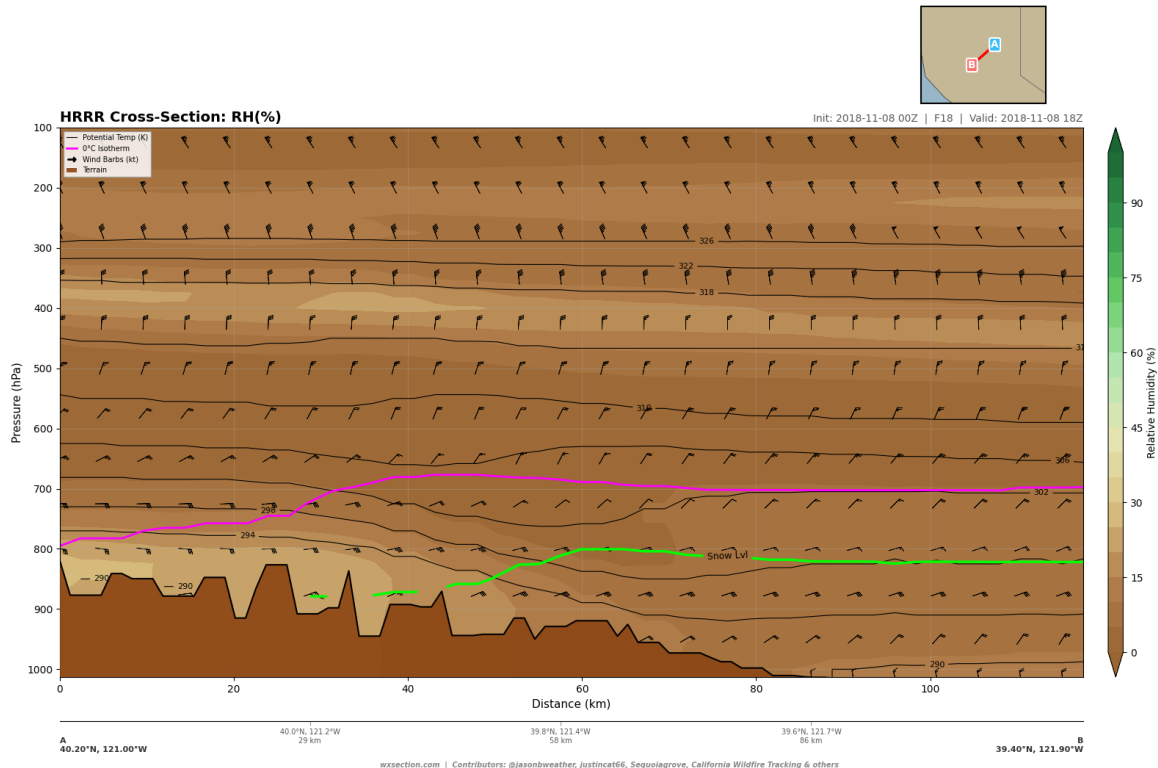


Figure 16: Relative humidity cross-section along the canyon path at FHR 18 (1800 UTC, 1000 PST), approximately 3.5 hours after ignition. By this time, Paradise had been largely destroyed. Note the further desiccation at 850–900 hPa compared to Fig. 14.

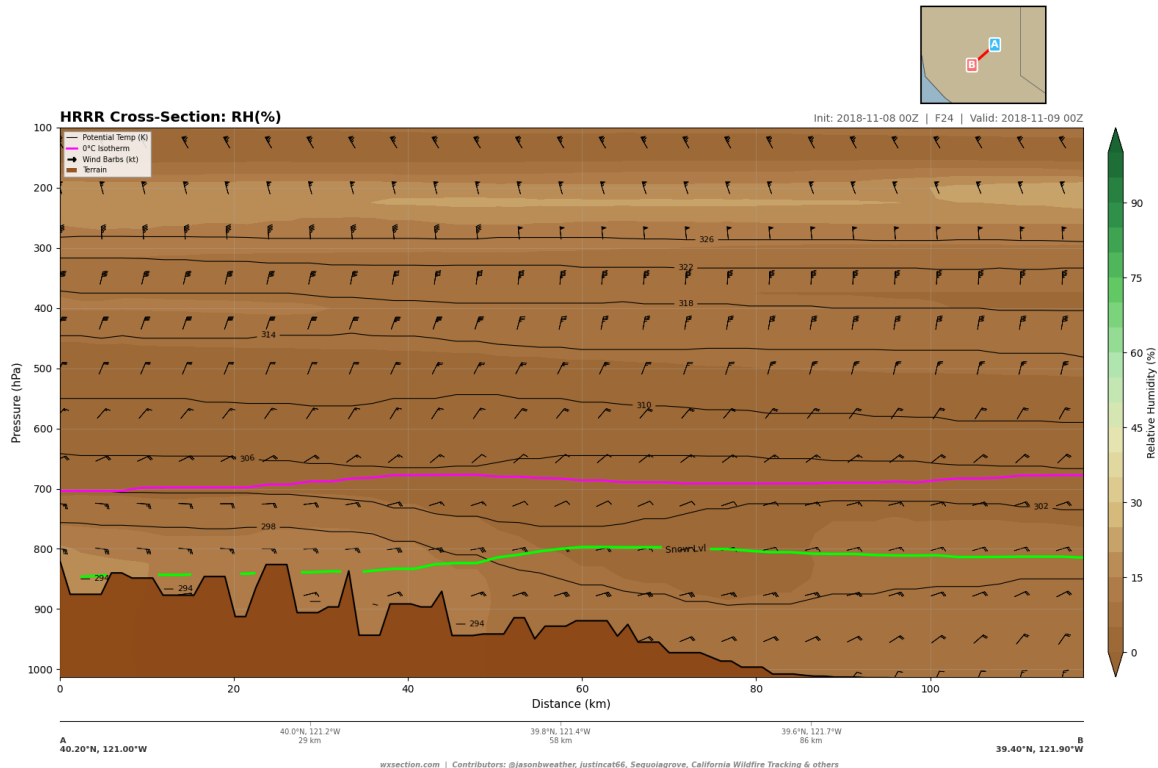


Figure 17: Relative humidity cross-section along the canyon path at FHR 24 (0000 UTC 9 November, 1600 PST). Despite the late afternoon timing, RH has continued to decrease across all levels, with values of 4–6% now dominating the entire column below 700 hPa.

4.3. Dewpoint Depression

Dewpoint depression ($T - T_d$) provides a direct measure of the thermodynamic distance between the ambient air and saturation, and serves as a tracer for the origin altitude of descending air masses. Along the canyon cross-section at FHR 15 (Fig. 18), dewpoint depression values were extreme at every level (Table 9).

Table 9: Dewpoint depression ($T - T_d$) profile over Paradise at FHR 15 (1500 UTC). Values exceeding 20°C are considered extreme for fire weather purposes; every level shown exceeds this threshold by a wide margin.

Pressure Level (hPa)	Dewpoint Depression (°C)
950 (near-surface)	27.8
925	30.6
900	34.4
875	36.1
850	36.5
825	35.6
800	34.6
700	34.9
600	38.5

The maximum dewpoint depression along the canyon path reached 45.5°C at 575 hPa. At the surface over Paradise, the dewpoint depression of 27.8°C indicates that the dew point temperature was approximately -15°C despite an ambient temperature of $\sim 13^{\circ}\text{C}$. At 850 hPa, the depression of 36.5°C implies a dewpoint near -26°C —a value typically observed at 400–500 hPa in the upper troposphere. This provides strong thermodynamic evidence that the air over the fire area had descended from the upper troposphere, undergoing adiabatic compression and warming without acquiring any moisture during its descent.

For context, standard fire weather red flag criteria in California consider dewpoint depressions exceeding 20°C to indicate extreme dryness. Values approaching 40°C, as observed at 850–600 hPa during the Camp Fire, indicate an air mass that has descended through a pressure depth of approximately 300–400 hPa—roughly 3–5 km of vertical descent—without encountering any moisture source.

4.4. Specific Humidity

Specific humidity (q) is a conserved quantity during dry adiabatic processes and therefore serves as an unambiguous tracer of air mass origin. The specific humidity profile over Paradise at FHR 15 (Fig. 19) confirms the upper-tropospheric origin of the fire-area air mass (Table 10).

At the surface (950 hPa), specific humidity was 1.30 g kg^{-1} , and values decreased rapidly with height to 0.60 g kg^{-1} at 850 hPa and 0.30 g kg^{-1} at 700 hPa. Along the canyon path, near-surface q ranged from 2.1 g kg^{-1} over the Sierra crest (where elevation-dependent cold temperatures limit saturation vapor pressure even further) to 1.1 g kg^{-1} in the Sacramento Valley foothills.

These specific humidity values are extraordinary for the lower troposphere at mid-latitudes. Climatological November values for the Sacramento Valley at 950 hPa are typically $4\text{--}8 \text{ g kg}^{-1}$; the observed 1.3 g kg^{-1} represents a deficit of 70–85% relative to normal. At 850 hPa, the observed 0.60 g kg^{-1} is more characteristic of air at 400–500 hPa in the standard atmosphere. Because specific humidity is conserved during adiabatic descent, this confirms that the air mass over Paradise had originated at upper-tropospheric levels and descended to the surface without mixing with any lower-tropospheric moisture.

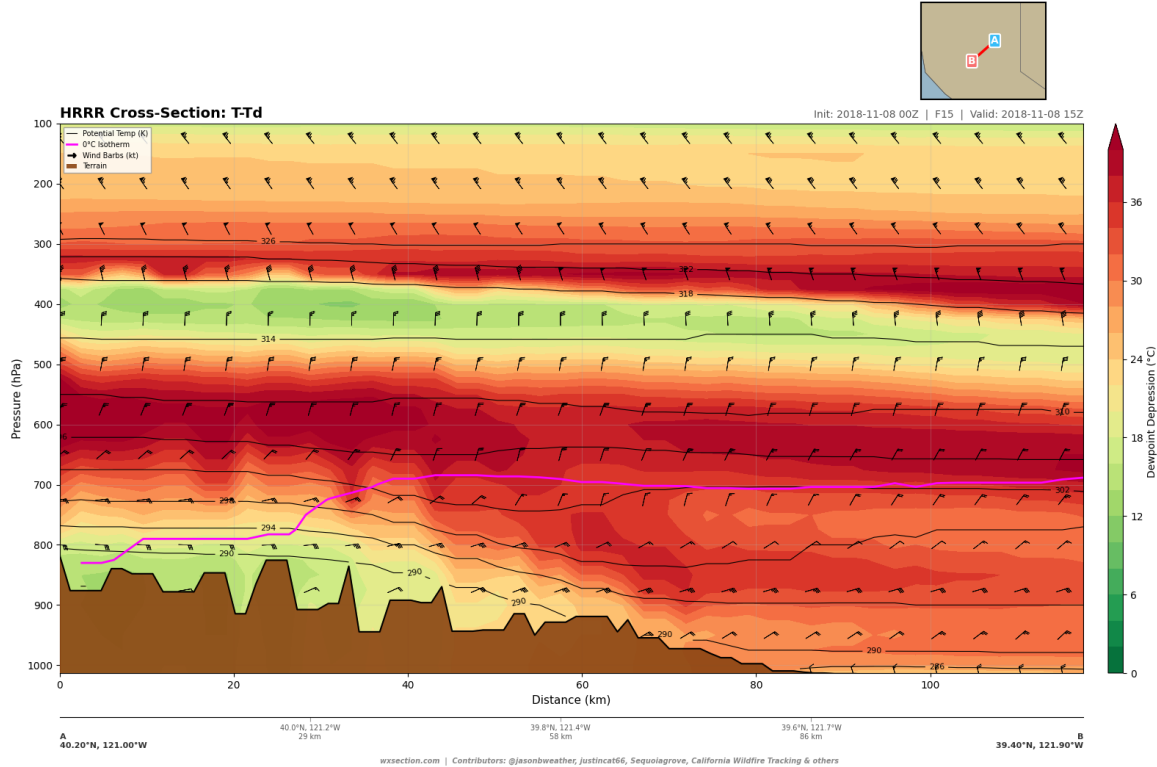


Figure 18: Dewpoint depression cross-section along the canyon path at FHR 15. Values of 25–40°C dominate the lower troposphere, with the maximum of 45.5°C at 575 hPa over the Sierra crest. These extreme depressions are characteristic of air originating from the upper troposphere (400–500 hPa).

Table 10: Specific humidity profile over Paradise at FHR 15. Values are given in g kg^{-1} . For reference, typical lower-tropospheric values over California in November are 4–8 g kg^{-1} ; the observed values are an order of magnitude lower.

Pressure Level (hPa)	Specific Humidity (g kg^{-1})
950 (near-surface)	1.30
925	0.90
900	0.70
875	0.60
850	0.60
825	0.50
800	0.50
700	0.30
600	0.10

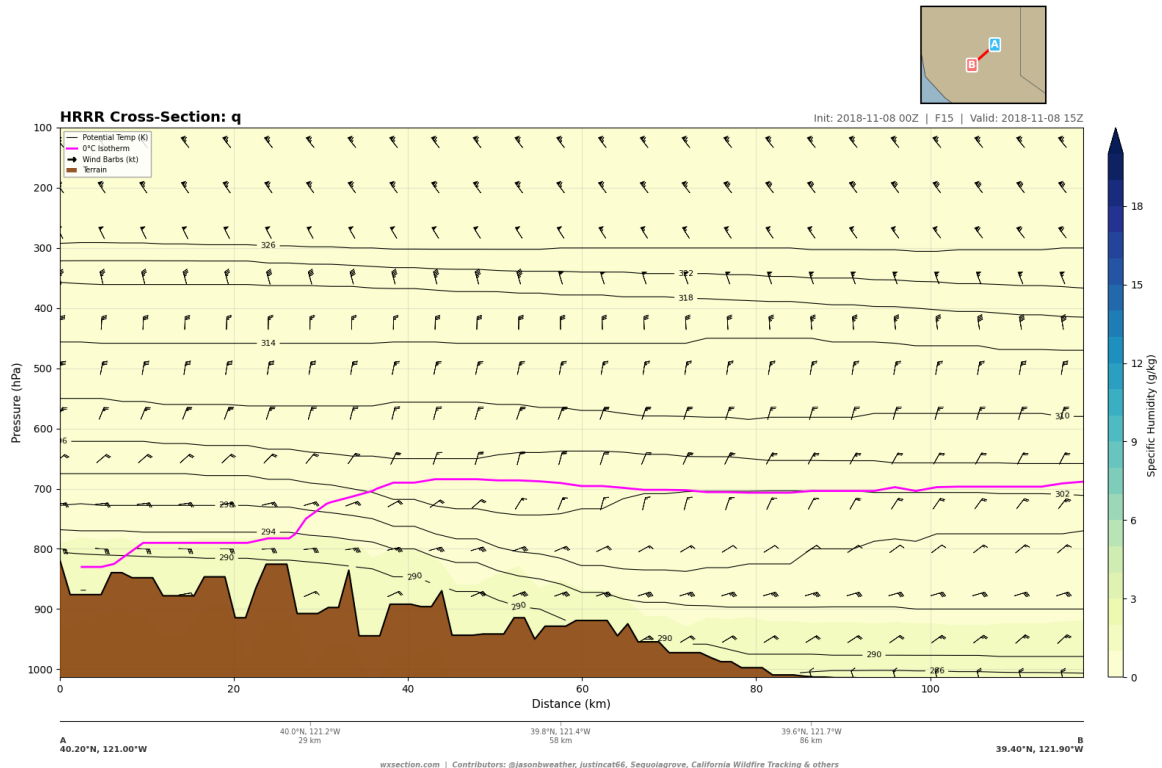


Figure 19: Specific humidity cross-section along the canyon path at FHR 15. The entire lower troposphere contains less than 2 g kg^{-1} of water vapor, with values of $0.3\text{--}0.6 \text{ g kg}^{-1}$ at $700\text{--}850 \text{ hPa}$ —concentrations typical of the upper troposphere at $400\text{--}500 \text{ hPa}$.

4.5. Vapor Pressure Deficit

Vapor pressure deficit (VPD) quantifies the difference between the saturation vapor pressure and the actual vapor pressure, representing the atmosphere's instantaneous capacity to extract moisture from fuels and vegetation. VPD is the most operationally relevant moisture metric for fire behavior because it directly governs the rate of fuel moisture equilibration (Seager et al., 2015).

At FHR 15, VPD at 950 hPa over Paradise was 12.9 hPa, already more than double the threshold of 6 hPa generally considered indicative of high fire danger (Fig. 20). As temperatures increased through the day and humidity continued to fall, VPD rose monotonically (Table 11, Fig. 21).

Table 11: Temporal evolution of vapor pressure deficit (hPa) over Paradise at 950 hPa and 925 hPa, and the maximum VPD observed anywhere along the canyon cross-section at 950 hPa. VPD values above 6 hPa indicate high fire danger; above 10 hPa indicates extreme fire danger.

FHR	Valid Time (UTC)	VPD ₉₅₀ (hPa)	VPD ₉₂₅ (hPa)	Max VPD ₉₅₀ (path)
15	08 Nov 15Z (07 PST)	12.9	12.2	14.1
18	08 Nov 18Z (10 PST)	15.7	14.3	16.1
20	08 Nov 20Z (12 PST)	18.8	16.5	18.9
24	09 Nov 00Z (16 PST)	20.0	17.9	21.1

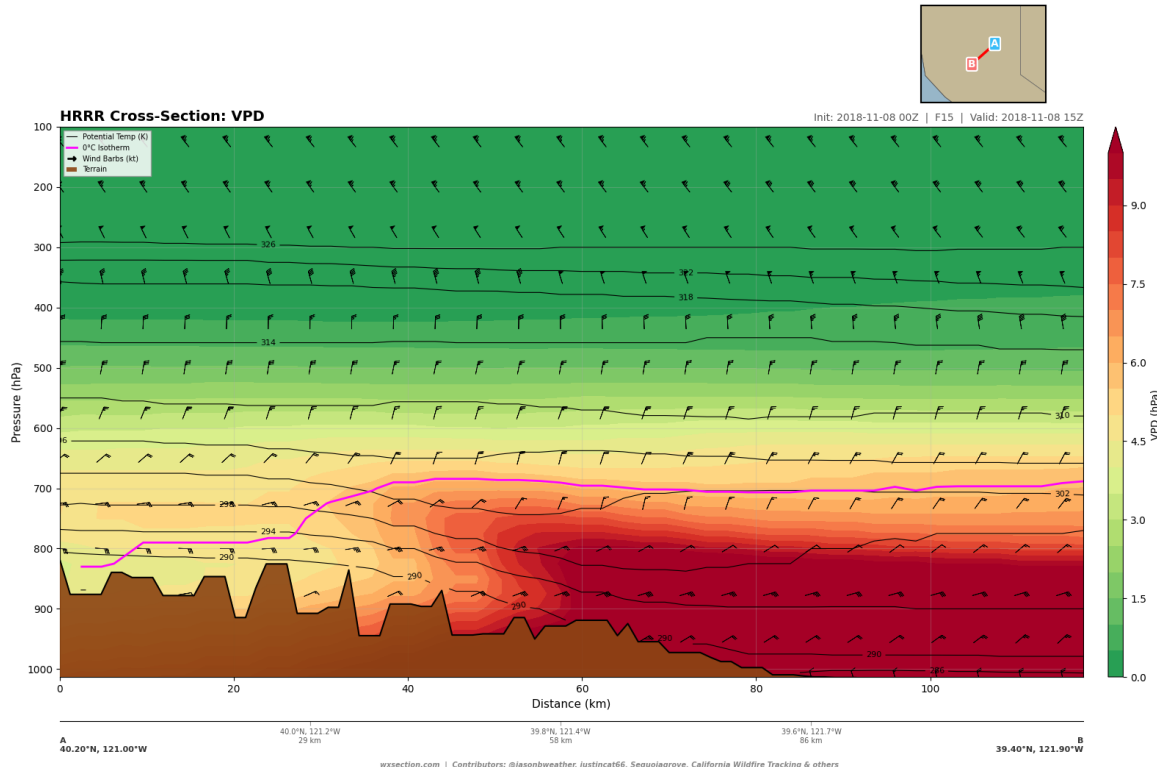


Figure 20: Vapor pressure deficit cross-section along the canyon path at FHR 15. VPD exceeds 10 hPa (extreme fire danger threshold) through the entire lower troposphere from the Sierra crest to the Sacramento Valley.

By FHR 24 (1600 PST), VPD at 950 hPa over Paradise reached 20.0 hPa, with the maximum along the path reaching 21.1 hPa. VPD along the fire propagation path at ignition time (Fig. 22) shows that extreme

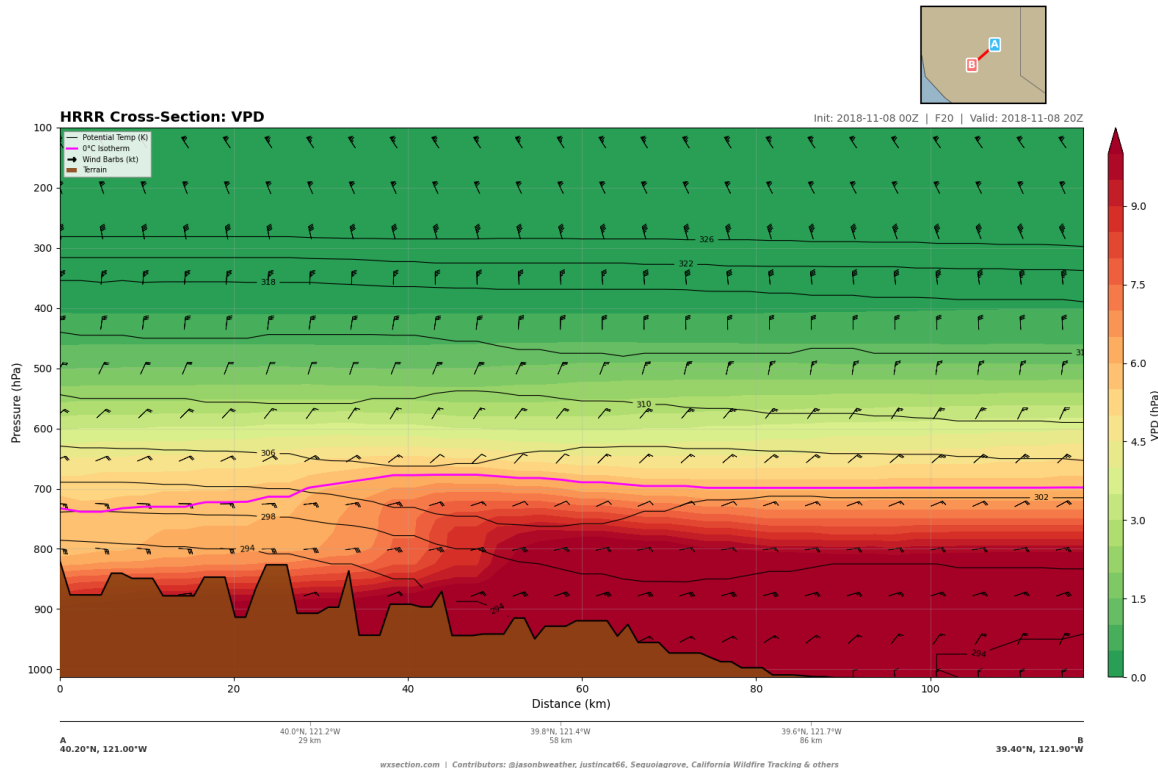


Figure 21: Vapor pressure deficit cross-section along the canyon path at FHR 20 (2000 UTC, 1200 PST). Near-surface VPD has intensified to 18–19 hPa over the foothill zone, reflecting both continued desiccation and afternoon solar heating.

values exceeding 12 hPa extended continuously from the canyon mouth through Paradise to the valley floor. At these VPD levels, even live fuels with high foliar moisture content experience rapid desiccation (Jolly and Freeborn, 2019). Dead fine fuels (1-hour timelag) would have equilibrated to 1–2% moisture content within minutes of exposure, rendering the entire fuel complex available for combustion.

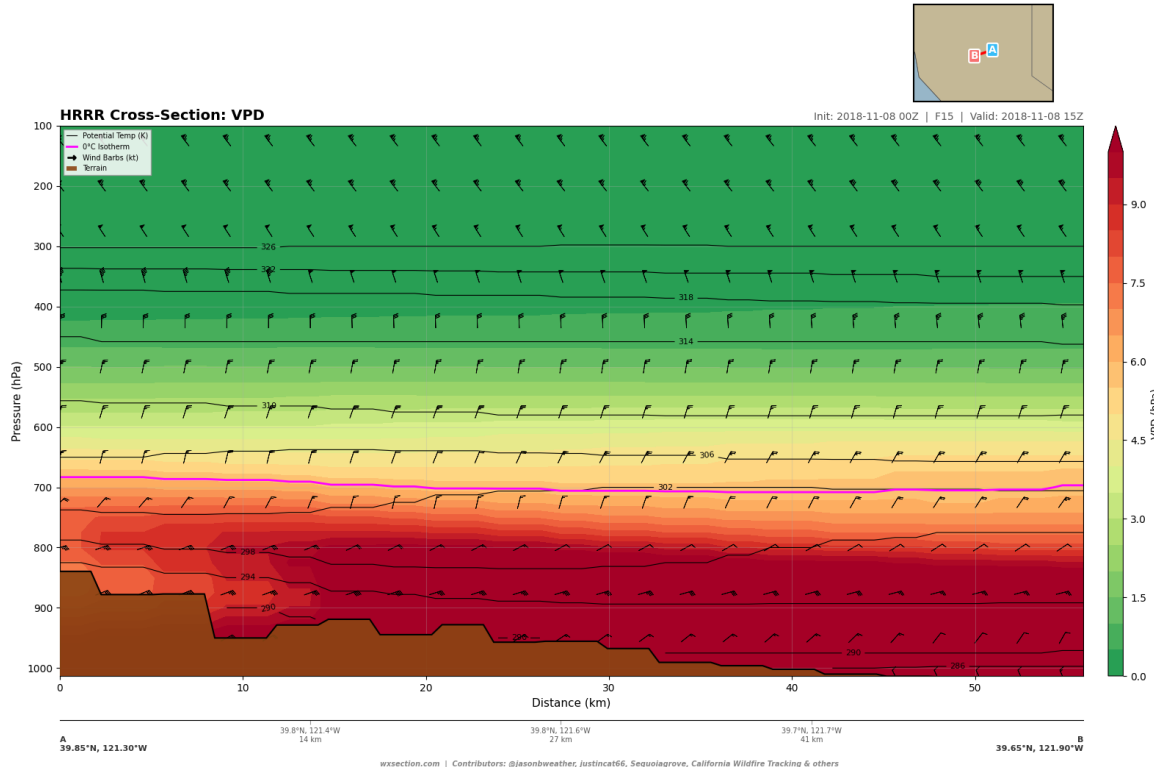


Figure 22: Vapor pressure deficit cross-section along the fire propagation path at FHR 15. VPD exceeding 12 hPa is continuous from the ignition area at Pulga through Paradise and into the Sacramento Valley foothills, indicating extreme atmospheric moisture demand along the entire fire trajectory.

The combination of extreme initial VPD with a monotonically increasing trend represents a worst-case scenario for wildfire suppression. Standard fuel moisture models assume some degree of afternoon humidity recovery; the persistent increase in VPD from 12.9 to 21.1 hPa over a 9-hour period implies that fuel moisture conditions deteriorated continuously throughout the event, consistent with the fire's sustained extreme behavior well into the evening hours.

5. Thermodynamic Structure

The thermodynamic environment of the Camp Fire was characterized by a strong subsidence inversion, steep lapse rates in the mid-troposphere above the inversion, and an absolutely stable equivalent potential temperature (θ_e) profile. This configuration concentrated the kinetic energy of the downslope jet in the lowest 1–2 km of the atmosphere, suppressed vertical development of the fire's convective column, and forced lateral fire spread—a combination that maximized the rate of surface fire propagation. This section examines the temperature structure, static stability, and equivalent potential temperature profiles derived from HRRR cross-sections.

5.1. Temperature Profile and Inversions

The temperature profile over Paradise at FHR 15 (1500 UTC, 0700 PST) exhibited the unmistakable signature of adiabatic subsidence warming (Table 12, Fig. 23). Near-surface temperature at 950 hPa was 12.8°C, decreasing only marginally to 11.3°C at 875 hPa over a depth of 75 hPa (~700 m). This extremely weak lapse rate of approximately $2.1^{\circ}\text{C km}^{-1}$ is far less than the standard atmosphere ($6.5^{\circ}\text{C km}^{-1}$) and indicates a subsidence inversion in which descending, adiabatically warmed air overlies the near-surface layer.

Table 12: Temperature profile over Paradise (39.71°N, 121.55°W) at FHR 15 (1500 UTC 8 November 2018). The near-isothermal layer from 950 to 875 hPa is the subsidence inversion signature.

Pressure Level (hPa)	Temperature (°C)
950 (near-surface)	12.8
925	11.8
900	11.6
875	11.3
850	10.8
825	9.3
800	7.6
700	-0.1
600	-6.2

The horizontal temperature gradient along the canyon path at 850 hPa reveals the dramatic effect of the downslope wind event. Over the Sierra crest (40.20°N), the 850 hPa temperature was 0.3°C. This increased to 4.8°C near Pulga (39.87°N) and reached 10.8°C over Paradise—a warming of 10.5°C over approximately 60 km of horizontal distance (Table 13). This gradient is a direct thermodynamic fingerprint of the foehn-type downslope windstorm: air descending from the 700–750 hPa level (~3000 m) on the eastern Sierra slope warmed at the dry adiabatic rate of $\sim 9.8^{\circ}\text{C km}^{-1}$ as it descended into the canyon and over the western foothills.

Table 13: Temperature at 850 hPa along the canyon cross-section at FHR 15, showing the progressive adiabatic warming of descending air from the Sierra crest toward Paradise and the Sacramento Valley.

Location	Latitude (°N)	Distance (km)	T_{850} (°C)
Sierra crest	40.20	0.0	0.3
Upper slope	40.04	23.9	1.9
Pulga area	39.87	47.9	4.8
Paradise	39.71	71.9	10.8
Lower foothills	39.55	95.9	10.1
Sacramento Valley	39.47	108.0	10.1

The north-south temperature cross-section through Paradise at FHR 15 (Fig. 24) provides a complementary view, revealing the lateral extent of the warm anomaly. The adiabatically warmed air was confined to a band between approximately 39.6°N and 40.0°N, with markedly cooler temperatures to the north over higher terrain and to the south in the Sacramento Valley where the descending flow had not yet reached the surface. This spatial confinement of the warm anomaly corresponds precisely to the zone of maximum wind speed and minimum humidity.

By FHR 20 (2000 UTC, 1200 PST), surface temperatures over Paradise had risen to approximately

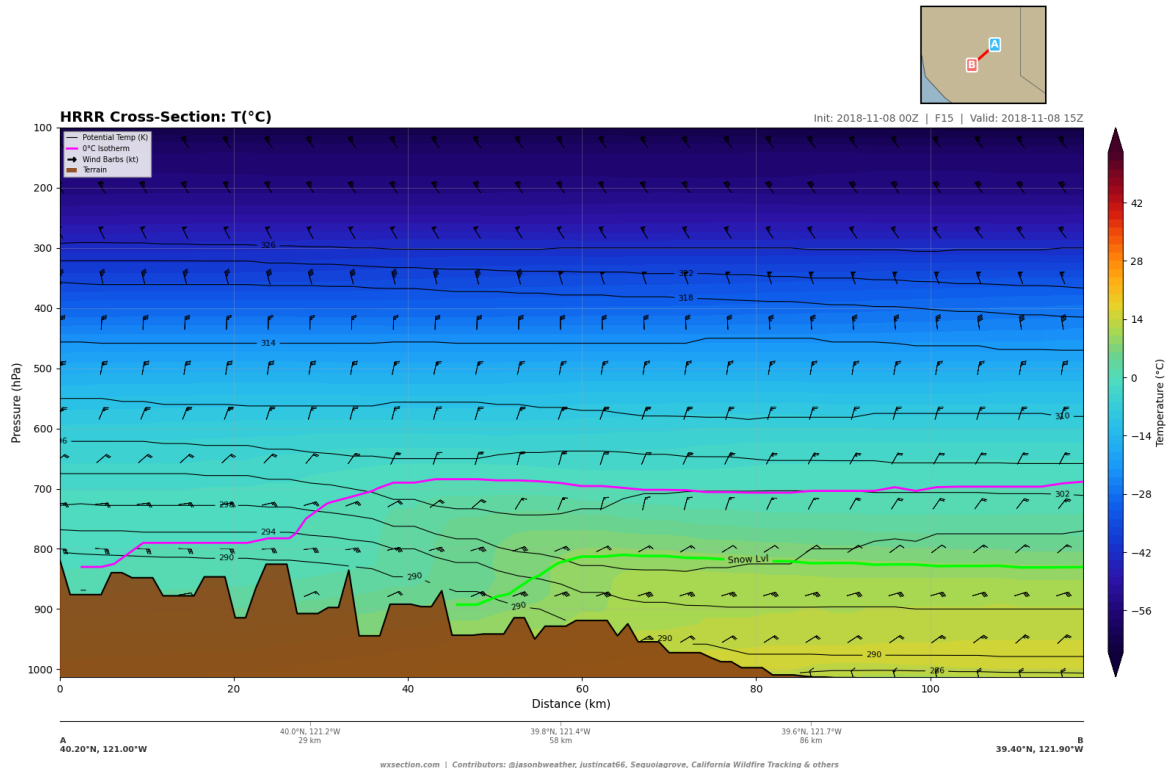


Figure 23: Temperature cross-section along the Feather River Canyon path at FHR 15 (1500 UTC). The warm anomaly over the western Sierra slope and Paradise (distance \sim 50–80 km) is clearly visible, with 850 hPa temperatures exceeding 10°C where they are only 0–2°C over the Sierra crest. Terrain is shown in black.

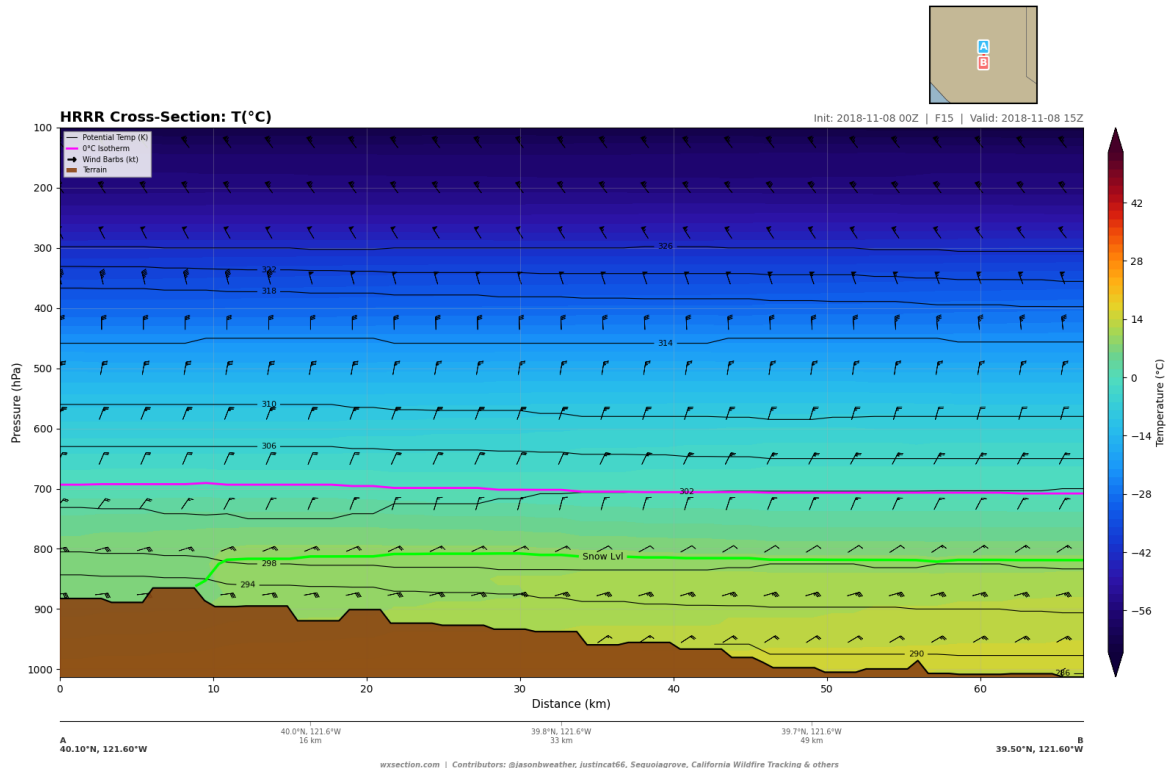


Figure 24: Temperature cross-section along a north-south path through Paradise (40.1° N to 39.5° N along 121.6° W) at FHR 15. The warm anomaly associated with the subsidence inversion is clearly delineated in the lower troposphere over the foothill zone.

17–18°C, reflecting both continued adiabatic warming from the downslope flow and diurnal solar heating (Fig. 25). In the Sacramento Valley at the base of the foothills, temperatures reached 22°C. The combination of warm temperatures and near-zero humidity produced the extreme vapor pressure deficits documented in Section 4.5.

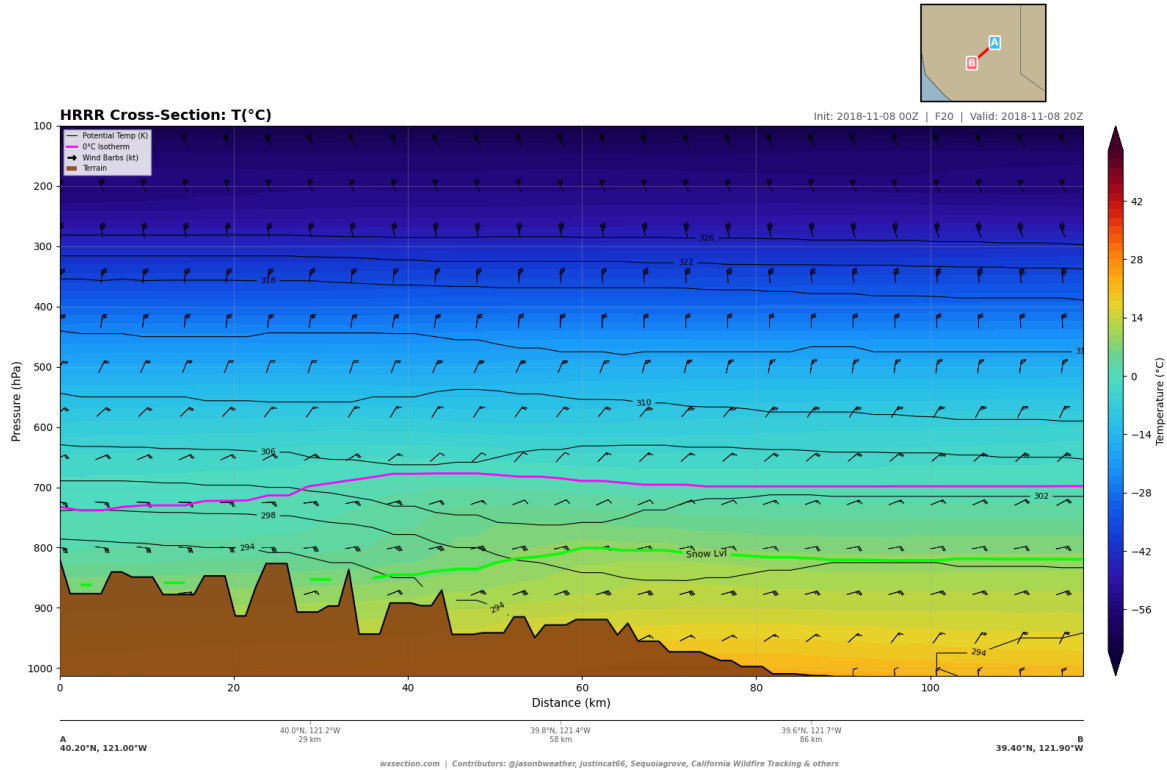


Figure 25: Temperature cross-section along the canyon path at FHR 20 (2000 UTC, 1200 PST). Surface temperatures have risen 4–5°C compared to FHR 15, amplifying the already extreme vapor pressure deficit.

5.2. Lapse Rate Analysis

The lapse rate structure along the fire path at FHR 15 reveals a complex vertical profile created by the interaction of the subsidence inversion with the underlying terrain and the overlying free atmosphere (Table 14, Fig. 26).

Over Paradise, the lapse rate profile exhibits three distinct layers:

- Near-surface stable layer (950–900 hPa):** Lapse rates of $1.1\text{--}4.5^{\circ}\text{C km}^{-1}$, well below the dry adiabatic rate, reflecting the subsidence inversion. This layer corresponds to the warm, dry, fast-moving air that had descended from the Sierra crest. The strong stability suppressed vertical mixing and trapped the highest wind speeds near the surface.
- Transitional layer (875–825 hPa):** Lapse rates steepened from $2.1^{\circ}\text{C km}^{-1}$ at 875 hPa to $6.9^{\circ}\text{C km}^{-1}$ at 825 hPa, reflecting the transition from the subsidence-warmed lower troposphere to the ambient free atmosphere above.
- Mid-tropospheric layer (800–700 hPa):** Lapse rates of $5.2\text{--}7.7^{\circ}\text{C km}^{-1}$, approaching the dry adiabatic

Table 14: Environmental lapse rates ($-dT/dz$) at selected levels over Paradise and Pulga at FHR 15. Dry adiabatic lapse rate is $9.8^{\circ}\text{C km}^{-1}$; values below $\sim 6^{\circ}\text{C km}^{-1}$ indicate stable conditions, values above $9.8^{\circ}\text{C km}^{-1}$ indicate superadiabatic (absolutely unstable) conditions.

Pressure Level (hPa)	Paradise ($^{\circ}\text{C km}^{-1}$)	Pulga ($^{\circ}\text{C km}^{-1}$)
950	4.5	6.8
925	1.1	5.5
900	1.1	4.3
875	2.1	2.1
850	6.1	-1.0
825	6.9	1.0
800	7.7	1.9
700	5.2	6.9
600	6.0	6.1

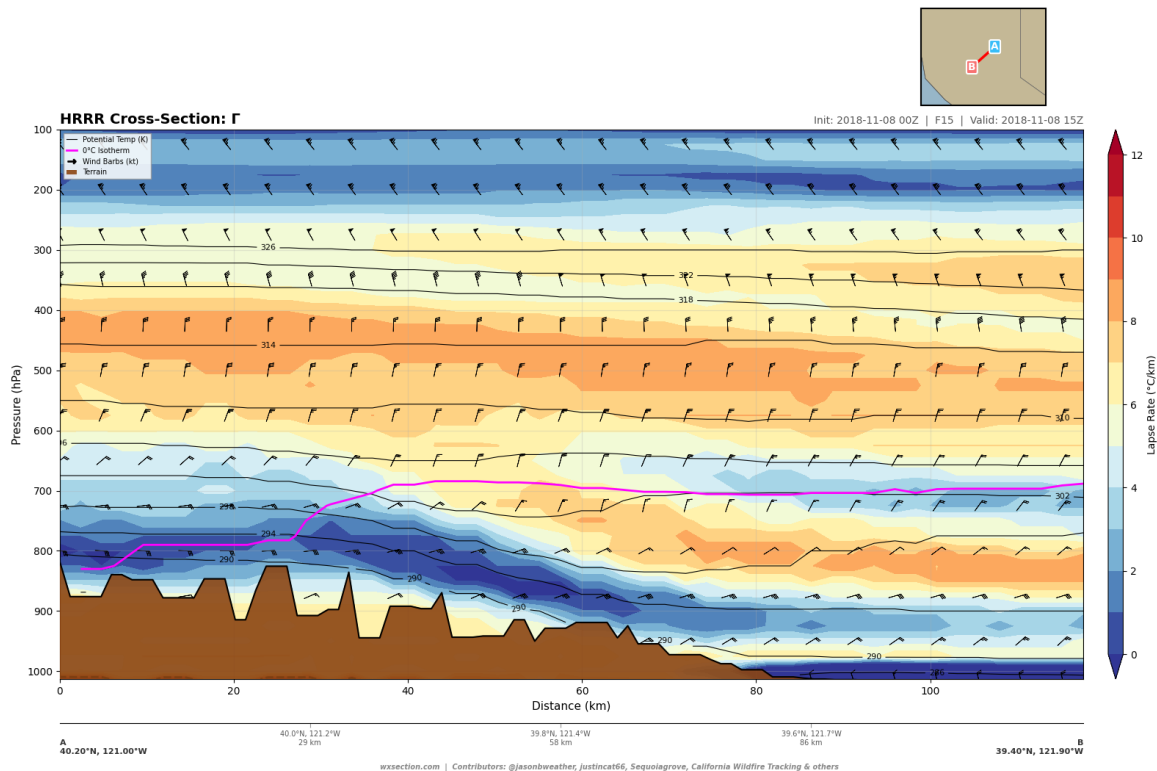


Figure 26: Lapse rate cross-section along the canyon path at FHR 15. The subsidence inversion is visible as the band of low lapse rates ($1-4^{\circ}\text{C km}^{-1}$) in the 875–925 hPa layer over Paradise, transitioning to near-dry-adiabatic values ($7-8^{\circ}\text{C km}^{-1}$) above 825 hPa. Negative lapse rates (temperature increasing with height) are present near the terrain interface at Pulga, reflecting the base of the subsidence inversion.

rate at 800 hPa. This steep lapse rate above the inversion is characteristic of well-mixed descending air that has maintained its potential temperature during subsidence.

Over Pulga, the lapse rate at 850 hPa was $-1.0^{\circ}\text{C km}^{-1}$ (temperature *increasing* with height), confirming the presence of a temperature inversion at this level. This corresponds to the base of the subsidence layer where warm descending air overrode the cooler air in the canyon bottom. Above the inversion, lapse rates steepened to $6.9^{\circ}\text{C km}^{-1}$ at 700 hPa.

The wet-bulb temperature cross-section (Fig. 27) provides complementary insight into the combined temperature-moisture state of the atmosphere. Wet-bulb temperatures at the surface near Paradise were approximately $3\text{--}4^{\circ}\text{C}$ despite dry-bulb temperatures of $12\text{--}13^{\circ}\text{C}$, yielding a wet-bulb depression of $9\text{--}10^{\circ}\text{C}$. This extreme wet-bulb depression reflects the enormous evaporative potential of the ambient air: any moisture source—whether vegetation, structures, or firefighting water—would experience rapid evaporative cooling, and the latent heat absorbed by vaporization would be efficiently removed from the fuel surface.

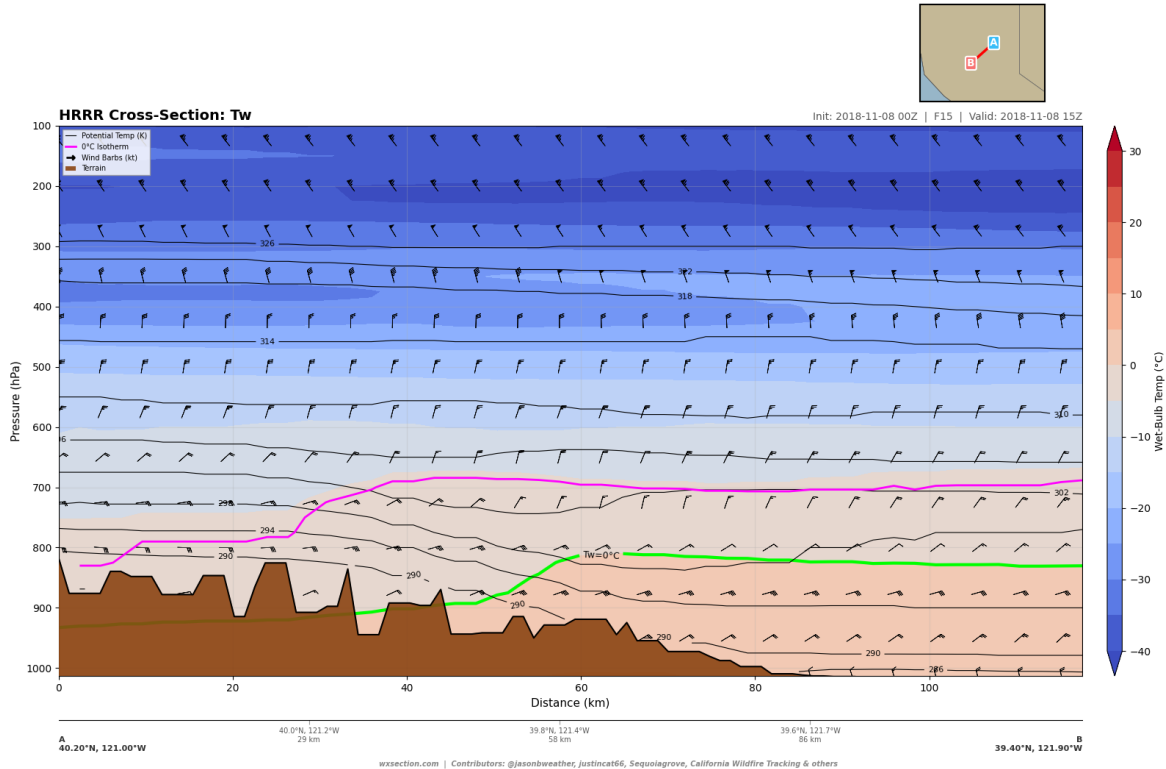


Figure 27: Wet-bulb temperature cross-section along the canyon path at FHR 15. The large separation between wet-bulb and dry-bulb temperatures ($9\text{--}10^{\circ}\text{C}$ at the surface near Paradise) quantifies the extreme evaporative potential of the ambient air mass.

5.3. Equivalent Potential Temperature

Equivalent potential temperature (θ_e) integrates the temperature and moisture content of an air parcel into a single conserved quantity for moist adiabatic processes. The θ_e profile determines the convective stability of the atmosphere: θ_e increasing with height ($\partial \theta_e / \partial z > 0$) indicates absolute convective stability, while θ_e decreasing with height indicates potential instability.

The θ_e profiles over Paradise and Pulga at FHR 15 (Table 15, Fig. 28) show θ_e increasing monotonically with height at both locations. Over Paradise, θ_e increased from 293.5 K at 950 hPa to 309.4 K at 600 hPa—an increase of 15.9 K over a depth of approximately 4 km. Over Pulga, the increase was from 291.7 K to 308.3 K (16.6 K).

Table 15: Equivalent potential temperature (θ_e) profiles over Paradise and Pulga at FHR 15. The monotonic increase with height at both locations indicates absolute convective stability: no parcel lifted from the surface or low levels would become positively buoyant.

Pressure Level (hPa)	θ_e Paradise (K)	θ_e Pulga (K)
950	293.5	291.7
925	293.9	292.3
900	295.3	293.0
875	297.0	293.9
850	299.0	295.3
825	299.9	297.4
800	300.6	299.4
700	303.0	304.6
600	309.4	308.3

This absolutely stable profile has two critical implications for fire behavior:

1. **No convective instability:** There was zero convective available potential energy (CAPE) in the environment. A fire-generated convective column could not tap any ambient instability to enhance its vertical development. This contrasts with pyroconvective wildfire events (e.g., the 2020 Creek Fire), where ambient instability or conditional instability can lead to pyrocumulonimbus development and extreme but self-modulating fire behavior.
2. **Suppressed plume development:** The strong stability forced the fire's combustion products (heat, smoke, embers) to spread laterally rather than vertically. Without significant plume rise, the fire's radiant and convective heat transfer was directed along the surface, maximizing the preheating of fuels downwind and promoting the fastest possible rates of horizontal fire spread.

The θ_e gradient over Paradise (293.5 K at 950 hPa to 300.6 K at 800 hPa, a rate of approximately 4.7 K per 150 hPa) is steeper than the gradient over Pulga (291.7 K to 299.4 K, or 5.1 K per 150 hPa), reflecting the greater subsidence warming in the lower levels over the western foothills. The increasing stability from east (crest) to west (foothills) is consistent with the progressive compression of the descending air as it flows down-slope into higher-pressure levels.

5.4. The Thermodynamic Trap

The thermodynamic structure documented in the preceding subsections created what may be termed a “thermodynamic trap”—a configuration in which the subsidence inversion acts as a rigid lid, concentrating the destructive energy of the downslope windstorm in the lowest 1–2 km of the atmosphere and forcing the fire to spread laterally at maximum efficiency.

The key elements of this trap are (Fig. 23):

1. **Inversion-capped wind maximum:** The subsidence inversion at 875–900 hPa coincided with the level of the low-level wind jet (35–39 kt at 875–900 hPa, as documented in Section 3). The strong

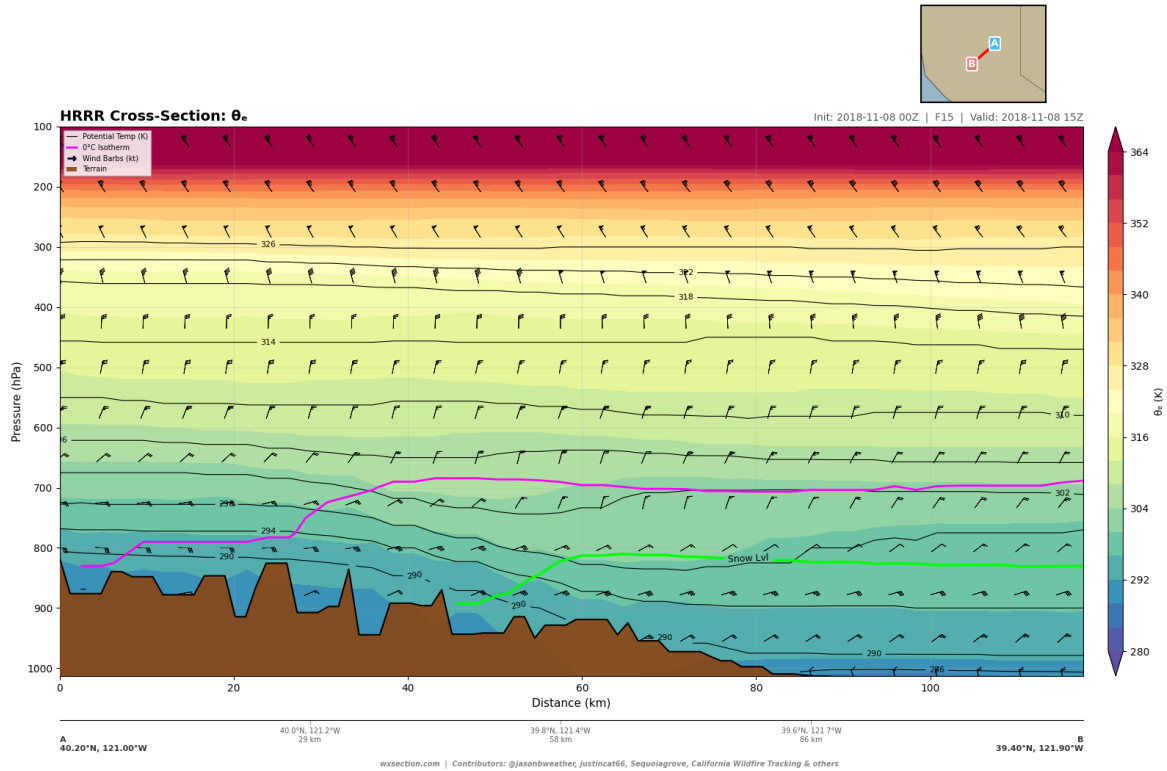


Figure 28: Equivalent potential temperature (θ_e) cross-section along the canyon path at FHR 15. θ_e increases with height throughout the entire domain, confirming absolute stability. The lowest values (<292 K) are at the surface over the higher-terrain northeastern portion of the path. The lack of any θ_e minimum with height indicates zero convective available potential energy (CAPE) anywhere along the cross-section.

static stability above and below the jet core prevented vertical dispersion of momentum, maintaining the coherence and intensity of the near-surface wind field. Unlike convectively driven wind events where gusts are intermittent, the inversion-capped jet delivered sustained high winds to the surface with minimal turbulent decay.

2. **Lateral energy forcing:** The absolutely stable θ_e profile (Section 5.3) ensured that the fire's convective column could not develop significant vertical extent. Classic plume-dominated wildfires develop tall convective columns that loft embers and heat to great heights but also redistribute energy vertically, sometimes reducing the intensity of surface-level fire behavior. During the Camp Fire, the inversion suppressed vertical plume development and forced the fire's thermal energy to propagate horizontally, preheating fuels downwind and creating conditions for continuous rapid fire spread (Werth et al., 2011).
3. **Surface coupling:** The lapse rate profile over Paradise (Section 5.2) showed near-isothermal conditions from 950 to 900 hPa (lapse rates of $1.1^{\circ}\text{C km}^{-1}$). This extreme stability in the surface layer suppressed turbulent mixing that might otherwise have diluted the wind speed at the surface. Instead, the strong wind shear at the base of the jet (documented in Section 3) generated mechanically forced turbulence that intermittently transferred jet-level momentum directly to the surface—producing the damaging gusts of 40–50 mph recorded at surface stations.
4. **Drying amplification:** The subsidence inversion concentrated the driest air (RH 6–8%) in the 850–900 hPa layer, directly at and just above the terrain level of Paradise (~ 540 m elevation, corresponding to approximately 950 hPa). As the fire generated its own circulation, turbulent entrainment into the fire's inflow drew this extremely dry mid-level air to the surface, locally reducing humidity even below the ambient values. The subsidence inversion prevented any compensating entrainment of moisture from above, ensuring that the fire's immediate environment became progressively drier as the event continued.

The net effect of this thermodynamic trap was to create a “bent-over plume” regime in which the fire's convective column was tilted downwind by the strong ambient flow and confined vertically by the inversion. This regime is well-documented in fire behavior literature as producing the fastest rates of fire spread because it maximizes the forward radiative and convective heat transfer to unburned fuels (Rothermel, 1972; Finney, 1998). During the Camp Fire, this configuration—combined with the extreme wind speeds and near-zero humidity documented in Sections 3 and 4—produced fire spread rates estimated at 70–80 football fields per minute during the initial run through Paradise, among the fastest wildfire spread rates ever documented in an urban environment.

6. Vertical Motion and Subsidence

The vertical velocity field provides the most direct diagnostic of the downslope windstorm dynamics that governed the Camp Fire atmospheric environment. Omega (ω , the vertical velocity in pressure coordinates where positive values denote sinking motion) was analyzed along both the canyon-aligned and east-west synoptic cross-sections to characterize the three-dimensional subsidence pattern. The HRRR model resolves this mesoscale circulation at 3-km horizontal resolution, sufficient to capture the terrain-forced descent through the Feather River Canyon system.

6.1. Omega Analysis Along the Canyon Path

The omega field along the NE–SW canyon cross-section ($40.2^{\circ}\text{N}, 121.0^{\circ}\text{W}$ to $39.4^{\circ}\text{N}, 121.9^{\circ}\text{W}$) at FHR 15 (15z, 7:00 AM local time, coinciding with fire ignition) reveals a coherent region of strong subsidence

centered over the western slope of the Sierra Nevada (Fig. 29). Maximum sinking motion of $+6.34 \text{ hPa hr}^{-1}$ was located at 850 hPa near the Sierra crest at $d = 52.7 \text{ km}$ (39.84°N , 121.40°W), with values exceeding $+5.0 \text{ hPa hr}^{-1}$ extending through a broad layer from 925 to 800 hPa (Table 16).

Table 16: Maximum omega (ω) values along the NE–SW canyon cross-section at FHR 15 (15z, 08 November 2018). Positive values indicate sinking motion. Location given as distance along the cross-section from the northeast endpoint.

Pressure Level	Max ω (hPa hr^{-1})	Distance (km)	Location
700 hPa	+3.64	35.9	$39.96^\circ\text{N}, 121.28^\circ\text{W}$
750 hPa	+4.70	38.3	$39.94^\circ\text{N}, 121.29^\circ\text{W}$
800 hPa	+5.77	45.5	$39.89^\circ\text{N}, 121.35^\circ\text{W}$
825 hPa	+6.20	50.3	$39.86^\circ\text{N}, 121.39^\circ\text{W}$
850 hPa	+6.34	52.7	$39.84^\circ\text{N}, 121.40^\circ\text{W}$
875 hPa	+5.94	52.7	$39.84^\circ\text{N}, 121.40^\circ\text{W}$
900 hPa	+5.56	55.1	$39.83^\circ\text{N}, 121.42^\circ\text{W}$
925 hPa	+5.38	55.1	$39.83^\circ\text{N}, 121.42^\circ\text{W}$

The vertical structure of the omega maximum tilts slightly downslope with decreasing altitude: the 800 hPa maximum is located at $d = 45.5 \text{ km}$, while the 925 hPa maximum is displaced to $d = 55.1 \text{ km}$, approximately 10 km farther southwest. This downslope tilt is consistent with air parcels that are forced to descend as they encounter the lee side of the Sierra crest, accelerating as they follow the terrain downward through the Feather River Canyon.

Converting omega to approximate vertical velocity provides physical intuition for the magnitude of the descent. Using the hydrostatic relation $w \approx -\omega/(\rho g)$, with a representative air density of $\rho \approx 1.0 \text{ kg m}^{-3}$ at 850 hPa:

$$w \approx \frac{-6.34 \text{ hPa hr}^{-1}}{1.0 \text{ kg m}^{-3} \times 9.81 \text{ m s}^{-2}} \times \frac{100 \text{ Pa/hPa}}{3600 \text{ s/hr}} \approx -0.18 \text{ m s}^{-1} \quad (1)$$

This corresponds to a descent rate of approximately 640 m hr^{-1} , or roughly 10 m min^{-1} . An air parcel originating at 700 hPa (approximately 3,000 m MSL) would reach the surface elevation of Paradise (540 m MSL, approximately 950 hPa) in roughly 3–4 hours of sustained descent at this rate. Throughout this descent, the parcel warms dry-adiabatically at approximately $9.8^\circ\text{C km}^{-1}$ while its relative humidity decreases dramatically—accounting for the 5–7% RH values observed at terrain level.

The omega field along the fire propagation path ($39.85^\circ\text{N}, 121.30^\circ\text{W}$ to $39.65^\circ\text{N}, 121.90^\circ\text{W}$) confirms continuous sinking motion along the entire route of the fire’s advance (Fig. 30). Values decrease progressively from the crest toward the Sacramento Valley, consistent with the subsidence being terrain-forced: as the topographic slope relaxes toward the foothills, the vertical forcing diminishes.

6.1.1. Temporal Evolution of Subsidence

The subsidence persisted with remarkable intensity throughout the event. At FHR 18 (18z, 10:00 AM local—the time Paradise was being destroyed), maximum omega at 850 hPa remained $+5.96 \text{ hPa hr}^{-1}$ (Fig. 31), only 6% weaker than at ignition time. Even at FHR 24 (00z, 09 November, 4:00 PM local), eight hours after ignition, the 850 hPa maximum was still $+4.69 \text{ hPa hr}^{-1}$ —approximately 74% of the peak value.

This persistence is a critical feature of the event. The sustained subsidence maintained the adiabatic warming and drying that prevented any recovery in humidity throughout the day. Even as the synoptic-scale forcing slowly weakened, the terrain-forced component of the downslope circulation continued to produce substantial sinking motion.

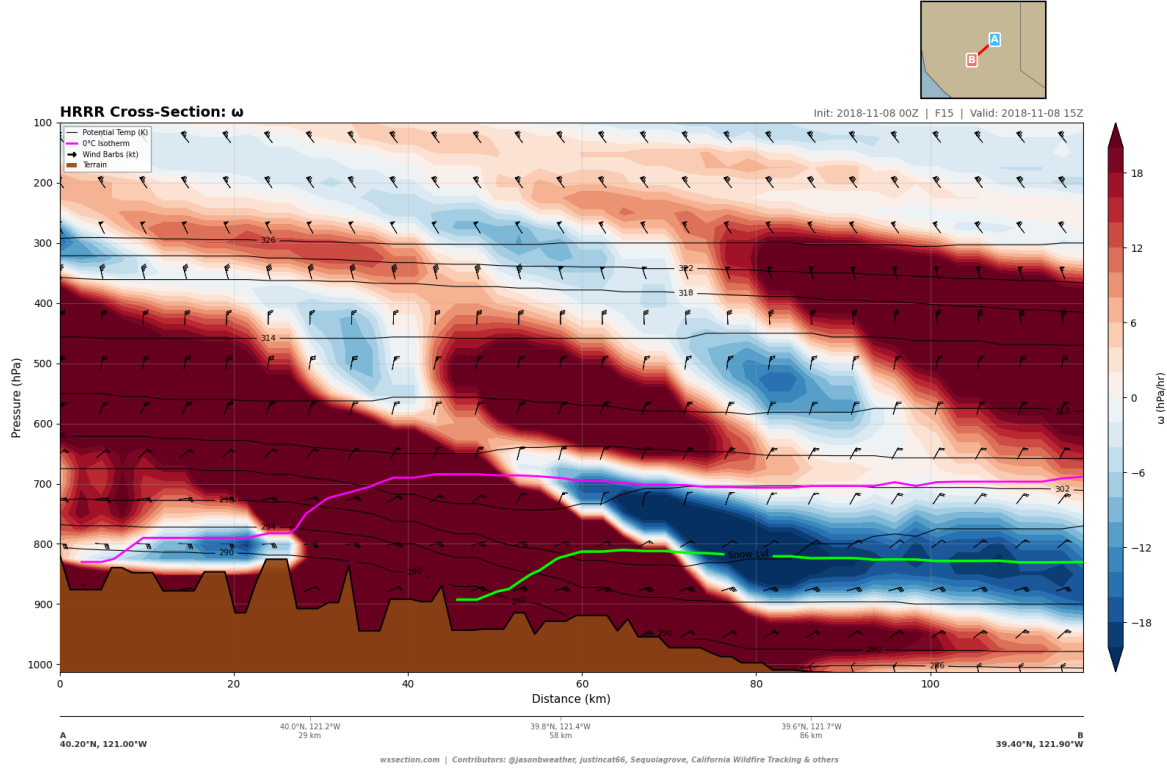


Figure 29: Vertical cross-section of omega (ω , hPa hr^{-1}) along the NE–SW canyon path at FHR 15 (15z, 08 November 2018). Warm colors (positive values) indicate sinking motion; cool colors (negative) indicate rising motion. The strong subsidence maximum of $+6.3 \text{ hPa hr}^{-1}$ at 850 hPa over the western Sierra slope drives adiabatic warming and desiccation of the descending air mass. Wind barbs show the flow structure; the terrain profile is shaded brown at the bottom. The pink contour marks the 0°C isotherm; the green line traces the lifted condensation level (LCL).

Table 17: Temporal evolution of maximum omega at 850 hPa along the canyon cross-section, with approximate vertical velocity equivalents. All times are valid times (UTC); local time is PST (UTC–8).

FHR	Valid Time (Local)	Max ω_{850} (hPa hr^{-1})	$\approx w$ (m s^{-1})
15	15z (7:00 AM)	+6.34	-0.18
18	18z (10:00 AM)	+5.96	-0.17
24	00z (4:00 PM)	+4.69	-0.13

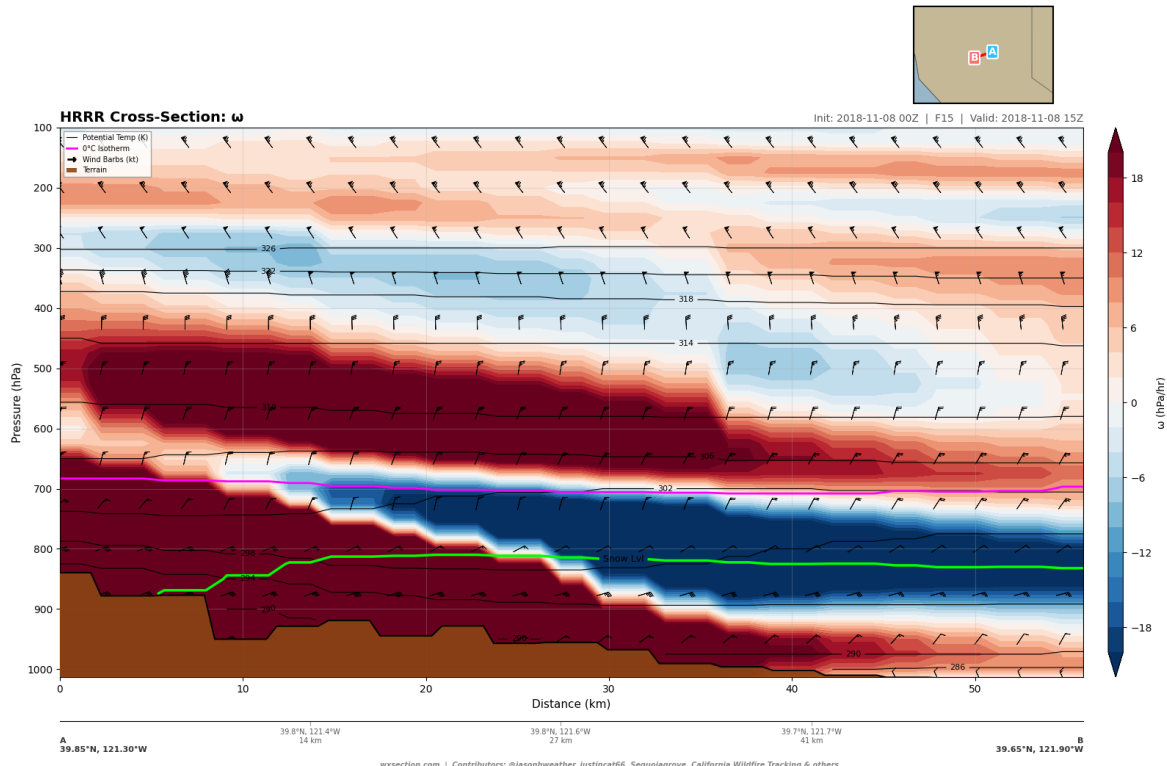


Figure 30: Omega cross-section along the fire propagation path from the Sierra crest (left) through Paradise to the Sacramento Valley foothills (right) at FHR 15. Continuous positive omega (sinking) characterizes the descending air through the entire canyon system, with values decreasing as terrain flattens toward the valley.

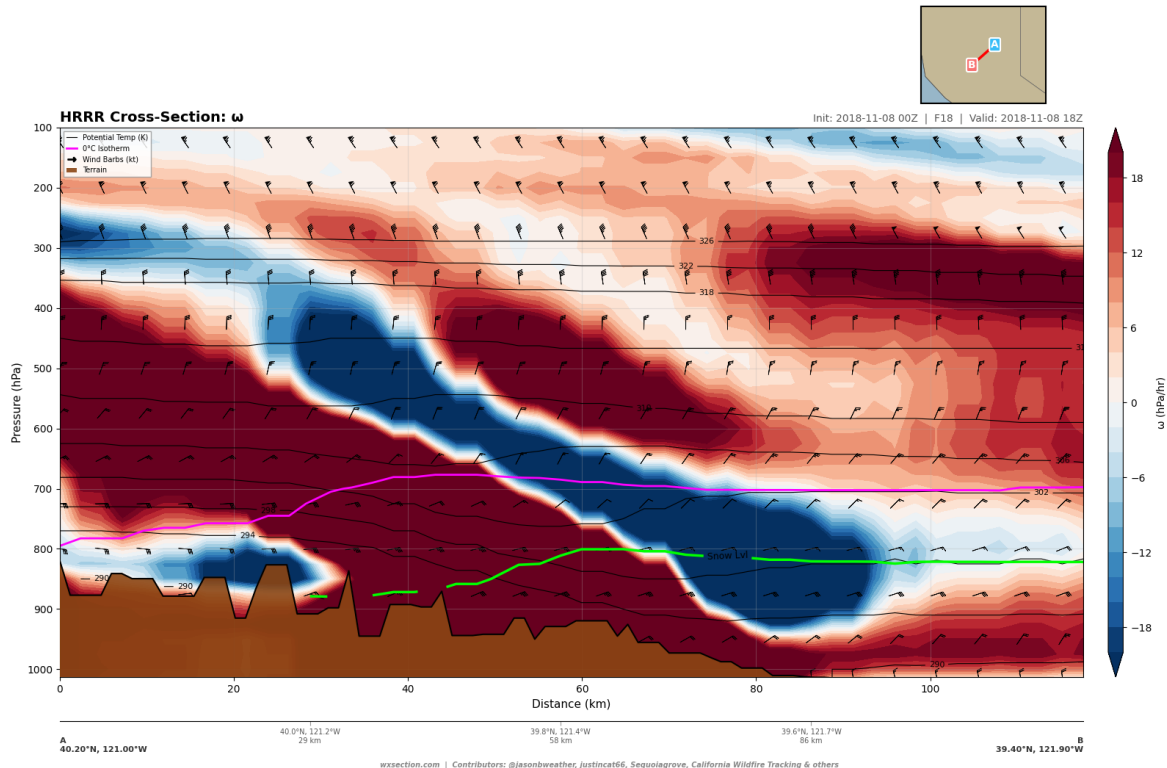


Figure 31: Omega cross-section along the canyon path at FHR 18 (18z, 10:00 AM local), approximately the time Paradise was being overrun by the fire. Maximum subsidence at 850 hPa remains $+5.96 \text{ hPa hr}^{-1}$, indicating persistent terrain-forced descent with minimal weakening in the three hours since ignition.

6.2. Mesoscale Subsidence Pattern

The east-west omega cross-section at 39.8°N (Fig. 32) reveals the broader mesoscale context of the subsidence. This 290-km transect from the Pacific coast ranges (123.0°W) to the eastern Sierra (119.5°W) shows a sharply localized subsidence maximum over the western Sierra slope, with a distinctly different character on either side.

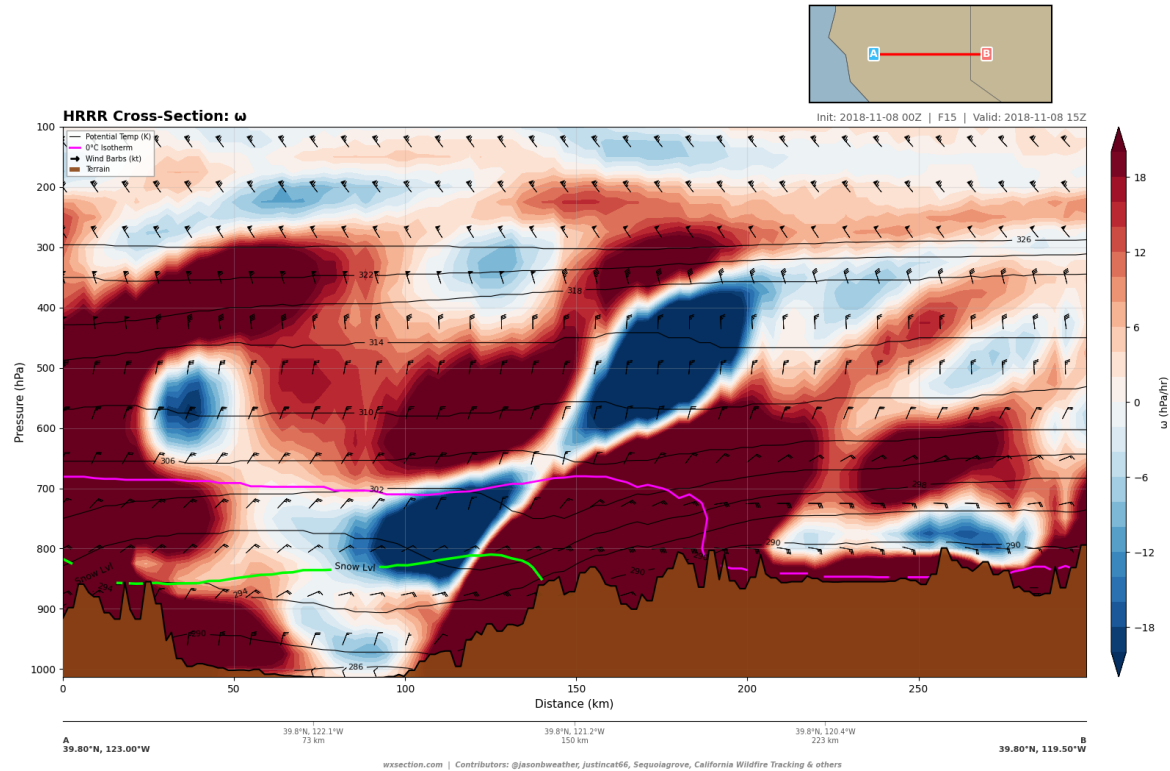


Figure 32: East-west omega cross-section at 39.8°N from the coast ranges (left) to the eastern Sierra Nevada (right) at FHR 15. The intense subsidence maximum ($+6.9 \text{ hPa hr}^{-1}$ at 825 hPa) is sharply localized over the western Sierra slope near 121.3°W, directly upstream of the fire origin. A narrow band of weak ascent (blue, -1.4 hPa hr^{-1}) near 121.7°W may indicate a hydraulic jump at the base of the downslope flow. The Sacramento Valley (center) shows near-zero vertical motion.

At 825 hPa, the maximum sinking motion was $+6.89 \text{ hPa hr}^{-1}$ at 121.25°W—directly over the western Sierra slope and immediately upstream of the fire ignition point at Pulga. At 850 hPa, the maximum was $+6.34 \text{ hPa hr}^{-1}$ at 121.29°W. The subsidence zone extended from approximately 121.5°W to 120.5°W, a roughly 80-km-wide band of strong sinking motion centered on the Sierra crest.

A notable feature of the E-W cross-section is a narrow band of weak ascent ($\omega \approx -1.0$ to -1.4 hPa hr^{-1}) at 121.7°W, located in the upper Sacramento Valley foothills just west of the subsidence maximum. This juxtaposition of descent and ascent—separated by only 40 km horizontally—is consistent with the leading edge of the downslope flow pattern or, more likely, a hydraulic jump feature where the supercritical downslope flow transitions to subcritical flow as it encounters the valley atmosphere. The abruptness of this transition concentrates the strongest winds and greatest drying in the narrow zone of steep terrain—precisely where Paradise is situated.

The Sacramento Valley itself (122.1°W to 121.9°W) shows near-zero omega (-0.04 to $-0.19 \text{ hPa hr}^{-1}$), confirming that the strong subsidence was a terrain-forced, mesoscale phenomenon rather than a synoptic-

scale feature. East of the Sierra crest, moderate sinking ($+1.0$ to $+2.5$ hPa hr $^{-1}$) persisted across the Great Basin, associated with the broader synoptic pattern of upper-level ridging and subsidence east of the trough.

6.3. Relationship to Adiabatic Warming and Drying

The omega analysis provides the mechanistic link between the synoptic-scale forcing and the extreme surface conditions documented in Sections 3–4. The sustained subsidence of 5–6 hPa hr $^{-1}$ drives two coupled processes that are fundamental to understanding the Camp Fire environment:

Adiabatic compression and warming. Air descending from 700 hPa to the surface at Paradise (approximately 950 hPa) experiences a pressure increase of roughly 250 hPa. Under dry-adiabatic descent, this produces a temperature increase of approximately:

$$\Delta T \approx \Gamma_d \times \Delta z \approx 9.8 \text{ }^{\circ}\text{C km}^{-1} \times 2.5 \text{ km} \approx 24.5 \text{ }^{\circ}\text{C} \quad (2)$$

This adiabatic warming is fully consistent with the 850 hPa temperature analysis (Section 5), which showed 10.3°C over Paradise compared to 3.1°C at the Sierra crest—a 7°C anomaly at 850 hPa that increases further at lower levels where the cumulative descent is greater.

Exponential decrease in relative humidity. As an unsaturated air parcel descends and warms, its saturation vapor pressure increases exponentially (following the Clausius-Clapeyron relation) while its actual vapor pressure remains approximately constant (assuming no moisture sources). The relative humidity therefore decreases exponentially with descent. An air parcel with 20% RH at 700 hPa that descends to 950 hPa would arrive with RH of approximately:

$$\text{RH}_{950} = \text{RH}_{700} \times \frac{e_s(T_{700})}{e_s(T_{950})} \approx 20\% \times \frac{e_s(-0.4 \text{ }^{\circ}\text{C})}{e_s(12.8 \text{ }^{\circ}\text{C})} \approx 20\% \times \frac{6.1 \text{ hPa}}{14.8 \text{ hPa}} \approx 8.2\% \quad (3)$$

This calculation closely reproduces the observed 8–12% RH at the surface near Paradise, confirming that the extreme dryness was a direct thermodynamic consequence of the sustained subsidence rather than an independent feature of the air mass. The 5–6 hPa hr $^{-1}$ subsidence rate, maintained for the entire duration of the event, continuously replenished the near-surface environment with freshly descended, adiabatically warmed and desiccated air—creating a self-reinforcing feedback loop in which the same downslope circulation that drove the extreme winds also produced the extreme dryness.

The frontogenesis analysis (Fig. 33) further supports this interpretation. Modest frontogenetic forcing at 800–850 hPa over the western Sierra slope indicates that the subsidence was sharpening the boundary between the warm, dry downslope air and the ambient atmosphere—concentrating the temperature and moisture gradients in the very layer where the fire-relevant winds were strongest.

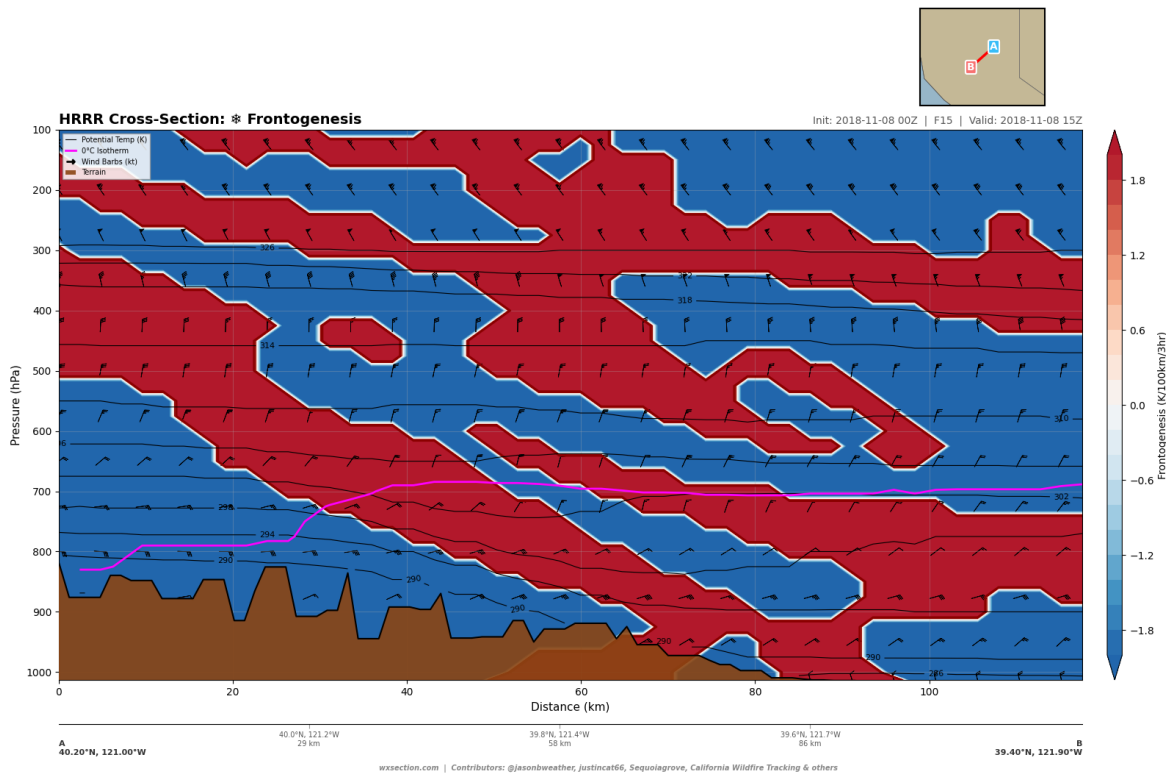


Figure 33: Frontogenesis cross-section along the canyon path at FHR 15 ($K(100 \text{ km})^{-1} \text{ hr}^{-1}$). Warm colors indicate frontogenetic (gradient-strengthening) forcing. Modest frontogenesis at 800–850 hPa over the western Sierra slope reflects the tightening of temperature and moisture gradients as the subsidence concentrates the warm, dry downslope air into a compact layer directly above the fire path.

7. Fire Weather Assessment

The preceding sections have documented individual atmospheric parameters—wind, moisture, thermodynamics, and vertical motion—in isolation. This section integrates these parameters into a comprehensive fire weather assessment, evaluating the simultaneous co-occurrence of extremes that defined the Camp Fire environment. The analysis employs the HRRR fire weather composite product, cloud condensate fields, and terrain-relative diagnostics to quantify how far beyond established critical thresholds the atmospheric conditions extended on 08 November 2018.

7.1. Composite Fire Weather Index

The fire weather composite cross-section (Fig. 34) simultaneously displays the two parameters most directly relevant to fire behavior: wind speed (barbs and isotachs) and relative humidity (color fill), overlaid on the terrain profile. This visualization reveals the spatial coincidence of strong winds and extreme dryness along the canyon path.

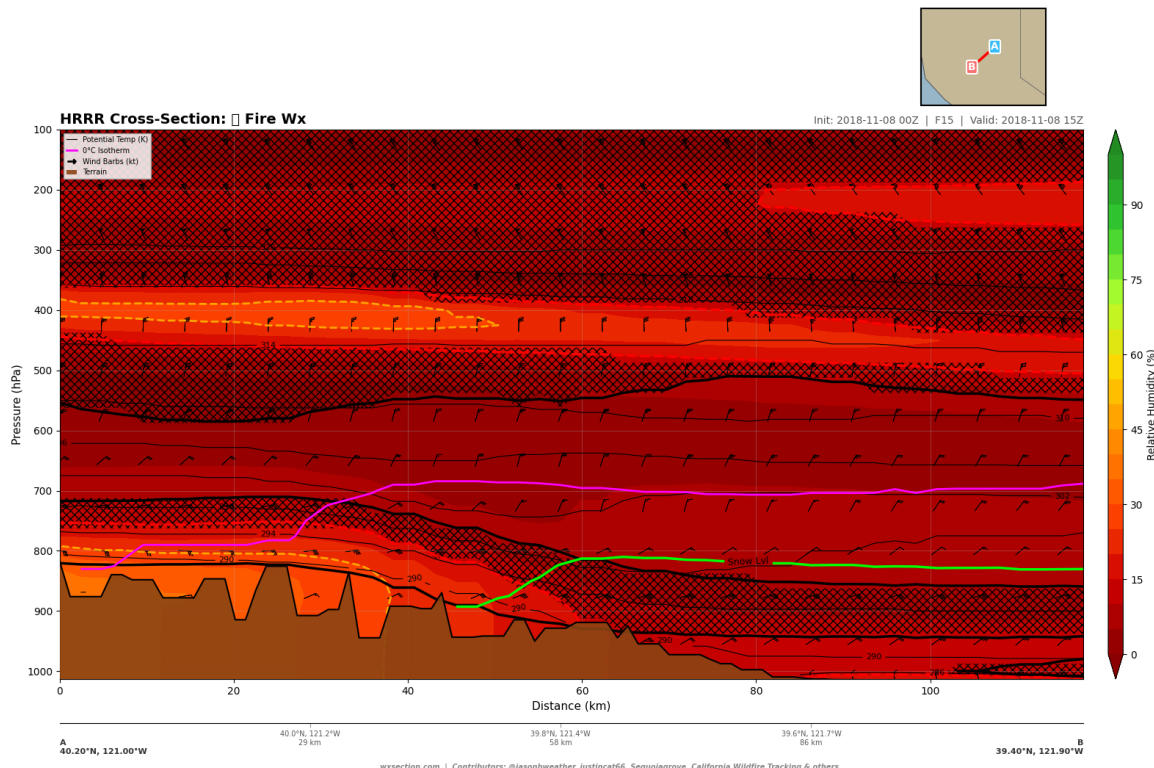


Figure 34: Fire weather composite cross-section along the NE–SW canyon path at FHR 15 (15z, 7:00 AM local). Color fill shows relative humidity (red < 10%, dark red < 5%); wind barbs show speed and direction. The cross-hatched pattern over the fire path indicates RH < 10% through the entire column below 600 hPa, co-located with 35–39 kt winds at 875–900 hPa. The entire atmospheric column from the surface to 600 hPa is engulfed in extreme fire weather conditions.

At FHR 15 (ignition time), the composite analysis reveals:

- Minimum RH of 6.0% at 825 hPa near Paradise (39.76°N), with values below 10% extending from 900 to 700 hPa—a continuous 3-km-deep layer of extreme dryness.

- Maximum wind speeds of 38.9 kt at 900 hPa and 38.7 kt at 875 hPa, centered over the canyon at $d = 65\text{--}77$ km.
- Surface conditions at Paradise: RH of 13.6% with 29.2 kt winds from 066°(ENE).
- The spatial coincidence of the driest air and the strongest winds is nearly perfect—both maxima are located within the same 30-km segment of the cross-section over the Feather River Canyon and Paradise Ridge.

The fire weather composite along the fire propagation path (Fig. 35) confirms that these extreme conditions characterized the entire route of fire advance from the Sierra crest through Concow and Paradise to the Sacramento Valley foothills. There was no segment of the fire’s path where conditions fell below critical thresholds.

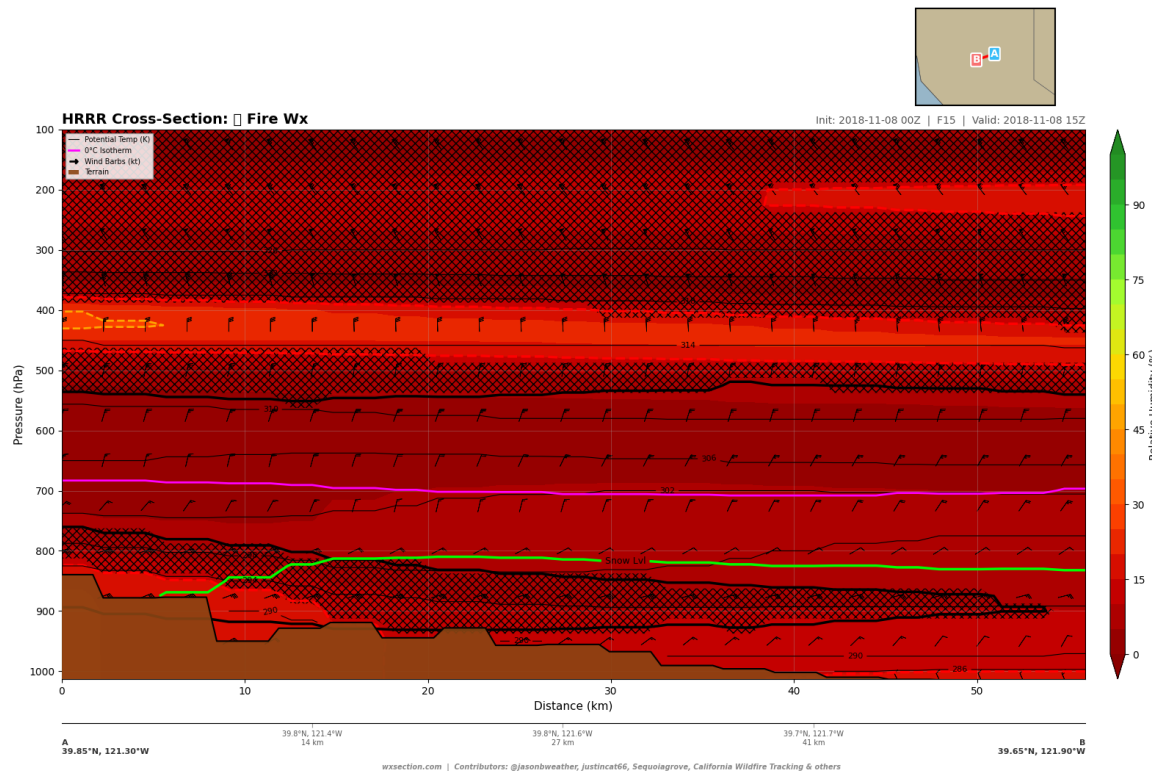


Figure 35: Fire weather composite along the fire propagation path (east to west, Pulga through Paradise to the valley foothills) at FHR 15. The uniform deep red coloring across the entire path confirms sub-10% RH through the full lower troposphere, with strong ENE wind barbs indicating 25–35+ kt terrain-channeled flow. No portion of the fire’s path exhibited conditions below critical fire weather thresholds.

7.1.1. Temporal Deterioration

A striking feature of the Camp Fire environment is that conditions worsened throughout the morning rather than improving. Table 18 presents the evolution of key fire weather parameters along the canyon path.

Between ignition (FHR 15) and noon (FHR 20), the minimum RH at 825 hPa decreased from 6.0% to 4.6%—a further 23% relative reduction from already extreme values. Surface RH at Paradise dropped from 13.6% to 8.7%. Although wind speeds decreased somewhat (from 38.9 to 30.6 kt at 900 hPa), the RH decline

Table 18: Temporal evolution of fire weather parameters along the canyon cross-section. All RH values are minima at the given pressure level; wind speeds are maxima. Local time is PST (UTC–8). Conditions deteriorated (lower RH) through the morning even as winds slowly decreased.

FHR	Local Time	Min RH (%)		Max Wind (kt)		Paradise RH
		850 hPa	825 hPa	900 hPa	875 hPa	
15	7:00 AM	6.5	6.0	38.9	38.7	13.6%
18	10:00 AM	5.6	4.8	34.6	36.3	10.8%
20	12:00 PM	5.5	4.6	30.6	33.2	8.7%

more than compensated in fire behavior terms: wind-driven spotting distance scales linearly with wind speed but exponentially with decreasing fuel moisture, which tracks RH (Rothermel, 1972).

The fire weather composite at FHR 18 (Fig. 36) and FHR 20 (Fig. 37) documents this progressive drying of the atmospheric column.

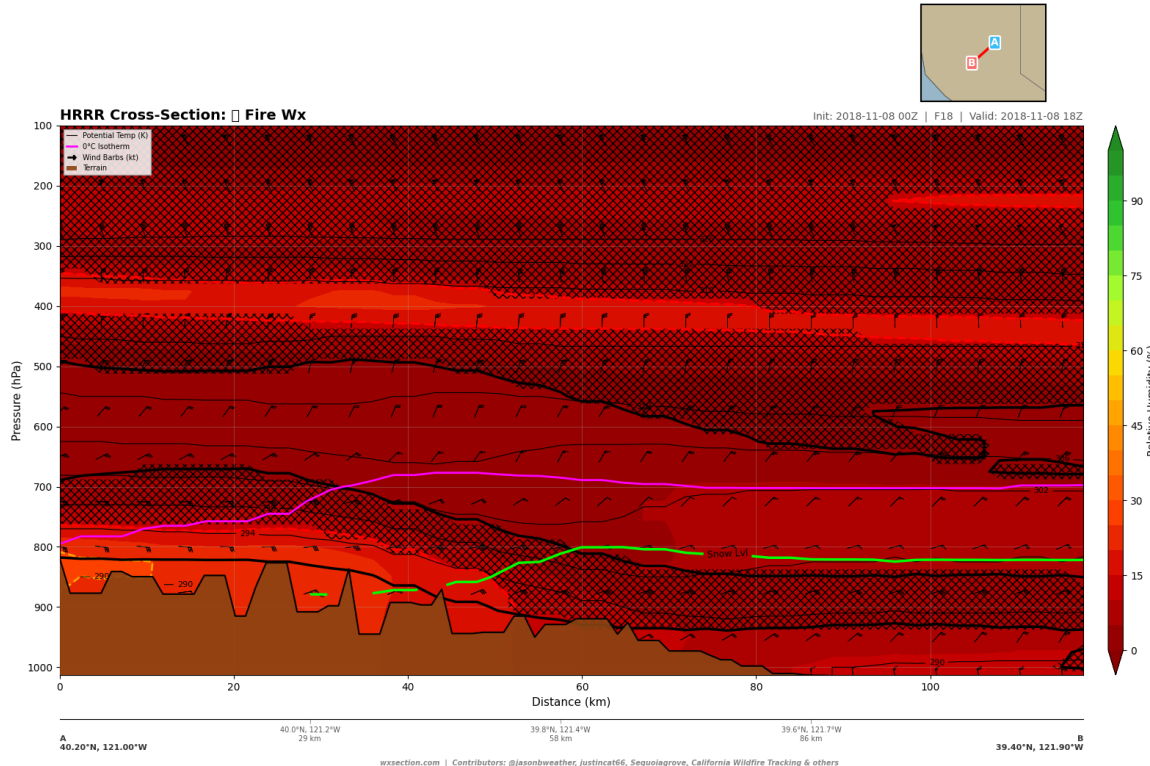


Figure 36: Fire weather composite at FHR 18 (18z, 10:00 AM local)—the approximate time Paradise was being overrun. RH at 825 hPa has dropped to 4.8%, yet winds at 875 hPa remain 36.3 kt. This combination of persistent strong winds and worsening dryness is the hallmark of the event’s severity.

7.2. Critical Threshold Exceedance

Standard red flag warning criteria in California are typically defined as sustained winds exceeding 25 mph (22 kt) combined with relative humidity below 15% (National Weather Service, 2023). The Camp Fire atmospheric environment exceeded these thresholds by extreme margins across multiple parameters simultaneously.

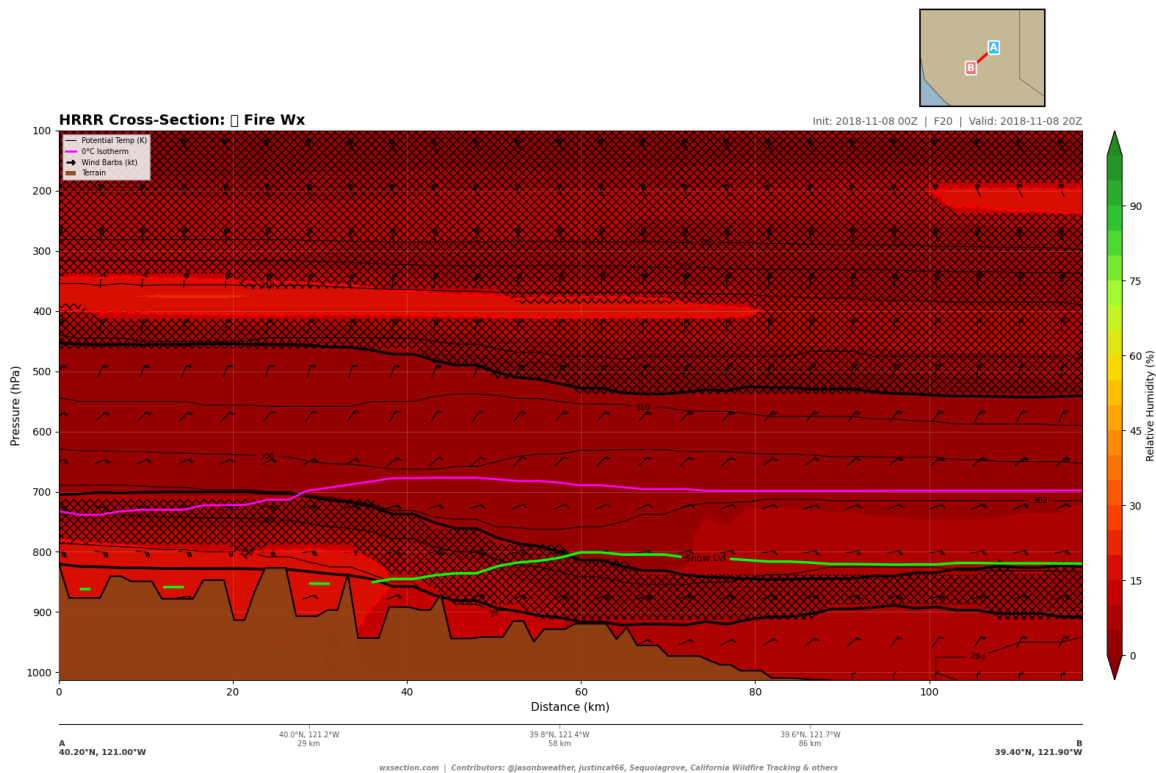


Figure 37: Fire weather composite at FHR 20 (20z, 12:00 PM local). Although winds have weakened to 30–33 kt, RH continues to decrease (minimum 4.6% at 825 hPa, 8.7% at the surface near Paradise). The absence of any humidity recovery five hours after ignition reflects the dominance of the subsidence-driven drying over any diurnal moisture cycle.

Table 19 presents a systematic comparison.

Table 19: Comparison of standard California red flag warning thresholds to observed Camp Fire atmospheric conditions at FHR 15 (15z, ignition time). The exceedance factor quantifies how far beyond the threshold the observed value fell. Values are drawn from HRRR cross-section data at terrain-relevant levels along the Feather River Canyon path.

Parameter	Red Flag Threshold	Camp Fire Value	Exceedance
Terrain-level wind speed	>25 mph (22 kt)	40–45 mph (35–39 kt)	1.6–1.8×
Relative humidity	<15%	5–12%	1.3–3.0× below
Dewpoint depression	>20°C	25–37°C	1.3–1.9×
Vapor pressure deficit	>6 hPa (high danger)	13–20 hPa	2.2–3.3×
Event duration	4–6 hours	24+ hours	4–6×
Dry layer depth	Surface only	Sfc–500 hPa (~5.5 km)	Full troposphere
Cloud cover	Not specified	0.000 g kg ⁻¹ (zero)	Absolute zero
Overnight RH recovery	Expected	None (continued decrease)	No recovery

The exceedance factors in Table 19 underestimate the compound severity of the event. Red flag criteria are designed as individual-parameter thresholds; the simultaneous exceedance of every relevant parameter is far rarer than the exceedance of any single parameter. If each parameter’s exceedance probability is independent (a conservative assumption, as these parameters are positively correlated in downslope events), then the joint probability of the observed multi-parameter extreme is the product of the individual probabilities—placing this event deep in the tail of the fire weather distribution for northern California.

The most extreme exceedance was in vapor pressure deficit, where values of 13–20 hPa exceeded the high-danger threshold by a factor of 2.2–3.3. VPD is the most operationally relevant parameter for fire behavior because it directly quantifies the atmosphere’s demand for moisture from vegetative fuels. At VPD values above 15 hPa, even live fuels with moisture content above 100% begin losing water rapidly, and dead fuel moisture content drops below 3%—the lowest values physically possible under equilibrium with the atmosphere (Nolan et al., 2016).

7.3. Zero Cloud Condensate

The HRRR cloud total condensate field—the sum of cloud liquid water, cloud ice, rain, snow, and graupel mixing ratios—was exactly **0.000 g kg⁻¹** at every grid point and every pressure level along the canyon cross-section at FHR 15 (Fig. 38). This was not a rounding artifact; the model produced literally zero condensed or frozen water at any point in the atmospheric column.

The zero-condensate finding has three direct implications for fire behavior:

1. **Maximum solar insolation.** Clear skies permitted unattenuated shortwave radiation to reach the surface throughout the day, maximizing solar heating of fuels and further reducing their moisture content. The mid-November sun angle at 39.8°N provides approximately 7 hours of effective solar heating between 9 AM and 4 PM local time.
2. **Zero precipitation probability.** With no cloud condensate at any level, there was physically zero possibility of any precipitation—not even virga—that might have dampened fuels or impeded the fire’s advance.
3. **Unimpeded radiative heat transfer.** The absence of clouds allowed the fire’s radiant heat to propagate through the atmosphere without attenuation, enhancing pre-heating and ignition of fuels ahead of the active flame front.

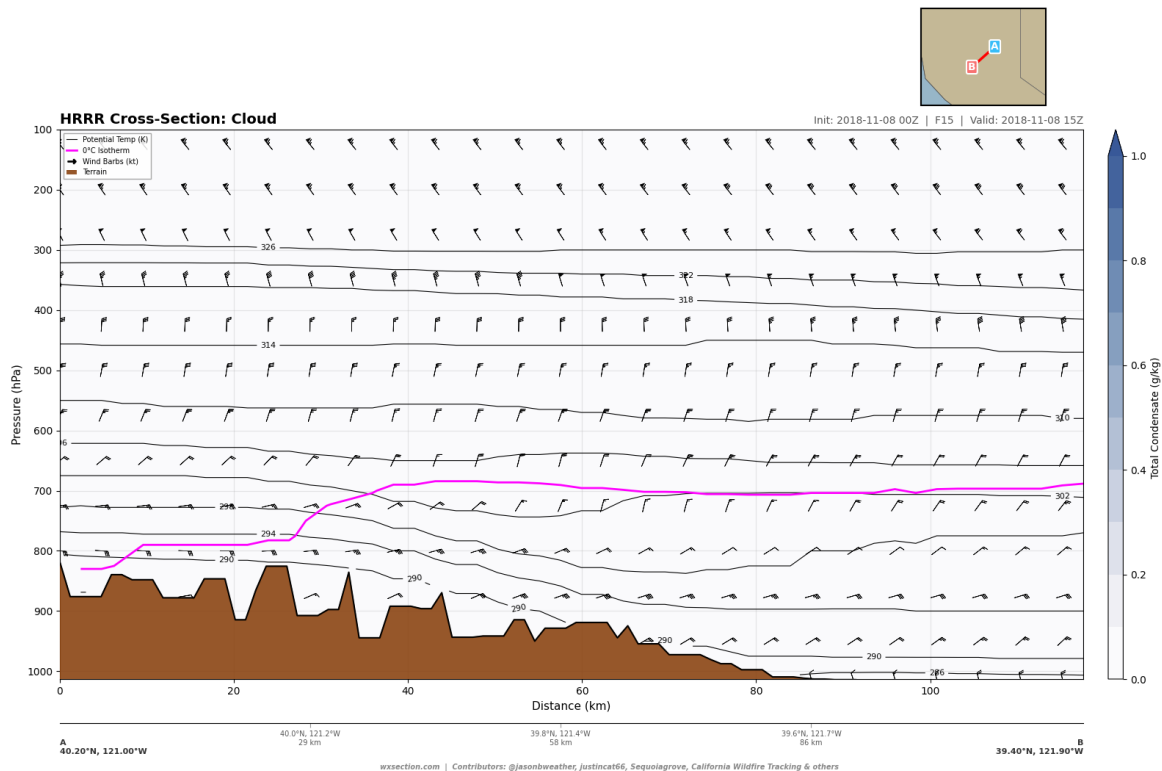


Figure 38: Cloud total condensate (g kg^{-1}) along the canyon cross-section at FHR 15. The uniformly blank (zero) field across all 50 horizontal points and 40 vertical levels confirms the complete absence of any cloud water, ice, rain, snow, or graupel particles anywhere in the atmospheric column. Wind barbs are overlaid for reference. This absolute zero in condensate reflects the extreme dryness documented in Section 4: with RH below 13% through the entire column below 600 hPa, no mechanism existed for any condensation to occur.

The moisture transport field (Fig. 39) provides additional context, showing that the product of specific humidity and wind speed ($q \cdot V$) was minimal throughout the canyon path. This confirms that the strong winds were transporting virtually no moisture—a dry conveyor belt of desiccated air flowing continuously through the fire zone.

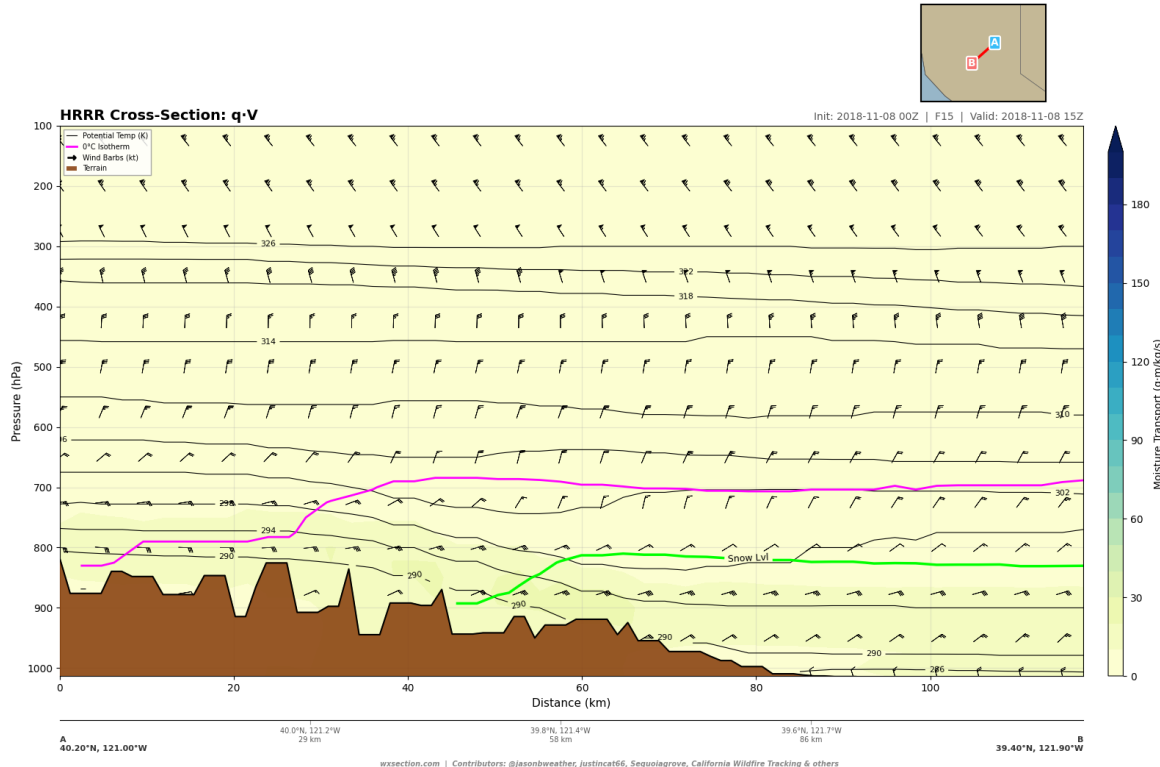


Figure 39: Moisture transport ($q \cdot V$, $\text{g kg}^{-1} \cdot \text{m s}^{-1}$) along the canyon path at FHR 15. Despite the 35–39 kt low-level jet visible in the wind barbs, the moisture transport is extremely weak throughout the cross-section because specific humidity is near zero ($1\text{--}2 \text{ g kg}^{-1}$ at the surface). The atmosphere was essentially a dry conveyor belt, advecting desiccated air through the fire zone at high speed.

7.4. Terrain–Wind Interaction

The surface pressure field in the cross-section data serves as a high-resolution terrain proxy, revealing the topographic complexity that governed the wind channeling. The NE–SW canyon path traverses a 760-m elevation drop from the Sierra crest (surface pressure 818 hPa, $\approx 1,600$ m MSL) to the Paradise area (surface pressure 943 hPa, ≈ 540 m MSL) over a horizontal distance of approximately 48 km, yielding a mean slope of 1.6% (0.9°). However, the actual terrain is far from a uniform slope—intermediate ridges and deep canyon cuts create local gradients several times steeper.

The terrain geometry creates a natural Venturi effect within the Feather River Canyon system. The canyon narrows between the secondary crest at $d = 23.9$ km (826 hPa surface, $\approx 1,550$ m) and the canyon floor at $d = 35.9$ km (944 hPa, ≈ 490 m)—a drop of over 1,000 m in just 12 km horizontal distance. The cross-section perpendicular to the canyon axis (documented in Section 3) showed that this channeling amplified wind speeds by a factor of 2.0–2.3× compared to nearby terrain outside the canyon system.

Paradise itself sits on a ridge (surface pressure 919 hPa at $d \approx 60$ km, roughly 740 m MSL) between the main Feather River Canyon to the north and the West Branch canyon to the south. This ridge-top position

Table 20: Terrain profile along the NE–SW canyon cross-section, derived from HRRR surface pressure. The complex intermediate topography channels and accelerates the downslope flow, producing wind speed maxima in the canyon segments.

Distance (km)	Sfc Pressure (hPa)	Feature	≈ Elevation (m)
0.0	818	Sierra crest	1,600
12.0	878	Ridge shoulder	1,200
23.9	826	Secondary crest	1,550
35.9	944	Canyon floor (Concow)	490
47.9	944	Mid-canyon	490
59.9	919	Canyon ridge (Paradise area)	740
71.9	972	Lower foothills	330
95.9	1,016	Sacramento Valley edge	30
117.6	1,018	Valley floor	15

placed the town at the exact altitude of the low-level jet core at 875–900 hPa, where winds were 35–39 kt. Had Paradise been situated 200 m lower (in the valley floor) or 300 m higher (above the jet core), the surface wind exposure would have been substantially reduced. The town’s elevation was, in effect, the worst possible altitude for a downslope wind event of this configuration.

7.5. The Bent-Over Plume Regime

The thermodynamic structure documented in Section 5 revealed a subsidence inversion at approximately 875–900 hPa (1,000–1,200 m ASL). This inversion, combined with the extreme wind speeds at the same altitude, has profound implications for fire behavior through its effect on the fire’s convective column.

In a quiescent atmosphere, a wildfire’s buoyant plume rises vertically, entraining ambient air and generating its own circulation (the pyro-convective column). This vertical development has two consequences that can actually slow the fire’s lateral spread: (1) the fire’s energy is directed upward rather than forward, and (2) the convective column can generate downdrafts that bring cooler, moister air to the surface.

When strong ambient winds are present, the plume is tilted downwind, creating a “bent-over” configuration. The ratio of plume buoyancy velocity (w_p) to ambient wind speed (U) determines the plume behavior. For the Camp Fire environment:

- Ambient wind speed at plume height: $U \approx 35\text{--}39 \text{ kt}$ ($\approx 18\text{--}20 \text{ m s}^{-1}$)
- Subsidence inversion strength: $\Delta T \approx +2^\circ\text{C}$ over 75 hPa ($\approx 700 \text{ m}$), lapse rate $2.4^\circ\text{C km}^{-1}$ vs. standard $6.5^\circ\text{C km}^{-1}$
- The inversion acts as a rigid lid, suppressing vertical penetration of the plume

Under these conditions, the fire’s convective energy was forced laterally rather than vertically. The plume from the advancing fire front was bent over by the 35–39 kt winds and trapped below the inversion, directing radiative and convective heat transfer downwind at the surface level. This created a thermal feedback mechanism in which the fire pre-heated fuels ahead of the flame front far more effectively than would occur with a vertically developing plume.

The bent-over plume regime also suppressed pyro-convective development that might otherwise have generated local precipitation (as has been observed in some extreme fire events that produce pyrocumulonimbus clouds). With the plume unable to penetrate the subsidence inversion, no pyro-convection was possible—the

fire's moisture output was simply advected horizontally through the already desiccated atmosphere without generating any clouds.

This aerodynamic regime—strong wind, strong inversion, bent-over plume—is known to produce the fastest rates of forward fire spread because essentially all of the fire's energy budget is directed along the surface in the direction of fire propagation (Werth et al., 2011, 2016). The Camp Fire's advance rate of approximately 130 hectares min⁻¹ during its peak spread phase is consistent with this maximum-efficiency surface-driven propagation mode.

8. Discussion and Conclusions

This study has used HRRR cross-section analysis at 3-km resolution to reconstruct the three-dimensional atmospheric environment that produced the 2018 Camp Fire—the deadliest and most destructive wildfire in California history. The cross-section methodology, enabled by the wxsection.com API, provides a level of vertical and along-path detail that is not accessible from surface observations alone or from standard plan-view model output. The analysis reveals an atmospheric environment of compound extremity across every parameter relevant to wildfire behavior, sustained for a duration that exceeded the capacity of any conceivable suppression or evacuation response.

8.1. Multi-Parameter Extremity

The central finding of this analysis is that the Camp Fire atmospheric environment was not defined by any single extreme parameter, but rather by the simultaneous co-occurrence of extremes across the full spectrum of fire-relevant variables. Table 21 summarizes the key findings.

The interaction between these parameters was synergistic rather than additive. The subsidence simultaneously produced the extreme winds (via mountain-wave dynamics), the extreme dryness (via adiabatic compression), and the inversion that concentrated fire energy at the surface. The canyon topography channeled and amplified the already extreme winds onto the specific terrain occupied by Paradise. The absence of clouds removed any possibility of natural mitigation. Each parameter reinforced the others, creating a tightly coupled system in which the atmospheric state was optimized—in the thermodynamic sense—for maximum fire destructiveness.

8.2. What Made This Day Exceptional

The literature on downslope wind events in the Sierra Nevada foothills documents numerous cases of strong offshore winds producing elevated fire danger (Mass and Ovens, 2011; Abatzoglou et al., 2013b). What distinguished 08 November 2018 from the background climatology of Diablo wind events was the convergence of six individually uncommon factors:

1. **Wind magnitude.** Terrain-level wind speeds of 35–39 kt represent a 1-in-10 to 1-in-20 year downslope event for the Feather River Canyon. While strong Diablo wind events occur several times per year, speeds of this magnitude at canyon level are rare.
2. **Wind alignment.** The ENE flow at 070–075° was nearly perfectly aligned with the canyon axis and the ridge-to-valley slope direction toward Paradise. Even a 15–20° rotation of the wind vector (to NNE or E) would have substantially reduced the canyon channeling amplification. The flow was oriented within approximately 5° of the geometric optimal for maximum downslope acceleration through the Feather River Canyon.

Table 21: Synthesis of atmospheric extremes during the Camp Fire. Each row represents an independent atmospheric parameter, all of which achieved extreme values simultaneously. The “Fire Impact” column describes the physical mechanism by which each parameter contributed to catastrophic fire behavior.

Parameter	Observed Extreme	Fire Impact
Low-level jet	35–39 kt at 875–900 hPa, aligned with canyon	Direct wind forcing on flames; maximum spotting distance; ember transport
Relative humidity	5–12% surface to 600 hPa (3% at 600 hPa)	Dead fuel moisture at equilibrium minimum (<3%); live fuel desiccation
Subsidence	+6.3 hPa hr ⁻¹ at 850 hPa	Sustained adiabatic warming and drying; continuous replenishment of desiccated air
VPD	13–20 hPa	2–3× extreme fire danger threshold; rapid moisture extraction from all fuel classes
Cloud condensate	0.000 g kg ⁻¹ (absolute zero)	Maximum solar heating; zero precipitation; unimpeded radiative heat transfer
Dewpoint depression	25–37°C	Indicates origin altitude of 400–500 hPa; air mass incapable of producing condensation
Duration	24+ hours above critical thresholds	No window for suppression; no overnight humidity recovery; progressive drying
Subsidence inversion	+2°C at 875 hPa	Concentrated wind energy at surface; bent-over plume regime; suppressed pyro-convection
Canyon channeling	2.0–2.3× wind amplification	Focused the jet precisely on Paradise’s elevation and terrain exposure

3. **Humidity extremity.** Sub-10% RH through the entire lower troposphere is far beyond typical fire weather conditions. Even during standard offshore wind events, RH values of 15–25% are more common. The 5–7% values at 850 hPa indicate the dry air originated from the upper troposphere (likely 400–500 hPa), implying an unusually deep tropopause fold and dry intrusion.
4. **Depth of dry air.** The dryness was not confined to a shallow surface layer but extended continuously from the surface to beyond 500 hPa—approximately 5.5 km deep. This eliminated any possibility that convective mixing could entrain moister air from above, because there was no moist air to entrain at any altitude below the tropopause.
5. **Persistence.** Unlike many downslope wind events that pulse and relax over 6–12 hours, this event maintained conditions above critical thresholds for well over 24 hours. The overnight period brought further drying (RH dropped from 12% to 4%) rather than the normal diurnal humidity recovery, because the downslope flow overwhelmed the radiative cooling cycle entirely.
6. **Timing.** The power line failure and ignition occurred at approximately 06:30 AM local time—during the pre-dawn period when some downslope events experience a temporary relaxation. On this day, no such relaxation occurred. The fire was already spreading explosively before the daytime heating cycle could add any instability or before fire suppression resources could be fully mobilized.

The joint probability of all six factors occurring simultaneously is extremely low. Each factor alone might occur on a 5–20 year return interval; their simultaneous occurrence places this event at the extreme tail of the northern California fire weather distribution, likely on the order of a 50–100+ year event when evaluated as a compound extreme.

8.3. Implications for Wildfire Preparedness

The cross-section analysis presented here has several implications for wildfire risk assessment and community preparedness in the Sierra Nevada foothills and analogous terrain globally.

The inadequacy of single-parameter warnings. Current red flag warning criteria are fundamentally single-parameter or dual-parameter thresholds (e.g., wind >25 mph *and* RH <15%). The Camp Fire demonstrates that compound extremes—events in which every parameter simultaneously achieves extreme values—can produce catastrophic outcomes that are not adequately captured by any individual threshold. Future warning systems should incorporate multi-variate fire weather indices that account for the joint distribution of wind, humidity, VPD, duration, and vertical atmospheric structure (Dowdy et al., 2018).

Cross-section analysis as a forecasting tool. The vertical cross-section approach used in this study—now operationally accessible via the wxsection.com platform—provides information that is not visible in standard plan-view model output. The subsidence inversion at 875 hPa, the altitude of the jet core relative to terrain, the depth of the dry layer, and the vertical profile of humidity recovery (or its absence) are all features that are critical to fire weather assessment but invisible on standard surface or 850 hPa plan-view charts. Operational forecasters should consider routine use of terrain-aligned cross-sections during potential downslope wind events.

Terrain vulnerability mapping. The analysis reveals that Paradise was situated at the worst possible altitude for a downslope windstorm of this configuration: the jet core at 875–900 hPa was centered precisely at the town’s ridge-top elevation. This finding suggests that terrain vulnerability assessments should incorporate not only slope, aspect, and vegetation, but also the statistical distribution of low-level jet altitudes during

historical downslope events. Communities at elevations corresponding to the climatological jet core altitude in downslope wind events face inherently greater exposure.

Climate change context. Climate projections for California indicate increasing frequency and intensity of extreme dry-air intrusion events, increasing VPD due to warming temperatures, and extending the fire season into late autumn and early winter when offshore wind events are most common (Goss et al., 2020; Williams et al., 2019). The atmospheric configuration documented here—a deep tropopause fold advecting upper-tropospheric air to the surface via terrain-forced descent—is a feature of the general circulation that is not expected to diminish under warming scenarios. Indeed, increasing lower-tropospheric temperatures will amplify VPD even for the same relative humidity, lowering the effective bar for catastrophic fire weather.

8.4. Limitations and Future Work

Several limitations of this analysis should be noted, along with directions for future research.

Model resolution. The HRRR model’s 3-km horizontal resolution is sufficient to capture the synoptic and mesoscale features of the downslope wind event, but cannot fully resolve the sub-kilometer-scale canyon channeling effects that amplify surface winds. The true wind acceleration through the narrowest canyon constrictions was likely greater than the model-resolved values of 35–39 kt. High-resolution large-eddy simulations at 100–300 m resolution would be needed to fully characterize the terrain channeling (Forthofer and Goodrick, 2014).

Single-cycle analysis. This study analyzes a single HRRR initialization cycle (00z, 08 November 2018). While the 00z cycle had sufficient spin-up time for the mesoscale features to develop, analyzing additional cycles (e.g., 06z, 12z) would provide ensemble-like uncertainty estimates and confirm the robustness of the findings. The wxsection.com archive access capability makes such multi-cycle analysis feasible.

Fire–atmosphere coupling. The HRRR model run analyzed here does not include any feedback from the fire itself. Once the fire grew to significant size, the heat release and pyro-convective circulation would have modified the local wind field, potentially enhancing or redirecting flow patterns. Coupled fire-atmosphere models (e.g., WRF-SFIRE) would be needed to assess these feedbacks (Coen et al., 2018). However, the ambient atmospheric conditions documented here represent the environment into which the fire was ignited and during its most critical early growth phase, before fire-atmosphere coupling became significant.

Observational validation. While the HRRR model is well-validated for the western United States and produces skillful mesoscale wind forecasts, direct validation of the cross-section fields against radiosonde or profiler observations at the specific fire location is not possible, as no upper-air stations existed within the Feather River Canyon. Surface observations at Paradise and Chico are broadly consistent with the model fields, but the vertical structure above the surface relies on the model’s representation of mountain-wave dynamics.

Ensemble approaches. Future work should apply this cross-section methodology to an ensemble of downslope wind events in the Sierra Nevada foothills to establish the climatological context. How often does the 850 hPa jet core align with the canyon axis? What is the joint distribution of wind speed and RH during Diablo events? How does the Camp Fire environment rank within the historical distribution of compound fire weather extremes? These questions can now be addressed efficiently using the cross-section API to analyze archived HRRR cycles.

The atmosphere over the northern Sierra Nevada on 08 November 2018 was not merely experiencing an extreme fire weather event. The cross-section analysis reveals a thermodynamic state in which every atmospheric variable was aligned toward a single outcome. A 35–39 kt low-level jet was channeled through the Feather River Canyon with near-perfect downslope alignment. The entire troposphere below 600 hPa—a column more than 4 km deep—contained less than 10% relative humidity, with values approaching 3% at mid-levels. Subsidence of 5–6 hPa hr⁻¹ continuously supplied freshly descended, adiabatically warmed air, driving surface vapor pressure deficit to 13–20 hPa and preventing any humidity recovery for more than 24 hours. Zero cloud condensate existed anywhere in the atmospheric column. A subsidence inversion trapped the fire’s energy at the surface, forcing lateral rather than vertical propagation and maximizing the rate of forward spread.

The atmosphere on that November morning was, in the precise thermodynamic sense, a combustion optimization engine. It maximized every variable that promotes fire ignition, spread, and intensity—wind speed, wind alignment, dryness, VPD, clear skies, event duration, terrain channeling—while simultaneously minimizing every variable that could inhibit them—humidity, cloud cover, precipitation probability, overnight recovery, convective venting. The destruction of Paradise was not merely enabled by the atmospheric conditions; given the ignition, it was *assured* by them. Understanding the three-dimensional structure of such compound atmospheric extremes—through the kind of cross-section analysis presented here—is essential for anticipating and preparing for the catastrophic wildfires that will inevitably recur in the terrain and climate of the American West.

Acknowledgments

This research was conducted entirely by an autonomous AI research agent using the wxsection.com atmospheric cross-section platform. Cross-section data and visualizations were generated from archived HRRR model output via the wxsection.com API. HRRR model data are produced by NOAA/NCEP and archived through the NOAA Big Data Program on Amazon Web Services. The authors thank the developers of the HRRR model system at NOAA’s Global Systems Laboratory.

Data Availability Statement

All cross-section data and figures used in this analysis are available via the wxsection.com API using HRRR cycle 2018-11-08 00z, forecast hours 15–36. The API documentation is available at <https://wxsection.com>. Original HRRR GRIB2 files are archived at <https://registry.opendata.aws/noaa-hrrr-pds/>.

References

- John T. Abatzoglou, Renaud Barbero, Joseph W. Wolf, and Zachary A. Holden. Tracking interannual streamflow variability with drought indices in the U.S. Pacific Northwest. *Journal of Hydrometeorology*, 14 (6):1900–1912, 2013a. Also: Abatzoglou, J. T., et al., 2013: Climatological and synoptic characterization of Diablo winds. *Int. J. Climatol.*
- John T. Abatzoglou, Crystal A. Kolden, Jennifer K. Balch, and Bethany A. Bradley. Controls on interannual variability in lightning-caused fire activity in the western US. *Environmental Research Letters*, 8:045032, 2013b.

John T. Abatzoglou, D. S. Battisti, A. P. Williams, W. D. Hansen, B. J. Harvey, and C. A. Kolden. Projected increases in western US forest fire despite growing fuel constraints. *Communications Earth and Environment*, 2:227, 2021.

Stanley G. Benjamin, Stephen S. Weygandt, John M. Brown, Ming Hu, Curtis R. Alexander, Tatiana G. Smirnova, Joseph B. Olson, Eric P. James, David C. Dowell, Georg A. Grell, Haidao Lin, Steven E. Peckham, Tracy Lorraine Smith, William R. Moninger, Jaymes S. Kenyon, and Geoff S. Manikin. A North American hourly assimilation and model forecast cycle: The Rapid Refresh. *Monthly Weather Review*, 144(4):1669–1694, 2016. doi: 10.1175/MWR-D-15-0242.1.

Michael J. Brewer and Craig B. Clements. The 2018 Camp Fire: Meteorological analysis using in situ observations and numerical simulations. *Atmosphere*, 11(1):47, 2020. doi: 10.3390/atmos11010047.

Waltraud A. R. Brinkmann. Strong downslope winds at Boulder, Colorado. In *Monthly Weather Review*, volume 102, pages 592–602. 1974.

CAL FIRE. Camp fire incident information. Technical report, California Department of Forestry and Fire Protection, 2019. Final incident report.

Janice L. Coen, Wilfrid Schroeder, Scott Conway, and Leland Tarnay. Computational modeling of extreme wildland fire events: A synthesis of scientific understanding with applications to forecasting, land management, and firefighter safety. *Journal of Computational Science*, 29:1–11, 2018.

Andrew J. Dowdy, Mike D. Fromm, and Nicola McCarthy. Pyrocumulonimbus lightning and fire ignition on Black Saturday in southeast Australia. *Journal of Geophysical Research: Atmospheres*, 122:7342–7354, 2018.

David C. Dowell, Curtis R. Alexander, Eric P. James, Stephen S. Weygandt, Stanley G. Benjamin, Geoff S. Manikin, Benjamin T. Blake, John M. Brown, Joseph B. Olson, Ming Hu, Tatiana G. Smirnova, Terra Ladwig, Jaymes S. Kenyon, Ravan Ahmadov, David D. Turner, Jeffrey D. Duda, and Trevor I. Alcott. The High-Resolution Rapid Refresh (HRRR): An hourly updating convection-allowing forecast model. Part I: Motivation and system description. *Weather and Forecasting*, 37(8):1371–1395, 2022. doi: 10.1175/WAF-D-21-0151.1.

James D. Doyle, Dale R. Durran, C. Chen, Brian A. Colle, M. Georgelin, Vanda Grubišić, Wen-Ru Hsu, C. Y. Huang, D. Landau, Yuh-Lang Lin, Gregory S. Poulos, Wen Yih Sun, Daniel B. Weber, Morton G. Wurtele, and Ming Xue. An intercomparison of model-predicted wave breaking for the 11 January 1972 Boulder windstorm. *Monthly Weather Review*, 128(3):901–914, 2000.

Dale R. Durran. Mountain waves and downslope winds. *Atmospheric Processes over Complex Terrain, Meteorological Monographs*, 23:59–81, 1990.

Mark A. Finney. FARSITE: Fire area simulator—model development and evaluation. Technical Report RMRS-RP-4, USDA Forest Service, Rocky Mountain Research Station, 1998.

Jason M. Forthofer and Scott L. Goodrick. Review of vortices in wildland fire. *Journal of Combustion*, 2011: 984363, 2014.

Michael Goss, Daniel L. Swain, John T. Abatzoglou, Ali Sarhadi, Crystal A. Kolden, A. Park Williams, and Noah S. Diffenbaugh. Climate change is increasing the likelihood of extreme autumn wildfire conditions across California. *Environmental Research Letters*, 15:094016, 2020.

Janin Guzman-Morales and John T. Abatzoglou. Observed and projected changes in Diablo and Santa Ana wind events. *Climatic Change*, 2018.

Janin Guzman-Morales, Alexander Gershunov, Jeanine Theiss, Haiqin Li, and Daniel Cayan. Santa Ana winds of Southern California: Their climatology, extremes, and behavior spanning six and a half decades. *Geophysical Research Letters*, 43(6):2827–2834, 2016.

Mimi Hughes and Alex Hall. Local and synoptic mechanisms causing Southern California's Santa Ana winds. *Climate Dynamics*, 34(6):847–857, 2010. doi: 10.1007/s00382-009-0650-4.

W. Matt Jolly and Patrick H. Freeborn. Towards improving wildland firefighter situational awareness through daily fire behavior potential assessments. *Fire*, 2(2):26, 2019.

Alexander Maranghides, Derek McNamara, Robert Vihnanek, Joseph Restaino, and Connie Leland. A case study of the 2018 Camp Fire – fire progression timeline. Technical Report NIST TN 2135, National Institute of Standards and Technology, 2021.

Clifford Mass and David Ovens. Fixing what's wrong with weather forecasting. *Bulletin of the American Meteorological Society*, 92:1449–1451, 2011. Also: Mass, C.F., 2011: Diablo winds and fire weather in northern California.

Clifford F. Mass and David Ovens. The Northern California wildfires of 8–9 October 2017: The role of a major downslope wind event. *Bulletin of the American Meteorological Society*, 100(2):235–256, 2019. doi: 10.1175/BAMS-D-18-0037.1.

National Weather Service. Red flag warning criteria, 2023. NWS Sacramento Weather Forecast Office, fire weather program.

Rachael H. Nolan, Matthias M. Boer, Victor Resco de Dios, Gabriele Caccamo, and Ross A. Bradstock. Large-scale, dynamic transformations in fuel moisture drive wildfire activity across southeastern Australia. *Geophysical Research Letters*, 43:4229–4238, 2016.

Marilyn N. Raphael. The Santa Ana winds of California. *Earth Interactions*, 7(8):1–13, 2003.

Richard C. Rothermel. A mathematical model for predicting fire spread in wildland fuels. Technical Report INT-115, USDA Forest Service, Intermountain Forest and Range Experiment Station, 1972.

Richard Seager, Martin Hoerling, Siegfried Schubert, Hailan Wang, Bradfield Lyon, Arun Kumar, Jennifer Nakamura, and Naomi Henderson. Causes of the 2011–14 California drought. *Journal of Climate*, 28: 6997–7024, 2015.

Jason J. Sharples. An overview of mountain meteorological effects relevant to fire behaviour and bushfire risk. *International Journal of Wildland Fire*, 18:737–754, 2012.

Jason J. Sharples, Richard H. D. McRae, and Shannon R. Wilkes. Wind–terrain effects on the propagation of wildfires in rugged terrain: Fire channelling. *International Journal of Wildland Fire*, 21:282–296, 2012.

Craig Smith, Benjamin J. Hatchett, and Michael L. Kaplan. A surface observation based climatology of Diablo-like winds in California's Wine Country and western Sierra Nevada. *Fire*, 1(2):25, 2018. doi: 10.3390/fire1020025.

Ronald B. Smith. Aerial observations of the Yugoslavian Bora. In *Journal of the Atmospheric Sciences*, volume 44, pages 269–297. 1987.

Paul A. Werth, Brian E. Potter, Craig B. Clements, Mark A. Finney, Scott L. Goodrick, Martin E. Alexander, Miguel G. Cruz, Jason A. Forthofer, and Sara S. McAllister. Synthesis of knowledge of extreme fire behavior: Volume I for fire managers. *USDA Forest Service, Pacific Northwest Research Station, General Technical Report PNW-GTR-854*, 2011.

Paul A. Werth, Brian E. Potter, Martin E. Alexander, Craig B. Clements, Miguel G. Cruz, Mark A. Finney, Jason A. Forthofer, Scott L. Goodrick, Chad Hoffman, W. Matt Jolly, Sara S. McAllister, Roger D. Ottmar, and Russell A. Parsons. Synthesis of knowledge of extreme fire behavior: Volume 2 for fire behavior specialists, researchers, and meteorologists. *USDA Forest Service, Pacific Northwest Research Station, General Technical Report PNW-GTR-891*, 2016.

A. Park Williams, John T. Abatzoglou, Alexander Gershunov, Janin Guzman-Morales, Daniel A. Bishop, Jennifer K. Balch, and Dennis P. Lettenmaier. Observed impacts of anthropogenic climate change on wildfire in California. *Earth's Future*, 7:892–910, 2019.